Organic particle formation in halogen-influenced environments

Inaugural-Dissertation

to obtain the academic degree

Doctor rerum naturalium (Dr. rer. nat.)

submitted to the Faculty of Biology, Chemistry and Geosciences

of the University of Bayreuth

by

Dipl.-Met. Katharina A. Kamilli

from Leipzig

July 2015

Science may set limits to knowledge, but should not set limits to imagination.

- Bertrand Russell -

The present thesis was prepared between April 2011 and July 2015 at the University of Bayreuth, Atmospheric Chemistry under the scientific supervision of Prof. Dr. Andreas Held.

This is a full reprint of the dissertation submitted to obtain the academic degree of Doctor of Natural Sciences (Dr. rer. nat.) and approved by the Faculty of Biology, Chemistry and Geosciences of the University of Bayreuth.

Date of submission: 21.07.2015

Date of defence: 04.12.2015

Acting Dean:

Prof. Dr. Stefan Schuster

Doctoral committee:

Prof. Dr. Andreas Held (1st reviewer)

Prof. Dr. Frank Keppler (2nd reviewer)

Prof. Dr. Christoph Thomas (chairman)

Prof. Dr. Cornelius Zetzsch

Abstract

Atmospheric aerosols are an important topic in atmospheric research, motivated by their impact on climate, human health and heterogeneous chemistry. Secondary aerosol formation from the reaction of organic trace gases and reactive halogen species can act as an important natural source of organic aerosol. In order to better understand these reactions, aerosol formation from the reaction of α-pinene with chlorine and bromine was studied in laboratory experiments. New particle formation was initiated about five times faster by chlorine than by bromine. While new particle formation was observed at mixing ratios of 2.5 ppb Cl_2 and 10 ppb α-pinene, new particle formation with bromine was not observed below 10 ppb Br_2 and 10 ppb α-pinene. The formation of halogenated organic aerosol was confirmed by infrared spectroscopy (FTIR). To investigate the role of halogens in natural organic aerosol formation, a salt lake region in Western Australia, which is rich in reactive halogen species and organic compounds, was chosen as measurement site. On nine out of eleven measurement days and at five lakes, new particle formation was identified by measuring particle size distributions with a custom-built mobility analyzer (DMPS). With a mobile Teflon chamber set up at the lakeshore, particle formation was directly related to salt lake emissions. Due to enrichment of organic precursors inside of the chamber, particle formation started earlier and particle growth was faster than in the ambient air. Based on these field measurements, a salt lake environment was simulated in the laboratory. By systematic variation of the experimental conditions, the presence of light and organic precursor gases were identified as essential for new particle formation. Iron salt concentrations in the lake mixture controlled the intensity and the growth rates during new particle formation. Iron salts may catalyze additional oxidation reactions of organic compounds in the aqueous phase by a Fenton-like reaction mechanism. In this work, high Fe^{II} concentrations led to less new particle formation, which indicates a competition of oxidation of organic compounds in the aqueous phase and the gas phase. Organic aerosol samples from the field and from the laboratory were analyzed by ultrahigh resolution mass spectrometry, Raman spectroscopy, and scanning electron microscopy combined with energy-dispersive X-ray spectroscopy. Halogenated organic compounds were unequivocally identified, however, their contribution to new particle formation seems to be minor. The results show a large contribution of oxidized organic compounds as well as nitrogen- and sulfur-containing organic compounds to the formed aerosol mass.

Zusammenfassung

Atmosphärische Aerosolpartikel sind wegen ihrer großen Bedeutung für das Klima, die menschliche Gesundheit und die heterogene Chemie ein bedeutsames Thema in der Atmosphärenforschung. Die sekundäre Aerosolbildung aus der Reaktion von organischen Spurengasen mit reaktiven Halogenverbindungen kann eine wichtige natürliche Quelle für organisches Aerosol sein. Zum besseren Verständnis dieses Reaktionsmechanismus wurde zunächst in Laborexperimenten die Aerosolbildung aus der Reaktion von α-Pinen mit Chlor bzw. Brom untersucht. Unter vergleichbaren experimentellen Bedingungen verlief die Partikelneubildung mit Chlor um ungefähr den Faktor fünf schneller als mit Brom. Während Partikelneubildung bereits bei Mischungsverhältnissen von 2.5 ppb Cl_2 und 10 ppb α-Pinen beobachtet wurde, fand Partikelneubildung mit Brom nicht unterhalb von 10 ppb Br_2 und 10 ppb α-Pinen statt. Die Bildung von halogeniertem organischen Aerosol konnte durch die chemische Analyse mittels Infrarotspektroskopie (FTIR) bestätigt worden. Um die Rolle von Halogenen bei der organischen Aerosolbildung in der Natur zu untersuchen, wurde eine Salzseeregion in Westaustralien gewählt, die reich an reaktiven Halogenverbindungen sowie organischen Verbindungen aus der Eukalyptus-Vegetation und der organisch angereicherten Bodenschicht ist. Mit einer mobilen Teflonkammer über der Randzone der Salzseen konnte an neun von elf Messtagen und fünf unterschiedlichen Seen durch Messung der Partikelgrößenverteilung mit einem speziell angefertigten Mobilitätsanalysator (DMPS) Partikelneubildung identifiziert und direkt den Salzseen zugeordnet werden. Die Partikelbildung setzte in der mobilen Kammer früher ein und das Partikelwachstum verlief schneller als in der Umgebung, was auf die Anreicherung an organischen Vorläufergasen im Inneren der Kammer zurückzuführen ist. Basierend auf diesen Feldmessungen wurde in Laborexperimenten ein Salzsee simuliert. Durch kontrollierte Variation der experimentellen Bedingungen wurde festgestellt, dass Licht sowie organische Vorläufergase unbedingt notwendig für die Partikelbildung sind. Die Konzentration von Eisensalzen in der Salzseemischung kontrollierte dagegen die Stärke und Geschwindigkeit der Partikelneubildung. Durch den Mechanismus der Fenton-Reaktion können die Eisensalze eine zusätzliche Oxidation organischer Verbindungen in der Flüssigphase katalysieren. In dieser Arbeit haben hohe Eisen-(II)-Konzentrationen zu einer schwächeren Partikelneubildung geführt, was somit einen kompetitiven Verbrauch organischer Verbindungen in der Flüssigphase zu Lasten der Gasphase nahelegt. Organische Aerosolproben aus dem Feldexperiment und den Laborexperimenten wurden mit ultrahochauflösender Massenspektrometrie, Ramanspektroskopie und Rasterelektronenmikroskopie kombiniert mit energiedispersiver Röntgenmikroanalyse chemisch analysiert. Dabei wurden halogenierte organische Verbindungen in den Proben eindeutig identifiziert, aber der Beitrag von Halogenen scheint nur eine untergeordnete Rolle bei der Partikelbildung gespielt zu haben. Die Ergebnisse heben den starken Beitrag von oxidierten organischen Verbindungen sowie Stickstoff enthaltenden und schwefelhaltigen organischen Verbindungen zu der gebildeten Aerosolmasse hervor.

Table of content

List of publications

This thesis consists of an implementation and synopsis of the performed research, based on the research articles I-III.

I. Ofner et al., 2013:

Ofner, J., **Kamilli, K. A.**, Held, A., Lendl, B., and Zetzsch, C.: **Halogen-induced organic aerosol (XOA): A study on ultra-fine particle formation and time-resolved chemical characterization**, Faraday Discussions, doi:10.1039/C3FD00093A, 2013.

II. Kamilli et al., 2015a:

Kamilli, K. A., Ofner, J., Krause, T., Sattler, T., Schmitt-Kopplin, P., Atlas, E., Eitenberger, E., Friedbacher, G., Lendl, B., Lohninger, H., Schöler, H. F., and Held, A.: **New particle formation induced by Western Australian salt lakes**, to be submitted 2015.

III. Kamilli et al., 2015b:

Kamilli, K. A., Ofner, J., Lendl, B., Schmitt-Kopplin, P., and Held, A.: **New particle formation above a simulated salt lake in aerosol chamber experiments**, Environmental Chemistry, 12, 489, doi:10.1071/EN14225, 2015.

Publications not topic of this work:

Kamilli, K. A., Poulain, L., Held, A., Nowak, A., Birmili, W., and Wiedensohler, A.: **Hygroscopic properties of the Paris urban aerosol in relation to its chemical composition**, Atmospheric Chemistry and Physics, 14(2), 737-749, 2014.

Healy, R. M., Evans, G. J., Murphy, M., Jurányi, Z., Tritscher, T., Laborde, M., Weingartner, E., Gysel, M., Poulain, L., **Kamilli, K. A.**, Wiedensohler, A., O'Connor, I. P., McGillicuddy, E., Sodeau, J. R., and Wenger, J. C.: **Predicting hygroscopic growth using single particle chemical composition estimates**, Journal of Geophysical Research: Atmospheres, 119(15), 9567-9577, 2014.

1 Introduction

1.1 Current state of scientific knowledge

Aerosol particles are ubiquitous in the atmosphere and involved in a variety of atmospheric processes. As effective cloud condensation nuclei (CCN) once grown above a diameter of 70 nm (Spracklen et al., 2008), aerosol particles directly influence the cloud formation, the radiative budget in the earth's atmosphere and thus play a central role in climate and climate change (IPCC, 2007). In recent years, significant progress was made in estimating the radiative forcing of different emitted compounds. However, the assessment in cloud and aerosol processes, and their interactions, were classified as low by the IPCC (2013), in contrast to the mediate to very high confidence levels e.g. for emitted greenhouse gases, which also influence the radiation budget. One reason for the still massive need for research in the field of atmospheric aerosols can be seen in the diverse formation and transformation pathway of the aerosol particles as well as their different sources, composition (Pöschl, 2005), and their influence on radiation and therefore the climate.

Aerosol particles, whether from natural or anthropogenic sources, are released either directly into the atmosphere or result from oxidation of gas-phase precursors (Kanakidou et al., 2005). Primary aerosol particles comprise the larger fraction of the size distribution beginning at about 50 nm in the so called upper Aitken mode. The main components of primary emitted particles are black carbon, sea salt, mineral dust and biological material. The release of nucleation mode particles can only be ensured by gas-to-particle-conversion and the associated formation of particle mass in the lower diameter range beginning at 3 nm (Seinfeld and Pandis, 2006). The transformation of inorganic gases such as sulfur dioxide, nitrogen dioxide and ammonia to secondary aerosol containing sulfate, nitrate and ammonium is well understood (Hallquist et al., 2009). Particulate matter resulting from volatile organic compounds (VOC), called secondary organic aerosol formation (SOA; Kroll and Seinfeld, 2008), was first suggested by Went (1960), who investigated the source of blue haze formed above forests. Contrary to previous assumptions that the haze may result from smoke, dust, water vapor or fog, they proposed the oxidation of organic vapors leading to condensable products involved in aerosol formation through gas-to-particle conversion. This blue haze was also observed commonly above the Australian eucalyptus forests (Went, 1960) suggesting the same formation pathway. Their hypothesis in new particle formation over forests was confirmed by numerous measurements (e.g. Mäkelä et al., 1997, Kavouras et al., 1999, Laaksonen et al., 2008). Organic compounds are supposed to make up an amount of at least 20 % of aerosol mass in the lower troposphere varying up to 90 % (Kanakidou et al., 2005) and are estimated to a number of 10 000 to 100 000 different organic compounds occurring in the atmosphere (Goldstein and Galbally, 2007). In the troposphere the organic compounds react mainly with hydroxyl (OH) radicals, nitrate (NO_3) radicals and ozone (O_3) (Atkinson and Arey, 2003). Each of those 10 000 to 100 000 different organic compounds can undergo various transformation and oxidation reactions before particle formation occurs, which gives rise to many uncertainties in the formation process of SOAs (Hallquist et al., 2009; Carslaw et al., 2010). Especially the SOA formation from natural VOCs is of importance, emphasized by the stronger emission source. Guenther et al. (2012) estimated the global VOC emission from biogenic sources to have a value of 1000 Tg yr^{-1} which corresponds to nearly the tenfold value of the global amount of anthropogenic VOC emissions, estimated to be 130 Tg yr^{-1}. Vegetation is a major source of VOCs to the atmosphere (Guenther et al., 1995),

with isoprene and its derivatives, e.g. monoterpenes and sesquiterpenes as the main groups of VOCs emitted (Kiendler-Scharr et al., 2009). Emission rates of the vegetation are coupled to temperature and light (Guenther et al., 1995).

Many studies were conducted in conifer or deciduous forests, where the substantial emission of reactive hydrocarbons, mainly monoterpenes or isoprene, was confirmed (e.g. Spracklen et al., 2008, Geron et al., 2006, Guenther et al., 2000 and references herein). Newly formed particles above forests were found to be mainly the result of organic compounds originating from photo-oxidized VOCs (e.g. Kavouras et al., 1998) and sulfates from sulfuric acid (e.g. Kulmala et al., 2004) acting as key reactants. Investigations in eucalyptus forests were neglected and only few studies focused on the topic of eucalyptus tree emissions. However, eucalyptus trees tend to produce a large amount of terpenes and isoprene (Ristovski et al., 2010, Kavouras et al., 1998; Winters et al., 2009), and therefore have a particle formation potential similar to other forests.

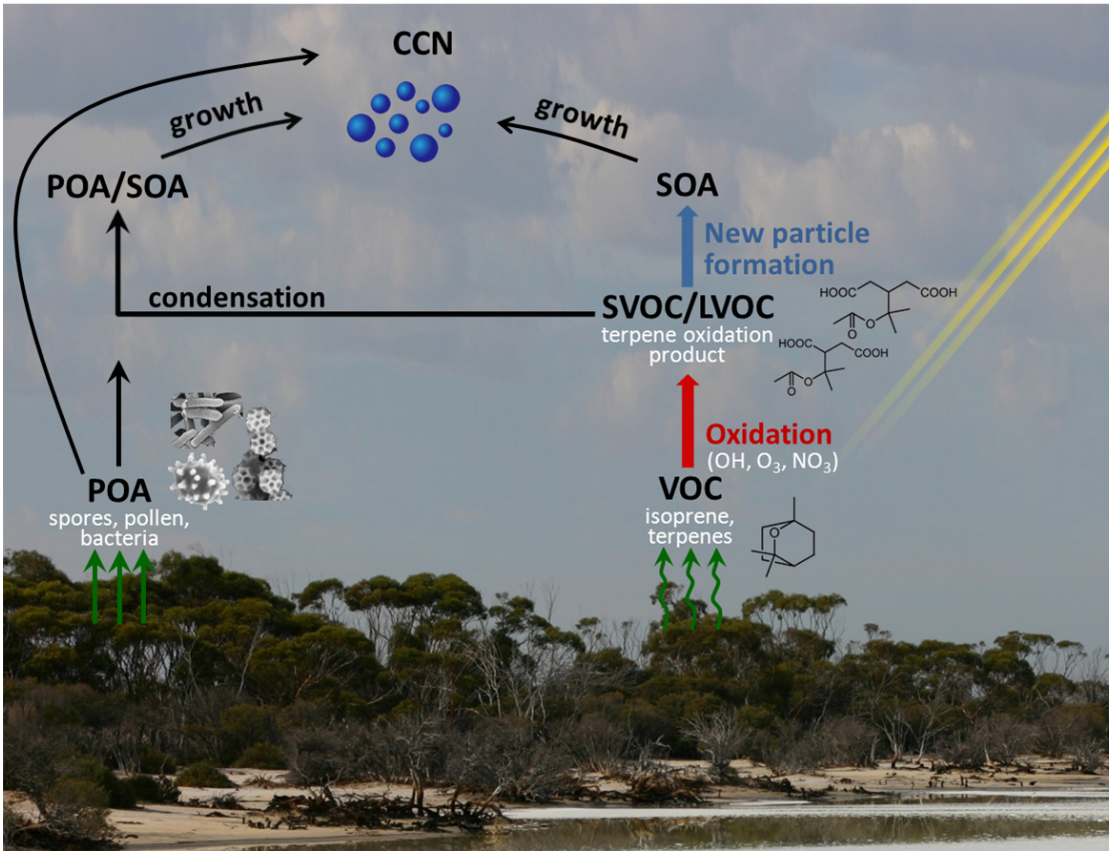

Figure 1 Scheme of primary and secondary aerosol formation from biogenic sources and subsequent growth to cloud condensation nuclei. One selected example of a SOA precursor is 1,8-cineole $C_{10}H_{18}O$, which is emitted by eucalyptus trees and may be oxidized after certain steps to diaterpenylic acid acetate $C_{10}H_{16}O_6$ and diaterebic acid acetate $C_9H_{14}O_6$ under the influence of irradiance. Subsequently, the oxidation products may undergo gas-particle partitioning to form SOA and grow to CCNs.

Nunes and Pio (2001) found eucalyptus to emit both isoprene and monoterpenes at high rates. One of the predominant monoterpene compounds emitted by eucalyptus trees is 1,8-cineole (Cerqueira et al., 2003; Fig. 1). This highly volatile OC with coincident high vapor pressure can be oxidized further in the atmosphere, most likely with OH radicals (Atkinson and Arey, 2003). The availability of oxidants is correlated with the highly energetic irradiation. Boy and Kulmala (2002) identified UV light as an important driver in instigating particle formation.

With increasing oxidation state the vapor pressure and the volatility of the organic gaseous compound are decreasing. In the example of 1,8-cineole, the later generation products diaterpenylic acid acetate and diaterebic acid acetate (Iinuma et al., 2009) can undergo gas-particle partitioning (Atkinson and Arey, 2003) and facilitate new particle formation (O'Dowd et al., 2002), which increases the atmospheric particle number. Alternatively, semi-volatile or low volatility organic compounds (SVOC/LVOC) condense on pre-existing primary emitted aerosol particles (Seinfeld and Pankow, 2003), which increases the atmospheric particle mass (Fig. 1). Regardless of the particle source or formation pathway, the organic particles have the ability to grow to relevant CCN sizes. The number of CCNs increases if organic vapor condenses on ultrafine aerosol ($Dp < 100$ nm), but decreases when the organic mass condenses mainly on particles with a diameter $Dp > 100$ nm, causing a loss of ultrafine particles (Riipinen et al., 2011). An enhanced source for ultrafine particles and a coincident low concentration of background aerosol leads to an enhancement of CCN number and has therefore a direct feedback to the climate.

An increased number of CCNs accompanied a decline in precipitation in the Western Australian salt lake area (Junkermann et al., 2009). The authors linked the phenomena to the formation of ultrafine particles with salt lakes as suggested particle source, without having chemical evidence for the formation pathway.

The Western Australian salt lakes are appropriate suppliers for ultrafine aerosol particles for different reasons. The salt lakes, formed after large-scale deforestation in the mid 20th century for agricultural purposes, are nowadays surrounded by the remains of the natural vegetation. Biogenic emissions in combination with an additional group of oxidants emitted by the salt lakes enlarge the common SOA formation pathway. Salt lakes have the potential to release high amounts of reactive halogens into the atmosphere (Stutz et al., 2002; Buxmann et al., 2012). Reactive halogen species (RHS) represent both an additional source in SOA formation (Cai and Griffin, 2006; Cai et al., 2008) and SOA transformation (George and Abbatt, 2010; Ofner et al., 2012). The coexistence of high concentrations of reactive halogen species (RHS) and organic precursor gases also allows for a halogen-induced secondary organic aerosol formation (XOA) under very low ozone mixing ratios. Due to their capability in ozone destruction, halogens directly increase the possibility of XOA formation or halogenation of previous formed SOA (Ofner et al., 2012). While the contribution of halogen-induced SOA formation has not been quantified in the natural environment so far, in laboratory experiments particle formation was observed from the reaction of terpenes with chlorine so far (Cai and Griffin, 2006). Theoretically, this particle formation pathway could take place in environments providing both halogen radicals and organic precursors, for example in salt lake environments. Due to the liquid layer of the salt lakes located above the salt crust and the organic enriched soil layer, which is also responsible for biogenic emissions, aqueous phase reactions are added to the possible SOA sources. In particular over the past decades, the aqueous phase has been established as an additional source for SOA (Hallquist et al., 2009; Lim et al., 2010; Carlton et al., 2006).

1.2 Objectives of this work

The overarching goal of this work is a better understanding of NPF resulting from gaseous precursors with organic origin, especially in halogen-influenced environments. In order to address this goal, ambient measurements as well as lab chamber experiments were conducted to shed light on the following questions:

I Is NPF from the interaction of reactive halogen species with organic precursor gases possible at atmospherically relevant concentrations?

II Are there indications for halogen-induced organic aerosol formation in ambient measurements?

III Which alternative pathways for NPF are possible in the studied environments?

IV Which role does halogen-induced organic aerosol formation play in the overall secondary organic aerosol formation process?

2 Halogen organic interaction

2.1 Physical investigation of NPF

The interaction of the organic precursor gas α-pinene and Cl- or Br-radicals released by reactive halogen species (RHS) was examined in aerosol-smog chamber experiments under close to ambient conditions with simulated sun light (details on the experimental setup can be found in Ofner et al., 2011, 2013). The decay of the aerosol precursor was analyzed by capillary gas chromatography coupled with flame-ionization detection (GC-FID). Simultaneously, the aerosol size distribution was measured using a Scanning Mobility Particle Sizer (SMPS; IfT Leipzig, Germany). Combining measurements of the aerosol size distribution and the decay of the aerosol precursor allowed to determine aerosol yields, which were then used to show the SOA formation potential (e.g. Pandis et al., 1993) according to the formula

$$Y = \frac{\Delta M_0}{\Delta VOC} \qquad (1)$$

The aerosol yield (Y) is defined by the aerosol mass formed (ΔM_0 in µg m^{-3}) divided by the amount of organic precursor gas (ΔVOC in µg m^{-3}) consumed in the aerosol formation process. The aerosol yield can either be quoted as the maximum yield obtained when the organic precursor is completely consumed with the coincident aerosol mass formed (Pandis et al., 1992), or as the progress of aerosol yield given from beginning particle formation to the end of particle growth (Ng et al., 2006; Hoffmann et al., 1997). The aerosol yields in Ofner et al. (2013) were derived in both ways and the initial conditions were varied in organic precursor concentration as well as the concentration of chlorine/ bromine atoms injected into the chamber as specified in Table 1.

Table 1 Initial conditions, aerosol mass ΔM_0 and aerosol mass yield Y of smog-chamber runs (revised and updated from Ofner et al., 2013).

Experiment	Cl_2 / Br_2 [ppb]	α-pinene [ppb]	ΔM_0 [µg m^{-3}]	Y
Cl-1	2.5	10	1.28E-03	3.73E-05
Cl-2	5	10	6.01E-02	2.00E-03
Cl-3	5	10	6.44E-02	9.78E-03
Cl-4	20	20	23.69	2.43E-01
Cl-5	100	20	12.41	1.09E-01
Cl-6	200	50	175.72	6.19E-01
Br-1	10	10	1.13E-02	3.37E-04
Br-2	20	20	8.49	7.98E-02
Br-3	100	20	16.29	1.78E-01
Br-4	200	50	56.45	2.87E-01

To ensure comparable results of the single measurement series, the experimental procedure was standardized and kept the same during all smog chamber runs as follows. After switching on the solar simulator at zero-air conditions, α-pinene was injected into the chamber. With the gas chromatograph coupled to a flame ionization detector (GC-FID) the homogeneous distribution of the organic precursor was monitored. With the SMPS, the self-initiated particle formation by photo-oxidation of the organic precursor was monitored. After 20 minutes, and equilibrium of the organic precursor was reached and one could exclude unintentional particle formation. Therefore the desired oxidant in the form of molecular chlorine or bromine was injected into the chamber. The molecular chlorine/bromine was rapidly photolyzed by the solar simulator, even at very low mixing ratios. For chlorine, the mixing ratios decrease to 2.5 ppb, while XOA formation initiated by bromine did not proceed below 10 ppb of bromine. Additionally, the time between injection of the RHS species and XOA formation differ between the experiments. Inside the illuminated smog chamber the NPF from chlorine was observed within two minutes in the low concentration experiments (Cl-1 to Cl-3) and immediately after injection for the high concentration experiments (Cl-4 to Cl-6). The NPF formation for bromine-induced events was about five times slower.

In experiments Cl-1 to Cl-3, the precursor mixing ratios tend to be realistic with respect to the atmosphere (cf. Tab. 1). The precursors are within one or two orders of magnitude found in environments supplying both increased halogen release and organic precursor gases emitted by natural or anthropogenic sources. The maximal aerosol yields for those experiments were in the range between $3.7x10^{-5}$ and $9.8x10^{-3}$ with SOA mass formed between $1.3x10^{-3}$ and $6.4x10^{-2}$ µg m^{-3} (Tab. 1), respectively. Comparing the yields of those experiments with the two-product model (2P-M, developed by Odum et al., 1996) applied to the data of Cai and Griffin (2006), Ofner et al. (2013) achieved reasonable agreement, but extended the aerosol yield to a range four orders of magnitude lower than what was measured by the previously mentioned study. In consistent measurement ranges (Cl-4 and Cl-5; Tab. 1), Ofner et al., 2013 could confirm the comparable work conducted by Cai and Griffin (2006) (Fig. 2b). The latter obtained maximum yields ranging from

$7.9x10^{-2}$ to $2.2x10^{-1}$ with coherent aerosol masses between 8.0 and 33.5 µg m^{-3} from oxidation of α-pinene by chlorine atoms. In experiment Cl-6, which was performed with exceeding mixing ratios of α-pinene as well as chlorine compared to Cai and Griffin (2006), Ofner et al. (2013) received higher yields than expected from the two-product model applied to data by Cai and Griffin (2006). Comparing the chlorine experiments with each other it can be assumed that in experiment Cl-5 the formed aerosol mass and consumed organic precursor was lower than expected from the initial conditions. With steadily increasing initial mixing ratios in experiment Cl-1 to Cl-6, the formed aerosol mass as well as the aerosol yield increased appropriate excluding Cl-5. Even if the precursor concentration was held constant from Cl-5 to Cl-6 due to the increased oxidation capacity, higher aerosol yields have been obtained. However, the relation between formed aerosol mass and aerosol yield coincide well with Cai and Griffin (2006).

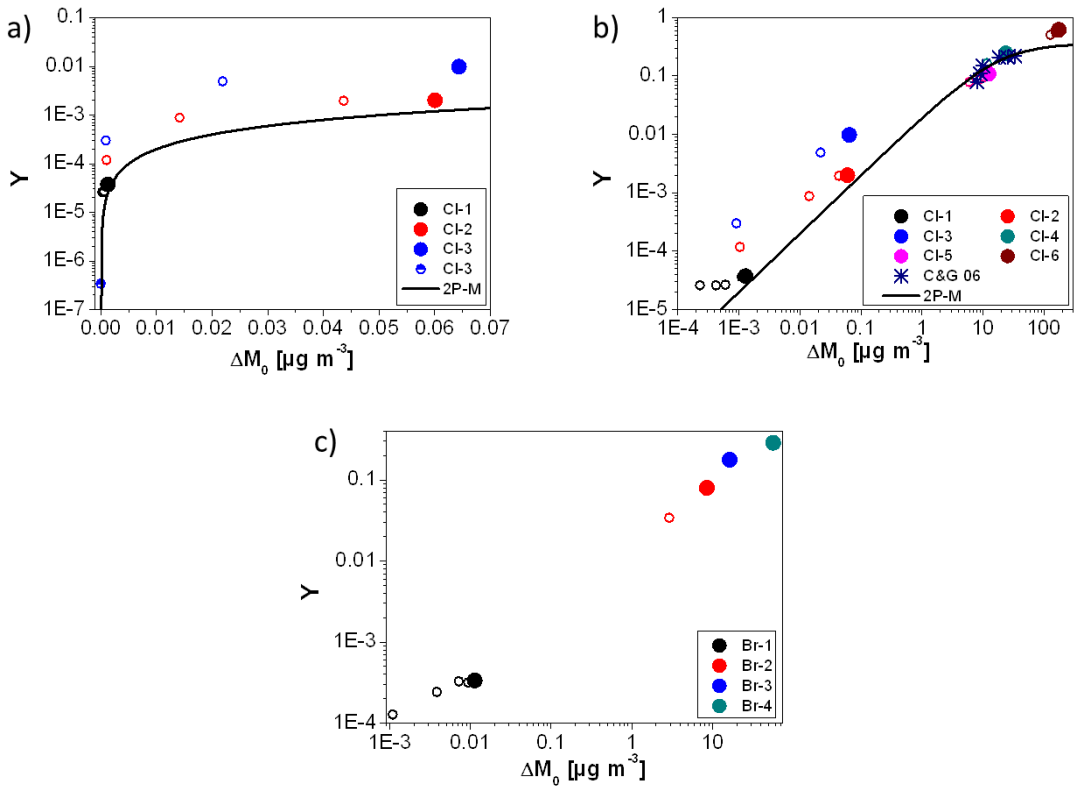

Figure 2 a) - b) Yield curves of α-pinene and chlorine as well as c) α-pinene and bromine (revised and updated from Ofner et al., 2013). The yield curves of six smog-chamber experiments conducted with varying α-pinene and chlorine mixing ratios were compared with the yield curve obtained applying a two-product model (2P-M) to the data of Cai and Griffin (2006) (C&G 06) in a) low concentration experiments Cl-1 to Cl-3 and b) all experiments Cl-1 to Cl-6. The data of four α-pinene and bromine experiments Br-1 to Br-4 are depicted in c) with no comparative data as no previous data are available on bromine-induced aerosol formation from organic precursors.

For the bromine experiments, aerosol yields between $3.4x10^{-4}$ and $2.9x10^{-1}$ with corresponding aerosol masses between $1.1x10^{-2}$ and 56.5 µg m^{-3} were obtained for the lowest and highest initial mixing ratios of the precursors, respectively (Tab. 1). In comparison to the chlorine experiments, the obtained maximal yields in the chlorine experiments were higher in obtained aerosol yields as well as aerosol mass formed, except for 20 ppb α-pinene and 100 ppb of the halogen molecules (Cl-5 vs. Br-3, Tab. 1). In the other

comparable chlorine and bromine experiments (Cl-4/Br-2; Cl-6/Br-4) the chlorine experiments resulted in two to three times higher maximal aerosol yields and masses. The bromine experiments could not be compared with similar data, as no comparative data on bromine-induced aerosol formation from organic precursors are available yet.

Even if the concentrations of the precursor gases are close to ambient conditions, the halogen-induced organic aerosol formation alone should hold organic aerosol masses between 1-10 µg m^{-3} to be of atmospheric relevance (McFiggans et al., 2013). Increasing the initial organic aerosol mass would have led to increased aerosol yields, as well as enhanced formed aerosol masses. When there was an initial organic mass present under so called heterogeneous conditions, Odum et al. (1996, 1997) found the transition from gas to particulate phase proceeding even below the saturation point of the high vapour pressure constituents. The initial organic aerosol mass served as core onto which the oxidized organic vapour could be absorbed.

Kroll and Seinfeld (2008) stated that yields obtained from the reaction of chlorine with monoterpenes are usually in the range of or lower than those from monoterpene photooxidation, and lower than the yields resulting from the addition of a hydroxyl or nitrate group. As the yields obtained from bromine in the current study were again typically lower than for chlorine, chlorine and bromine obviously lower the vapor pressure of the organic precursor less effective than other oxidants. Nevertheless, in the current study Ofner et al. (2013) showed the formation possibility of halogenated organic aerosol from the gas phase without an initial aerosol mass (homogeneous nucleation) at very low precursor concentrations in the absence of ozone.

2.2 Chemical investigation of NPF

The consumption of the organic precursor was monitored by GC-FID and compared to the theoretical decay based on the available molecular chlorine and associated chlorine atoms (described in detail in Ofner et al, 2013). It is assumed that every chlorine atom reacts with the organic precursor molecule and is subsequently consumed. The release of the chlorine atom for further oxidation of other organic molecules is neglected. For the low chlorine experiments (Cl-1 to Cl-3) the measured decay of the organic precursor was nearly twice as high after one hour as computed for the 2.5 ppb Cl_2 (5 ppb Cl) initial value. The result showed that contrary to the assumption, one chlorine atom may be regenerated after oxidation with one organic molecule and released for additional reactions. In the 5 ppb Cl_2 (10 ppb Cl) experiment computed and measured organic precursor decay show a better agreement than for 2.5 ppb Cl_2. For experiments with higher concentrations in Cl-3 to Cl-6, a comparison between computed and measured value becomes invalid due to the decreased diffusion of both chlorine and RHS (Ofner et al., 2013).

The detailed chemical information was retrieved with flow-reactor measurements coupled to a Fourier transform infrared (FTIR; Bruker IFS 113v) spectrometer in parallel to the aerosol-smog chamber experiments. The obtained dataset was analyzed by 2D correlation spectroscopy (Noda, 1993; Noda et al., 2000; Muik et al., 2007), where the chemical transformation of the organic precursor was examined during the aerosol formation and aging process to distinguish between SOA and XOA formation.

In general, radical initiated oxidations by OH, NO_3 or halogens cause either an abstraction of a hydrogen atom, or addition to a C–C double bond (Kroll and Seinfeld, 2008). In contrast to the addition reaction the vapor pressure of the organic product was not lowered by the abstraction reaction leading to an ineffective reaction for initiating particle formation. In the current work, evidence for both pathways was identified in the flow-reactor measurements. The Cl addition pathway to α-pinene, which breaks the double bond, was indicated by the formation of C–Cl bonds visible in the FTIR-spectra. The formation of HCl gave hints for H-atom abstraction from α-pinene in the reaction with chlorine. The resulting aerosol was halogen induced, and therefore, the formation of XOA established. After XOA formation, XOA was transformed by oxygen or oxygen-containing functional groups added to the radical site of the organic structure. The transformation gave the XOA a more SOA appearance, where the remaining C–Cl bond in the FTIR-spectra still gave evidence on the origin of the organic aerosol. With further transformation and aging via reactive species the XOA appearance of the organic aerosol got lost gradually until the aerosol looked like common SOA.

3 Particle formation in salt lake environments

3.1 Measurement sites

The field measurements were conducted in Western Australia in the wheat belt area around Lake King, where a plenty of salt lakes are present. The Australian salt lakes show a great diversity in measured pH values and other chemical parameters in the liquid and the subjacent layers, such as iron content, even between adjacent lakes (Bowen and Benison, 2009). The conditions for NPF are therefore diverse and provide an interesting measurement site worth studying. The experimental setup with a new approach using a mobile chamber and used instrumentation can be found in Kamilli et al. (2015a). Under irradiance organic precursor gases are released from the salt lake to the atmosphere, enriched in the chamber, where they are oxidized mainly by OH, O_3 and NO_3 resulting in SOA formation (Fig. 3a). Those newly formed particles were observed at nearly every examined salt lake in Western Australia and showed distinct particle growth.

An attempt was made to simulate new particle formation above salt lakes. To simulate a salt lake environment, a home-made structure was built and mounted into the 700 L glass chamber, which was also used for examination of halogen organic interaction (cf. chapter 2). A salt lake mixture containing dissolved organic compounds was introduced into the chamber and illuminated by the solar simulator to reproduce conditions and processes similar to Western Australia (Fig. 3b). The experiments were conducted as described in detail in Kamilli et al. (2015b).

At both measurement sites filters were loaded at the end of experiments when NPF was concluded and the particles had grown. The subsequent analysis gave a comprehensive chemical characterization of organic aerosol in salt lake environments and enabled the comparison of both measurement sites.

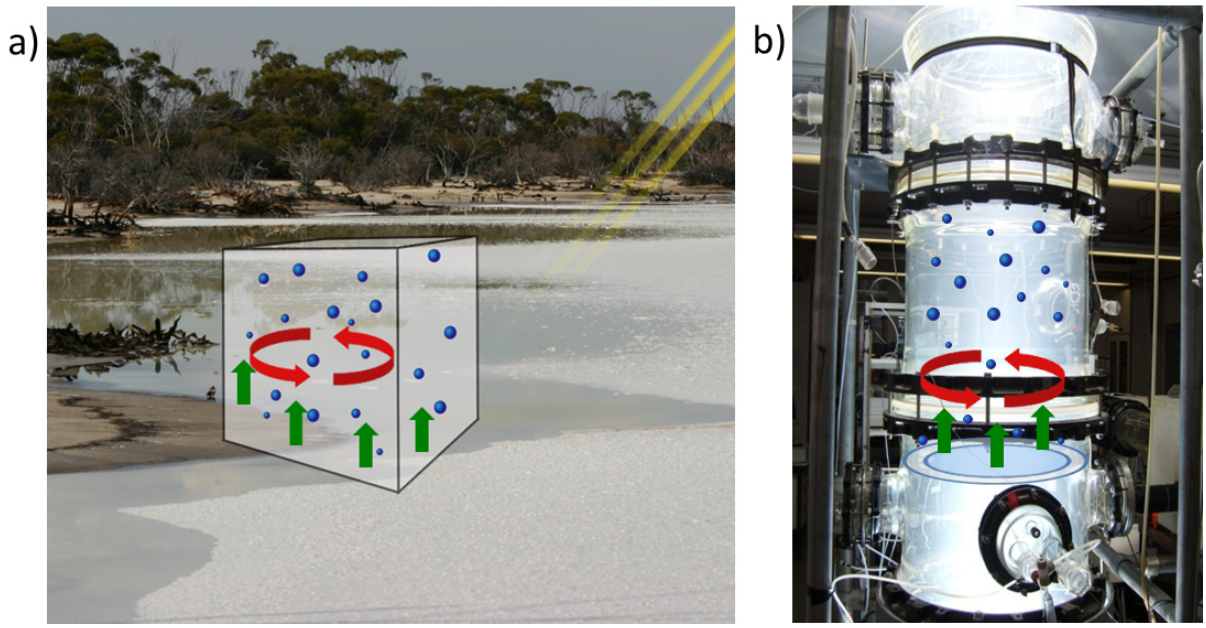

Figure 3 Under irradiance the VOCs emissions (green arrows) arising from the salt lake are oxidized (red arrows) leading to NPF (blue spheres) and subsequent particle growth (a) in natural environments as well as (b) in simulation experiments carried out in the laboratory.

3.2 Possible pathways leading to NPF

In salt lake environments the formation pathways leading to NPF are diverse due to the following reasons

a) Release of high amounts of VOCs to the gas phase,
b) The aqueous phase as reaction volume in addition to the gas phase,
c) Combination of high irradiation, low pH values and supply of reactive iron species,
d) Release of RHS.

Those requirements promote the following processes (cf. Figure 4)

a) SOA formed in the gas phase,
b) Further oxidation in the aqueous phase,
c) Occurrence of Fenton reaction,
d) Formation of organosulfates,
e) Halogen activation: Formation of XOA or halogenated SOA.

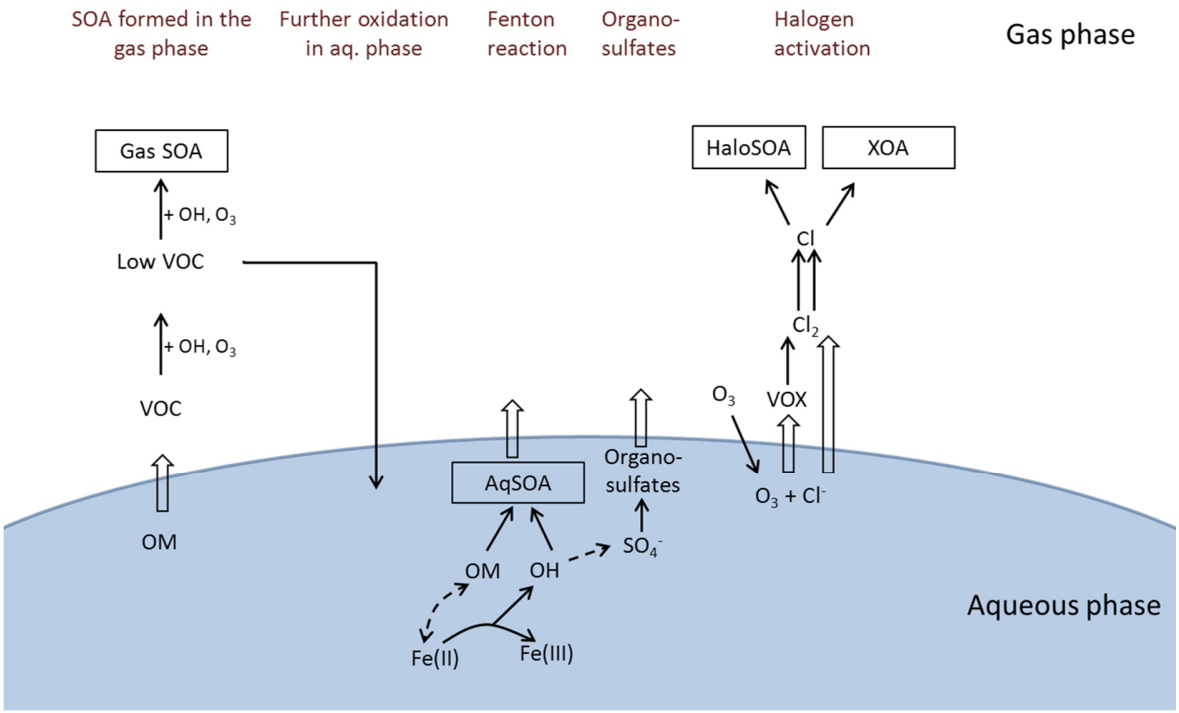

Figure 4 Possible processes leading to NPF in irradiated salt lake environments due to the interaction between aqueous and gas phase chemistry. The salt lake contains a mixture of salts and organic matter (OM). Kamilli et al., (2015b).

SOA formation in the gas phase

In natural salt lakes the organic matter is stored in the sediment layer of the soil directly below the salt crust. The organic matter originates mainly from decomposed leaves from surrounding eucalyptus trees that had fallen into the salt lake. 1,8-cineole as main organic compound released by eucalyptus leaves (Cerqueira et al., 2003) may be released from the soil layer to the overlaying salt crust and the thin liquid film. Therefore, 1,8-cineole is dissolved in the aqueous phase. Once the dissolved organic matter is released into the gas phase, it is quickly oxidized by OH radicals (Corchnoy and Atkinson, 1990) leading to low volatility organic compounds. These LVOCs may either transit back into the aqueous phase for further oxidation (Bateman et al., 2011) or contribute to SOA formation in the gas phase (Fig. 4).

The organic mixture in the aqueous phase of the simulated salt lakes, composed of 1,8-cineole and limonene, may undergo processes similar to processes in natural salt lake environments. Subsequent to the release of organic precursors into the gas phase, 1,8-cineole is oxidized by OH radicals (Corchnoy and Atkinson, 1990) and limonene is oxidized by ozone as well as OH radicals (Calogirou et al., 1999). Besides the oxidation of organic compounds in the gas phase leading to new particulate matter, the formed SOA mass can be expanded by oxidation pathways in the aqueous phase (Hallquist et al., 2009) in salt lake environments.

Fenton reaction

Fenton reactions take place in aqueous media and are favored at locations with high irradiation, low pH values and the supply of reactive iron species (Krause et al., 2014; Southworth and Voelker, 2003). Most of the Western Australian salt lakes were extremely acidic with values less than 4 (Benison et al., 2007). Krause et al. (2014) measured a total iron content between 0.46 and 3.6 weight percent of the sampled sediments and the dissolved iron contents of the water samples ranged from below the detection limit with 0.2 mg l^{-1} and a value of 173 mg l^{-1}. The latter parameter showed a correlation with pH values detected between 8.7 and 2.4. Due to a constant supply of high irradiation, the occurrence of the Fenton reaction can be assumed in this area.

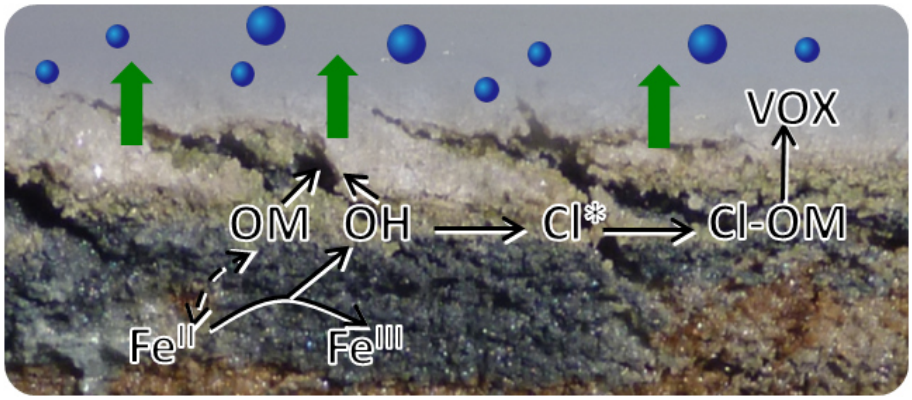

Figure 5 Detail of a salt lake soil with the black layer enriched in organic matter (OM) and colouring FeS/FeS_2 minerals positioned under the salt crust. The Fenton reaction provides the conditions for the oxidation of OM by OH radicals and subsequent release of the oxidation products from the soil to the atmosphere with transition from the gas to the particulate phase. Additionaly, OH radicals may react with dissolved chloride to form reactive chlorine species Cl*, like Cl_2, HOCl, OCl^-, Cl_2^-, Cl radical, reacting with OM to form SOA precursors such as halogenated volatile organic carbons (VOX).

Organic matter (OM), stored under the salt crust is a potential electron donor for the reduction of oxygen to hydrogenperoxide (Voelker and Sulzberger, 1996; Voelker et al., 1997). In the presence of light, the electrons in the OM may be promoted to a higher energetic state from which they can be transferred to oxygen, forming oxygen radicals. Oxygen radicals are further reduced by iron forming with hydrogen ions (H^+), present in high extent in the liquid phase of acidic lakes, and hydrogen peroxide (H_2O_2). In a Fenton reaction, which is likely to happen in the liquid layer of the lakes, ferrous iron (Fe^{II}; Fe^{2+}) is oxidized by H_2O_2 to ferric iron (Fe^{III}; Fe^{3+}) under formation of a hydroxyl anion (HO^-) and OH radicals (cf. reaction (2); Cooper et al., 1988; Remucal and Sedlak, 2011; Haber and Weiss, 1932; Mazellier and Sulzberger, 2001):

$$Fe^{2+} + H_2O_2 \rightarrow Fe^{3+} + HO^- + OH^{\cdot} \qquad (2)$$

The OM in the aqueous phase can be oxidized by aqueous OH radicals, resulting from the Fenton reaction, which is expected to be one of the main mechanisms for their oxidation in the aqueous phase (Southworth and Voelker, 2003). Less-volatile organic products resulting from OH oxidation may lead to

SOA formation in the gas phase if the products are released from the aqueous phase. However, competitive effects of gas phase reactions and aqueous phase chemistry have the possibility to reduce SOA formation in the gas phase as observed by Chu et al. (2014) and Kamilli et al. (2015b). The reasons suggested for reducing already formed SOA mass are OH radicals breaking down the organic oxidation products at the wet surface of the SOA layer (Chu et al., 2014) and the decreasing availability of the organic precursor before further oxidation already in the aqueous phase (Kamilli et al., 2015b). The latter impact is supposed to arise from the formation of complexes consisting of organic compounds and irradiated iron (Voelker et al., 1997) and the chelating effect of specific organic compounds for Fe^{II} (Joshi et al., 2008).

Halogen activation

Beside direct oxidation of OM, the OH radicals in the aqueous phase may yield oxidants in the form of reactive halogen species. OH radicals from the Fenton reaction may react with dissolved chloride to form reactive chlorine species (Yu and Barker, 2003; Cl* in Fig. 5) after certain intermediate reactions (3a-3d).

$$OH^{\cdot} + Cl^{-} \rightarrow HOCl^{\cdot -} \rightarrow Cl^{\cdot} + OH^{-} \quad (3a)$$

$$Cl^{\cdot} + Cl^{-} \rightarrow Cl^{\cdot}_{2}^{-} \quad (3b)$$

OH radicals react with chloride to Cl radicals, which react with another Cl anion to form a Cl_2 radical anion (Anbar and Thomas, 1964; Jayson et al., 1973). Further, the Cl_2 radical anion may undergo self-reaction, or react with another Cl radical to form Cl_2 (Yu and Barker, 2003).

$$Cl^{\cdot}_{2}^{-} + Cl^{\cdot}_{2}^{-} \rightarrow 2\,Cl^{-} + Cl_2 \quad (3c)$$

$$Cl^{\cdot} + Cl^{\cdot}_{2}^{-} \rightarrow Cl^{-} + Cl_2 \quad (3d)$$

Ozone merging from the gas phase into the aqueous phase may also lead to the production of RHS in form of HOCl shown in reactions (4a-b).

$$O_3 + Cl^{-} \rightarrow ClO^{-} + O_2 \quad (4a)$$

$$ClO^{-} + H^{+} \rightarrow HOCl \quad (4b)$$

The resulting HOCl may subsequently react with dissolved chloride under acidic conditions resulting in molecular chlorine (Barcellos da Rosa, 2003), which is released into the gas phase. This pathway results in a release of RHS, which might oxidize SOA precursors in the gas phase (Ofner et al., 2013), as such molecular chlorine is photolyzed to chlorine radicals under the influence of radiation. The other possibility after reaction (4b) is the reaction of HOCl with the organic compounds in the aqueous phase (Fig. 5) to chlorinated organic matter (Cl–OM), which is released in form of VOX to the gas phase and might act as a SOA precursor.

Formation of Organosulfates

Another possible oxidant for SOA formation are sulfate radicals formed in the aqueous phase (Herrmann, 2003), e.g. in salt lakes (Kamilli et al., 2015b). Irradiated solutions that contain sulfate and organic compounds lead to organosulfate formation (Nozière et al. 2010), indicating a radical chemistry. In particular, the sulfate radical formation is induced by the photochemical reaction of OH radicals and bisulfate ions (HSO_4^-):

$$OH^{\cdot} + HSO_4^- \rightarrow SO^{\cdot}{}_4^- + H_2O \qquad (5)$$

The OH radicals may be produced by the Fenton reaction (Herrmann et al., 2005), photochemically by H_2O_2 (Warneck, 1999) or other processes, possibly involving organic compounds (Nozière et al. 2010).

For monoterpenes, like α-pinene and limonene, which are also present at salt lakes, the sulfate radical is added to the double bond, followed by the addition or oxidation by OH radicals and/or oxygen (Nozière et al. 2010). The formation of organosulfates with 1,8-cineole as parent compound has not been studied so far, but is expected to occur at a smaller rate compared to the oxidation by OH radicals, as it is the main oxidation pathway accompanied by H-abstraction and subsequent ring opening (Iinuma et al., 2009). Additionally, reaction (5) is reversible (Tang et al., 1988), so that SO_4 and OH radicals coexist, which supports the former line of reasoning. However, in Australian field samples a potential organosulfate ($C_{10}H_{17}O_9S$) derived from 1,8-cineole was identified (Kamilli et al., 2015a).

3.3 Chemical characterization of aerosol samples

Particles collected above the salt lakes with the Sioutas impactor and open-faced filter holders were analyzed subsequently for their chemical composition to validate the potential formation pathways presented in section 3.2 and in Kamilli et al. (2015b). Impactor samples in the size range between 250 nm and 10 µm were examined using chemical imaging and electron microscopy by a combination of Raman microscopy and scanning electron microscopy with energy-dispersive x-ray spectroscopy (SEM-EDX). Results obtained from these methods are not discussed here, but can be found in Kamilli et al. (2015a, b). The following discussion is based on results obtained from ultrahigh resolution mass spectrometry.

The loaded filters from the open filter holders were analyzed with ultrahigh resolution mass spectrometry without size segregation (Kamilli et al., 2015a, b). Due to limitations in the sampling method chemical information about the freshly nucleated particles were not in the direct focus of examination, but conclusions about the formation may be drawn anyway. The filters were analyzed for (oxygenated) organics (CHO), chlorinated organics (CHOCl), sulfur-containing organics (CHOS) and nitrogen-containing organics (CHON) for field and lab samples, respectively. In the van Krevelen diagrams (Fig. 6a, b left panel) the H/C and the O/C ratios for the identified compounds are shown. The associated average carbon oxidation state (OS_c) dependent on the carbon number (n_c) are depicted in Fig. 6a, b in the right panels.

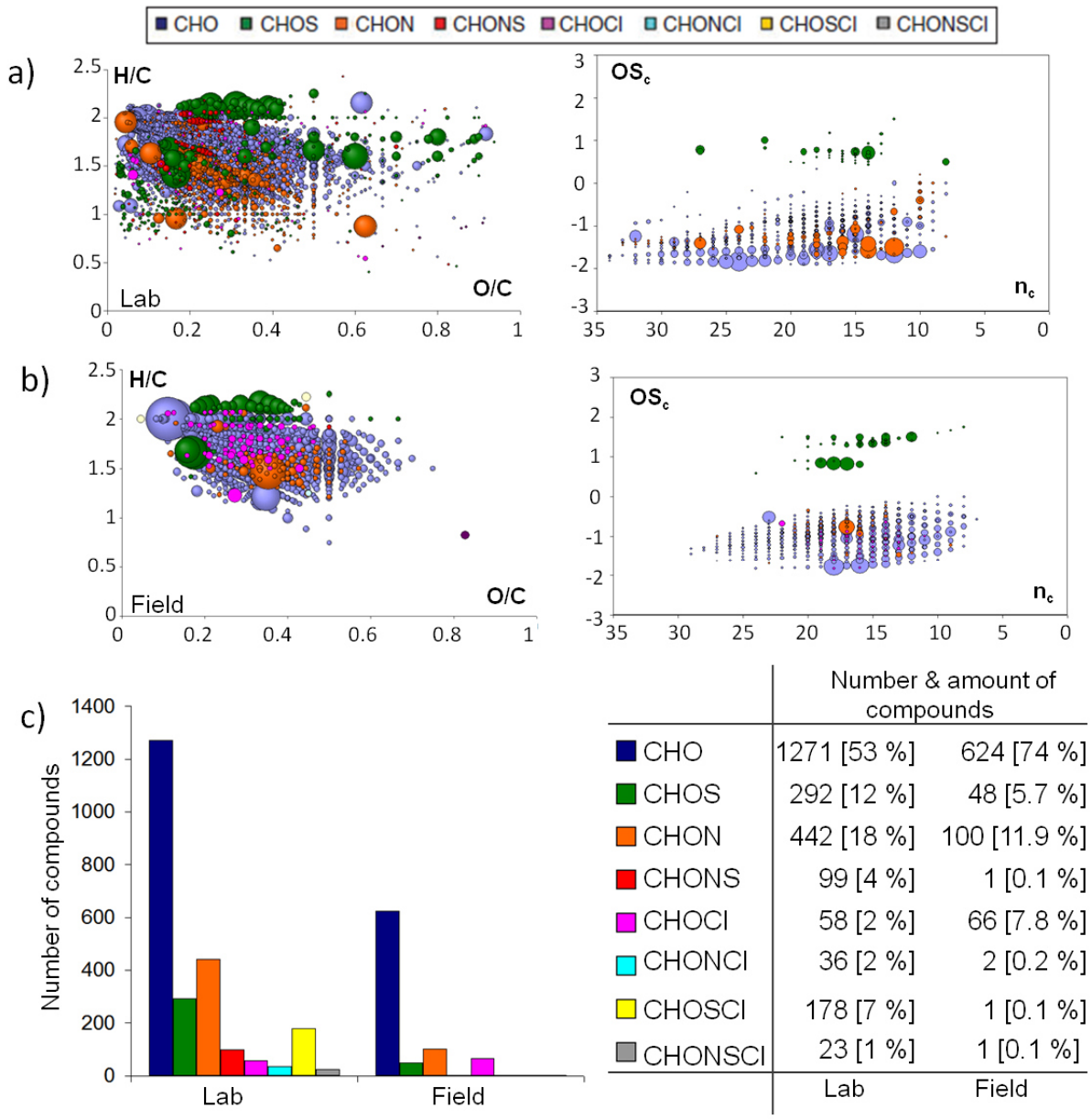

Figure 6 Van Krevelen diagrams of the ultrahigh resolution mass spectra (a, b left), and corresponding carbon oxidation states (a, b right) of filter samples taken during a lab experiment with the standard Fe (II) concentration (a) and in a field experiment at Lake Shot (b). The bubble size is proportional to the signal intensity in the mass spectra and the color code indicates the composition. The comparison of field and lab experiments regarding the number and total amount of compounds in percent is depicted in c).

For comparison, one lab sample with the normal amount of Fe^{II} in the salt lake mixture (Kamilli et al., 2015b), which is comparable to natural salt lake composition, is contrasted to a field sample taken at Lake Shot. Figure 6c shows the number of individual organic compounds found in both samples. It is obvious that in the lab sample, corresponding to a simulated salt lake, more individual compounds have been found, namely 2400 in contrast to about 850. Moreover, the compounds are more distributed in the

van Krevelen diagrams, particular the whole range of O/C ratios. More CHO compounds are identified at high H/C and low O/C ratio in the field than in the lab (Fig. 6a, b; left). Whereas in the field CHO compounds represent 2/3 of the total amount of organic compounds, they are about half of the compounds in the lab. The reason is the higher number of other compounds formed in the lab. The CHOS compounds with an O/C ratio below 0.4 are indeed similarly distributed in both samples, but in the lab CHOS compounds with higher O/C ratios are found. In contrast to the field sample, the lab sample exhibits not only more long-chained CHO compounds, but also those compounds might be oxidized by sulfur more often resulting in a higher number of CHOS compounds in the lab. An additional group of compounds nearly absent in the field are CHONS. Even if they are identified with low intensities in the lab, they are evenly distributed between O/C ratio 0.1 and 0.3 in the lab sample. A total amount of 4 % in the lab is contrasted with 0.1 % of CHONS compounds in the field. Also, in the lab sample CHON are identified more frequently and with higher intensities in the van Krevelen diagrams (Fig. 6a, b; left). The oxidation of CHO compounds by nitrogen appears to occur more often in the lab, as CHON compounds are found at an OS_c between -2 and 0 in a wide range of carbon numbers in the lab sample compared to only one distinct group of CHON compounds with 17 carbon atoms in the field sample (Fig. 6b; right). CHOCl is visible in the van Krevelen diagrams. Obviously, the oxidation by halogens occurs more often in the field than in the lab, since CHOCl compounds are more abundant in the field sample.

Examinations in laboratory experiments above a simulated salt lake mixture by Kamilli et al. (2015b) identified that the Fenton reaction has a direct effect on the formation of sulfur-containing and halogenated organic compounds, which is in agreement with section 3.2. Without iron-addition, the ultrahigh resolution mass spectra identified less chemical diversity in the aerosol particles (Fig. 7a, b; C3). With Fe^{II} in the salt lake mixture the amount of CHOS and halogenated organic compounds increased, respectively (Fig. 7a, b; C1). By enhancing the Fe^{II} concentration, the relative abundance of CHOS and halogenated organic compounds increased further, while the relative abundance of CHO compounds decreased (Fig. 7a, b; C2).

Kamilli et al. (2015b) suggested that the bond of Fe^{II} to the organic matter in the aqueous phase results in less release of organic compounds into the gas phase, and therefore leads to reduced formation of particulate matter with increasing Fe^{II} concentration. This assumption is supported by the observed complexing of organic compounds by irradiated iron oxide in Voelker et al. (1997) and the chelating properties of Fe^{II} and 1,8-cineole-containing oils (Joshi et al., 2008).

While halogenated organic compounds were not only identified in the aerosol samples with ultrahigh resolution mass spectrometry, but also with SEM-EDX, Raman spectroscopy in both the field and lab samples, a mixture of (oxygenated) organic, sulfur- and nitrogen-containing organic compounds seems to play a major role in new particle formation in the salt lake environments. Beside the important effect of organic species in NPF, the interplay with inorganically dominated coarse mode particles by coating of the salts could also be shown with Raman microscopy (Kamilli et al., 2015a).

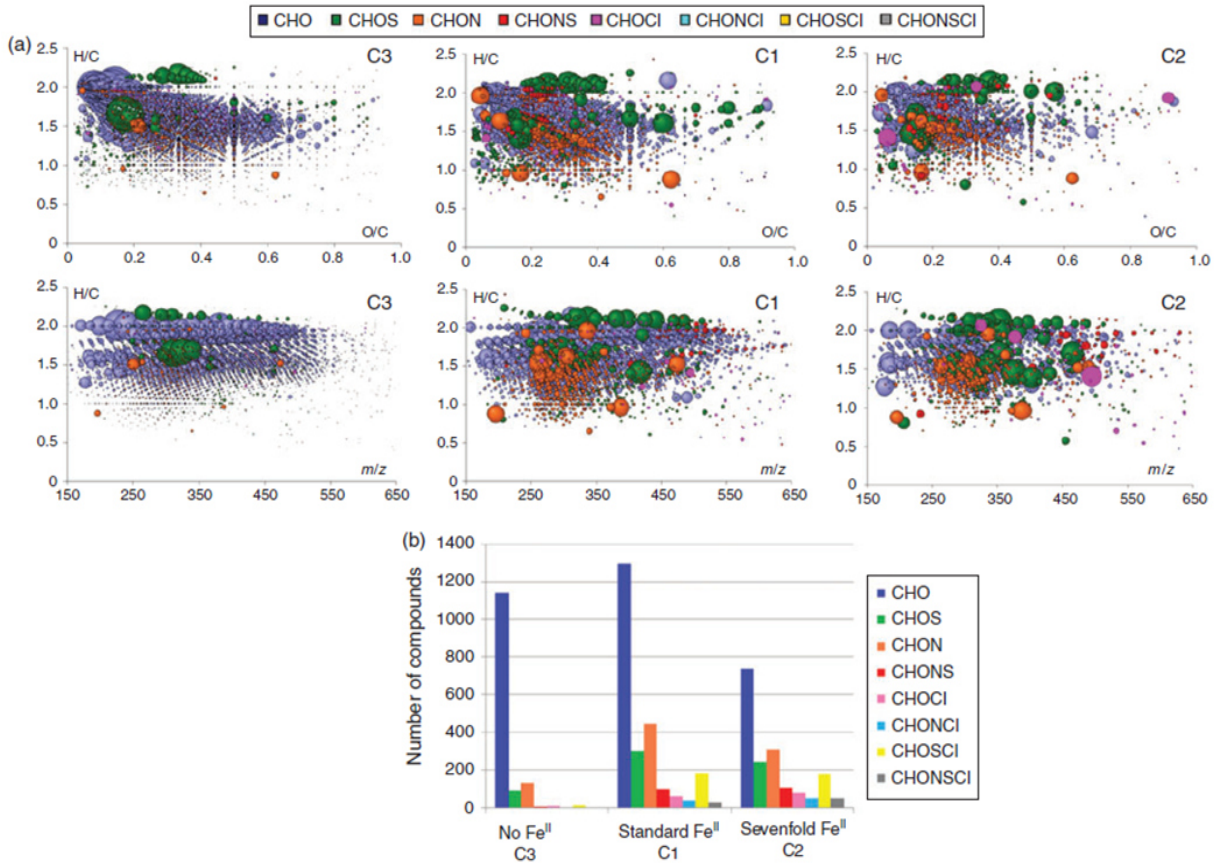

Figure 7 The increasing chemical diversity with increasing Fe^{II} concentration (C3 → C1 → C2) in the aerosol samples is depicted in a) Van Krevelen diagrams derived by ultrahigh resolution mass spectrometry and is summarized in b). The color code indicates the type of compositions and the bubble size corresponds to the signal intensity in the mass spectra. Kamilli et al. (2015b).

4 Conclusions and outlook

This thesis is mainly aimed at investigating NPF resulting from gaseous organic precursors in halogen-influenced environments. As a first approach, chamber experiments were conducted examining halogen oxidation of organic precursors and tracing the evolution of the chemical composition excluding other oxidation pathways (Ofner et al., 2013). Thereafter, an environment with increased halogen release was chosen for examination in the natural environment. The salt lake region in Western Australia fulfilled the requirements for halogen induced organic aerosol formation, and was therefore chosen for investigation (Kamilli et al., 2015a). Based on the field measurements, simulation experiments were conducted in the lab to specify the influencing factors on NPF in salt lake environments (Kamilli et al., 2015b).

Considering the four research questions of this work, the major conclusions are:

I Lab chamber experiments demonstrated the initiation of NPF by the interaction of halogens and an organic precursor. NPF was observed at atmospherically realistic mixing ratios of the precursor gases chlorine and α-pinene, with 5 ppb and 10 ppb, respectively (Ofner et al., 2013). Bromine induced organic aerosol formation did proceed in the lab chamber experiments, but is not expected to play an important role in the atmosphere. A bromine mixing ratio of 10 ppb and even higher needed to initiate NPF is unlikely in the atmosphere.

Experiments with precursor gas concentrations close to ambient conditions yielded organic aerosol masses of atmospheric relevance between 1-10 µg m^{-3}, as expected under heterogeneous conditions (McFiggans et al., 2013). Nevertheless, Ofner et al. (2013) showed that the formation of halogenated organic aerosol is possible from the gas phase from homogeneous nucleation at low precursor concentrations in the absence of ozone. In the atmosphere, halogens may be more involved in heterogeneous particle formation, as they lower the vapor pressure of the organic precursor less effectively than other oxidants (Kroll and Seinfeld, 2008).

II Filter samples taken at two Australian salt lakes, Lake Shot and Lake Dune, were examined with both Raman microscopy and ultrahigh resolution mass spectrometry. The single vibrational Raman spectrum of the organic particle layer of both lakes exhibits fundamental vibrations related to carbon-chlorine bonds. Also, in the characterization of the organic particle phase by ultrahigh resolution mass spectrometry, a contribution of chlorinated organics was identified. It was striking that the daytime sample collected at Lake Shot showed a higher intensity of CHOCl than the night-time sample collected at Lake Dune, which underlined the importance of photochemistry for the formation of CHOCl, and therefore the importance for the halogenation processes (Kamilli et al., 2015b).

III The simultaneous occurrence of gas and aqueous phases broadens the possible oxidation pathways for the organic precursor leading to NPF in the studied environments. Beside the halogen-induced aerosol formation, the particles formed by common SOA formation in the gas phase may be further oxidized in the aqueous phase (Bateman et al., 2011). The combination of low pH values, with high irradiation and the supply of reactive iron species enables the proceeding of the Fenton reaction in aqueous media (Krause et al., 2014; Southworth and Voelker, 2003). Clear indications for the occurrence of the Fenton reaction were found in lab chamber experiments simulating a salt lake environment (Kamilli et al., 2015b). The influence of varying Fe^{II} concentrations on the particle number concentration and chemical diversity indicated a coupling of aqueous phase chemistry and particle formation (Kamilli et al., 2015b). Due to the complexity of the natural system, the individual role of chemical processes could not be deduced. Nevertheless, there were hints for the proceeding of the Fenton reaction in natural salt lakes (Kamilli et al., 2015a). Aqueous phase chemistry also provides the possibility of organic precursor oxidation by sulfate radicals resulting in organosulfates (Nozière et al., 2010). Organosulfates were identified to contribute to the particulate matter both in the lab and in the field samples (Kamilli et al., 2015a, b).

IV While halogenated organic compounds were found in the aerosol samples, the formation of (oxygenated) organics, organosulfates and organonitrates that were identified with SEM-EDX, Raman spectroscopy, and mass spectrometry is proposed to control new particle formation in both study areas (Kamilli et al., 2015a, b). However the transformation of aged halogen-induced organic aerosol to common SOA in the aging process (Ofner et al., 2013) may have led to underestimating halogens in the particle formation process due to to the offline analysis.

This study gave an extensive physical and chemical characterization of organic particle formation in halogen-influenced environments. Especially in salt lake environments, the complex interaction of gas and aqueous phase chemistry was important for NPF. More studies have to be carried out to better understand the interactions between both media. The influence of initial conditions on the different formation pathways have to be assessed. Concerning the future, the area of halogen-influenced environments may grow due to the persistent salinization of soils (Williams, 1999), covering an area of already ~3.6 x 10^6 km² on a global scale (Stutz et al., 2002). Furthermore, the role of NPF from those environments might become more important. Increased NPF would lead to an enhanced number of CCNs with an impact on the future precipitation pattern and the climate of the Western Australian salt lake areas (Junkermann et al., 2009).

References

Anbar, M., and Thomas, J. K.: Pulse radiolysis studies of aqueous sodium chloride solutions, J. Phys. Chem., 68, 3829-3835, doi:10.1021/j100794a050, 1964.

Atkinson, R., and Arey, J.: Gas-phase tropospheric chemistry of biogenic volatile organic compounds: a review. Atmospheric Environment, 37, 197-219, 2003.

Barcellos da Rosa, M.: Untersuchungen heterogener troposphärenrelevanter Reaktionen von Schwefel- und Halogenverbindungen, PhD thesis, 2003.

Bateman, A. P., Nizkorodov, S. A., Laskin, J., and Laskin, A.: Photolytic processing of secondary organic aerosols dissolved in cloud droplets, Phys. Chem., 13, 12199–12212, 2011.

Benison, K. C., Bowen, B. B., Oboh-Ikuenobe, F. E., Jagniecki, E. A., LaClair, D. A., Story, S. L., Mormile, M. R., and Hong, B. Y.: Sedimentology of acid saline lakes in southern Western Australia: newly described processes and products of an extreme environment, Journal of Sedimentary Research, 77(5), 366-388, 2007.

Bowen, B. B., and Benison, K. C.: Geochemical characteristics of naturally acid and alkaline saline lakes in southern Western Australia, Appl. Geochem., 24, 268–284, doi:10.1016/j.apgeochem.2008.11.013, 2009.

Boy, M., and Kulmala, M.: Nucleation events in the continental boundary layer: Influence of physical and meteorological parameters, Atmos. Chem. Phys., 2, 1-16, 2002.

Buxmann, J., Balzer, N., Bleicher, S., Platt, U., and Zetzsch, C.: Observations of bromine explosions in smog chamber experiments above a model salt pan, Int. J. Chem. Kinet., 44, 312-326, 2012.

Cai, X., and Griffin, R. J.: Secondary aerosol formation from the oxidation of biogenic hydrocarbons by chlorine atoms, Journal of Geophysical Research: Atmospheres (1984–2012), 111, D14206, 2006.

Cai, X., Ziemba, L. D., and Griffin, R. J.: Secondary aerosol formation from the oxidation of toluene by chlorine atoms, Atmospheric Environment, 42(32), 7348-7359, 2008.

Calogirou, A., Larsen, B. R., and Kotzias, D.: Gas-phase terpene oxidation products: a review, Atmospheric Environment, 33(9), 1423-1439, 1999.

Carlton, A. G., Turpin, B. J., Lim, H.-J., Altieri, K. E., and Seitzinger, S.: Link between isoprene and secondary organic aerosol (SOA): Pyruvic acid oxidation yields low volatility organic acids in clouds, Geophys. Res. Lett., 33, L06822, 2006.

Carslaw, K. S., Boucher, O., Spracklen, D. V., Mann, G. W., Rae, J. G. L., Woodward, S., and Kulmala, M.: A review of natural aerosol interactions and feedbacks within the Earth system, Atmos. Chem. Phys., 10, 1701-1737, doi:10.5194/acp-10-1701-2010, 2010.

Cerqueira, M. A., Pio, C. A., Gomes, P. A., Matos, J. S., and Nunes, T. V.: Volatile organic compounds in rural atmospheres of central Portugal, Science of The Total Environment, 313(1), 49-60, 2003.

Chu, B., Liu, Y., Li, J., Takekawa, H., Liggio, J., Li, S.-M., Jiang, J., Hao, J., and He, H.: Decreasing effect and mechanism of $FeSO_4$ seed particles on secondary organic aerosol in a-pinene photooxidation, Environ. Pollut., 193, 88, doi:10.1016/J.ENVPOL.2014.06.018, 2014.

Cooper, W. J., Zika, R. G., Petasne, R. G., and Plane, J. M. C.: Photochemical formation of hydrogen peroxide in natural waters exposed to sunlight, Environ. Sci. Technol., 22, 1156–1160, 1988.

Corchnoy, S. B., and Atkinson, R.: Kinetics of the gas-phase reactions of hydroxyl and nitrogen oxide (NO3) radicals with 2-carene, 1,8-cineole, p-cymene, and terpinolene, Environ. Sci. Technol., 24(10), 1497-1502, 1990.

George, I. J., and Abbatt, J. P. D.: Heterogeneous oxidation of atmospheric aerosol particles by gas-phase radicals, Nature Chemistry, 2(9), 713-722, 2010.

Geron, C., Owen, S., Guenther, A., Greenberg, J., Rasmussen, R., Bai, J. H., Li, Q. J., and Baker, B.: Volatile organic compounds from vegetation in southern Yunnan Province, China: Emission rates and some potential regional implications, Atmospheric Environment, 40(10), 1759-1773, 2006.

Goldstein, A. H., and Galbally, I. E.: Known and unexplored organic constituents in the earth's atmosphere, Environ. Sci. Technol., 41, 1514–1521, 2007.

Guenther, A., Hewitt, C. N., Erickson, D., Fall, R., Geron, C., Graedel, T., Harley, P., Klinger, L., Lerdau, M., Mckay, W. A., Pierce, T., Scholes, B., Steinbrecher, R., Tallamraju, R., Taylor, J., and Zimmerman, P.: A global model of natural volatile organic compound emissions, Journal of Geophysical Research: Atmospheres (1984–2012), 100(D5), 8873-8892, 1995.

Guenther, A., Geron, C., Pierce, T., Lamb, B., Harley, P., and Fall, R.: Natural emissions of non-methane volatile organic compounds, carbon monoxide, and oxides of nitrogen from North America, Atmospheric Environment, 34 (12-14), 2205-2230, 2000.

Guenther, A. B., Jiang, X., Heald, C. L., Sakulyanontvittaya, T., Duhl, T., Emmons, L. K., and Wang, X.: The Model of Emissions of Gases and Aerosols from Nature version 2.1 (MEGAN2. 1): an extended and updated framework for modeling biogenic emissions, Geoscientific Model Development, 5, 1471–1492, 2012.

Haber, F., and Weiss, J.: Über die Katalyse des Hydroperoxydes, Naturwissenschaften, 20, 948–950, 1932.

Hallquist, M., Wenger, J. C., Baltensperger, U., Rudich, Y., Simpson, D., Claeys, M., Dommen, J., Donahue, N. M., George, C., Goldstein, A. H., Hamilton, J. F., Herrmann, H., Hoffmann, T., Iinuma, Y., Jang, M., Jenkin, M. E., Jimenez, J. L., Kiendler-Scharr, A., Maenhaut, W., McFiggans, G., Mentel, Th. F., Monod, A., Prévôt, A. S. H., Seinfeld, J. H., Surratt, J. D., Szmigielski, R., and Wildt, J.: The formation, properties and impact of secondary organic aerosol: current and emerging issues, Atmos. Chem. Phys., 9, 5155-5236, doi:10.5194/acp-9-5155-2009, 2009.

Herrmann, H.: Kinetics of aqueous phase reactions relevant for atmospheric chemistry, Chem. Rev., 103, 4691–4716, doi:10.1021/cr020658q, 2003.

Herrmann, H., Tilgner, A., Barzaghi, P., Majdik, Z., Gligorovski, S., Poulain, L., and Monod, A.: Towards a more detailed description of tropospheric aqueous phase organic chemistry: CAPRAM 3.0, Atmos. Environ., 39, 4351–4363, 2005.

Hoffmann, T., Odum, J. R., Bowman, F., Collins, D., Klockow, D., Flagan, R. C., and Seinfeld, J. H.: Formation of organic aerosols from the oxidation of biogenic hydrocarbons, Journal of Atmospheric Chemistry, 26(2), 189-222, 1997.

Iinuma, Y., Böge, O., Keywood, M., Gnauk, T., and Herrmann, H.: Diaterebic Acid Acetate and Diaterpenylic Acid Acetate: Atmospheric Tracers for Secondary Organic Aerosol Formation from 1,8-Cineole Oxidation, Environ. Sci. Technol., 43 (2), 280-285, 2009.

Intergovernmental Panel on Climate Change (IPCC): Climate Change 2007: The Physical Science Basis, Cambridge University Press, UK, 2007.

Intergovernmental Panel on Climate Change (IPCC): Climate Change 2013: The Physical Science Basis. Contribution of Working Group I to the Fifth Assessment Report of the Intergovernmental Panel on Climate Change, Cambridge University Press, Cambridge, United Kingdom and New York, NY, USA, 1535 pp, doi:10.1017/CBO9781107415324, 2013.

Jayson, G. G., Parsons, B. J., and Swallow, A. J.: Some simple, highly reactive, inorganic chlorine derivatives in aqueous solution. Their formation using pulses of radiation and their role in the mechanism of the Fricke dosimeter, J. Chem. Soc. Farad. T. 1, 69, 1597-1607, doi:10.1039/F19736901597, 1973.

Joshi, S., Chanotiya, C. S., Agarwal, G., Prakash, O., Pant, A. K., and Mathela, C. S.: Terpenoid Compositions, and Antioxidant and Antimicrobial Properties of the Rhizome Essential Oils of Different Hedychium Species, Chemistry & Biodiversity, 5, 299–309, 2008.

Junkermann, W., Hacker, J., Lyons, T., and Nair, U.: Land use change suppresses precipitation, Atmos. Chem. Phys., 9, 6531–6539, 2009.

Kamilli, K. A., Ofner, J., Krause, T., Sattler, T., Schmitt-Kopplin, P., Eitenberger, E., Friedbacher, G., Lendl, B., Lohninger, H., Schöler, H. F., and Held, A.: New particle formation induced by Western Australian salt lakes, to be submitted, 2015a.

Kamilli, K. A., Ofner, J., Lendl, B., Schmitt-Kopplin, P., and Held, A.: New particle formation above a simulated salt lake in aerosol chamber experiments, Environmental Chemistry, 12, 489, doi:10.1071/EN14225, 2015b.

Kanakidou, M., Seinfeld, J. H., Pandis, S. N., Barnes, I., Dentener, F. J., Facchini, M. C., Van Dingenen, R., Ervens, B., Nenes, A., Nielsen, C. J., Swietlicki, E., Putaud, J. P., Balkanski, Y., Fuzzi, S., Horth, J., Moortgat, G. K., Winterhalter, R., Myhre, C. E. L., Tsigaridis, K., Vignati, E., Stephanou, E. G., and Wilson, J.: Organic aerosol and global climate modelling: a review, Atmos. Chem. Phys., 5, 1053-1123, 2005.

Kavouras, I. G., Mihalopolous, N., and Stephanou, E. G.: Formation of atmospheric particles from organic acids produced by forests, Nature, 395, 683–686, 1998.

Kavouras, I. G., Mihalopoulos, N., and Stephanou, E. G.: Secondary organic aerosol formation vs primary organic aerosol emission: In situ evidence for the chemical coupling between monoterpene acidic photooxidation products and new particle formation over forests, Environ. Sci. Technol., 33(7), 1028-1037, 1999.

Kiendler-Scharr, A., Wildt, J., Dal Maso, M., Hohaus, T., Kleist, E., Mentel, T. F., Tillmann, R., Uerlings, R., Schurr, U., and Wahner, A.: New particle formation in forests inhibited by isoprene emissions, Nature, 461(7262), 381-384, 2009.

Krause, T., Tubbesing, C., Benzing, K., and Schöler, H. F.: Model reactions and natural occurrence of furans from hypersaline environments, Biogeosciences, 11, 2871-2882, 2014.

Kroll, J. H., and Seinfeld, J. H.: Chemistry of secondary organic aerosol: Formation and evolution of low-volatility organics in the atmosphere, Atmospheric Environment, 42(16), 3593-3624, 2008.

Kulmala, M., Vehkamäki, H., Petäjä, T., Dal Maso, M., Lauri, A., Kerminen, V.-M., Birmili, W., and McMurry, P. H.: Formation and growth rates of ultrafine atmospheric particles: a review of observations, Journal of Aerosol Science, 35 (2), 143-176, 2004.

Laaksonen, A., Kulmala, M., O'Dowd, C. D., Joutsensaari, J., Vaattovaara, P., Mikkonen, S., Lehtinen, K. E. J., Sogacheva, L., Dal Maso, M., Aalto, P., Petäjä, T., Sogachev, A., Yoon, Y. J., Lihavainen, H., Nilsson, D., Facchini, M. C., Cavalli, F., Fuzzi, S., Hoffmann, T., Arnold, F., Hanke, M., Sellegri, K., Umann, B., Junkermann, W., Coe, H., Allan, J. D., Alfarra, M. R., Worsnop, D. R., Riekkola, M. -L., Hyötyläinen, T., and Viisanen, Y.: The role of VOC oxidation products in continental new particle formation, Atmos. Chem. Phys., 8, 2657-2665, 2008.

Lim, Y. B., Tan, Y., Perri, M. J., Seitzinger, S. P., and Turpin, B. J.: Aqueous chemistry and its role in secondary organic aerosol (SOA) formation, Atmos. Chem. Phys., 10, 10521-10539, 2010.

Mäkelä, J. M., Aalto, P., Jokinen, V., Pohja, T., Nissinen, A., Palmroth, S., Markkanen, T., Seitsonen, K., Lihavainen, H., and Kulmala, M.: Observations of ultrafine aerosol particle formation and growth in boreal forest, Geophysical Research Letters, 24(10), 1219-1222, 1997.

Mazellier, P., and Sulzberger, B.: Diuron degradation in irradiated, heterogeneous iron/oxalate systems: The rate-determining step, Environ. Sci. Technol., 35, 3314, 2001.

McFiggans, G., Lewis, A., Reid, J., Kiendler-Scharr, A., and Herrmann, H.: Tropospheric Aerosol-Formation, Transformation, Fate and Impacts, Faraday Discussions, 165, 151-179, doi: 10.1039/C3FD90032K, 2013.

Muik, B., Lendl, B., Molina-Diaz, A., Valcarcel, M., and Ayora-Cañada, M. J.: Two-dimensional correlation spectroscopy and multivariate curve resolution for the study of lipid oxidation in edible oils monitored by FTIR and FT-Raman spectroscopy, Analytica chimica acta, 593(1), 54-67, 2007.

Ng, N. L., Kroll, J. H., Keywood, M. D., Bahreini, R., Varutbangkul, V., Flagan, R. C., Seinfeld, J. H., Lee, A., and Goldstein, A. H.: Contribution of first-versus second-generation products to secondary organic aerosols formed in the oxidation of biogenic hydrocarbons, Environ. Sci. Technol., 40(7), 2283-2297, 2006.

Noda, I.: Generalized two-dimensional correlation method applicable to infrared, Raman, and other types of spectroscopy, Appl. Spectrosc, 47(9), 1329-1336, 1993.

Noda, I., Dowrey, A. E., Marcott, C., Story, G. M., and Ozaki, Y.: Generalized two-dimensional correlation spectroscopy, Appl. Spectrosc, 54(7), 236A-248A, 2000.

Nozière, B., Ekström, S., Alsberg, T., and Holmström, S.: Radical-initiated formation of organosulfates and surfactants in atmospheric aerosols, Geophys. Res. Lett., 37, L05806, 2010.

Nunes, T. V., and Pio, C. A.: Emission of volatile organic compounds from Portuguese eucalyptus forests, Chemosphere - Global Change Science, 3(3), 239-248, 2001.

O'Dowd, C. D., Aalto, P., Hmeri, K., Kulmala, M., and Hoffmann, T.: Aerosol formation: Atmospheric particles from organic vapours, Nature, 416(6880), 497-498, 2002.

Odum, J. R., Hoffmann, T., Bowman, F., Collins, D., Flagan, R. C., and Seinfeld, J. H.: Gas/particle partitioning and secondary organic aerosol yields, Environ. Sci. Technol., 30, 2580-85, 1996.

Odum, J. R., Jungkamp, T. P. W., Griffin, R. J., Forstner, H. J. L., Flagan, R. C., and Seinfeld, J. H.: Aromatics, reformulated gasoline, and atmospheric organic aerosol formation, Environ. Sci. Technol., 31, 1890-97, 1997.

Ofner, J., Balzer, N., Buxmann, J., Grothe, H., Schmitt-Kopplin, P., Platt, U. and Zetzsch, C.: Halogenation processes of secondary organic aerosol and implications on halogen release mechanisms, Atmos. Chem. Phys., 12(13), 5787–5806, doi:10.5194/acp-12-5787-2012, 2012.

Ofner, J., Kamilli, K. A., Held, A., Lendl, B., and Zetzsch, C.: Halogen-induced organic aerosol (XOA): a study on ultra-fine particle formation and time-resolved chemical characterization, Faraday discussions, 165, 135-149, 2013.

Pandis, S. N., Harley, R. A., Cass, G. R., and Seinfeld, J. H.: Secondary organic aerosol formation and transport, Atmospheric Environment. Part A. General Topics, 26(13), 2269-2282, 1992.

Pandis, S. N., Wexler, A. S., and Seinfeld, J. H.: Secondary organic aerosol formation and transport–II. Predicting the ambient secondary organic aerosol size distribution, Atmospheric Environment. Part A. General Topics, 27(15), 2403-2416, 1993.

Pöschl, U.: Atmospheric Aerosols: Composition, Transformation, Climate and Health Effects, Angew. Chem. Int. Edit., 44, 7520–7540, 2005.

Remucal, C. K., and Sedlak, D. L.: The Role of iron coordination in the production of reactive oxidants from ferrous iron oxidation by oxygen and hydrogen peroxide, Aquatic Redox Chemistry (ACS Symposium Series), 1071, 177–197, 2011.

Riipinen, I., Pierce, J. R., Yli-Juuti, T., Nieminen, T., Häkkinen, S., Ehn, M., Junninen, H., Lehtipalo, K., Petäjä, T., Slowik, J., Chang, R., Shantz, N. C., Abbatt, J., Leaitch, W. R., Kerminen, V.-M., Worsnop, D. R., Pandis, S. N., Donahue, N. M., and Kulmala, M.: Organic condensation: a vital link connecting aerosol formation to cloud condensation nuclei (CCN) concentrations, Atmos. Chem. Phys., 11, 3865–3878, 2011.

Ristovski, Z. D., Suni, T., Kulmala, M., Boy, M., Meyer, N. K., Duplissy, J., Turnipseed, A., Morawska, L., and Baltensperger, U.: The role of sulphates and organic vapours in growth of newly formed particles in a eucalypt forest, Atmospheric Chemistry and Physics, 10(6), 2919-2926, 2010.

Seinfeld, J. H., and Pandis, S. N.: Atmospheric Chemistry and Physics: From Air Pollution to Climate Change, 2nd edition, J. Wiley, New York, 2006.

Seinfeld, J. H., and Pankow, J. F.: Organic atmospheric particulate material, Annual Review of Physical Chemistry, 54(1), 121-140, 2003.

Southworth, B. A., and Voelker, B. M.: Hydroxyl radical production via the photo-Fenton reaction in the presence of fulvic acid, Environ. Sci. Technol., 37, 1130–1136, 2003.

Spracklen, D. V., Bonn, B., and Carslaw, K. S.: Boreal forests, aerosols and the impacts on clouds and climate, Philosophical Transactions of the Royal Society A: Mathematical, Physical and Engineering Sciences, 366(1885), 4613-4626, 2008.

Stutz, J., Ackermann, R., Fast, J. D., and Barrie, L.: Atmospheric reactive chlorine and bromine at the Great Salt Lake, Utah, Geophys. Res. Lett., 29, 18-11–18-14, 2002.

Tang, Y., Thorn, R. P., Mauldin III, R. L., and Wine, P. H.: Kinetics and spectroscopy of the SO_4 – radical in aqueous solution, J. Photochem. Photobiol. A, 44, 243–258, doi:10.1016/1010-6030(88)80097-2, 1988.

Voelker, B. M., and Sulzberger, B.: Effects of fulvic acid on Fe (II) oxidation by hydrogen peroxide, Environ. Sci. Technol., 30, 1106-1114, 1996.

Voelker, B. M., Morel, F. M. M., and Sulzberger, B.: Iron Redox Cycling in Surface Waters: Effects of Humic Substances and Light, Environ. Sci.Technol., 31, 1004-1011, 1997.

Warneck, P.: The relative importance of various pathways for the oxidation of sulfur dioxide and nitrogen dioxide in sunlit continental fair weather clouds, Phys. Chem. Chem. Phys., 1, 5471-5483, 1999.

Went, F. W.: Blue hazes in the atmosphere, Nature 187, 641–643, 1960.

Williams, W. D.: Salinisation: a major threat to water resources in the arid and semi-arid regions of the world, Lakes Reservoirs: Res. Manage, 4, 85, 1999.

Winters, A. J., Adams, M. A., Bleby, T. M., Rennenberg, H., Steigner, D., Steinbrecher, R., and Kreuzwieser, J.: Emissions of isoprene, monoterpene and short-chained carbonyl compounds from Eucalyptus spp. in southern Australia, Atmos. Environ., 43, 3053–3043, 2009.

Yu, X.-Y., and Barker, J. R.: Hydrogen peroxide photolysis in acidic aqueous solutions containing chloride ions. I. Chemical mechanism, J. Phys. Chem. A, 107(9), 1313-1324, 2003.

Individual contribution to the included manuscripts

Ofner, J., **Kamilli, K. A.**, Held, A., Lendl, B., and Zetzsch, C.: **Halogen-induced organic aerosol (XOA): A study on ultra-fine particle formation and time-resolved chemical characterization**, Faraday Discussions, doi:10.1039/C3FD00093A, 2013.

The preparation and conduction of the laboratory measurements were made in collaboration with J. Ofner in equal shares. The research idea was discussed within all co-authors. The analysis of SMPS data and conjunction with GC-FID data for calculation of the SOA formation potential was performed by myself. The interpretation of particle data was largely my work. A. Held and J. Ofner helped in interpreting the obtained particle data. I took an active part in discussing the cumulative results, writing and editing the manuscript. The main part of the manuscript was written by J. Ofner. The result part "halogen-induced ultra-fine particle formation" was written by myself and edited by A. Held. A. Held, B. Lendl and C. Zetzsch helped in editing the entire manuscript.

Kamilli, K. A., Ofner, J., Lendl, B., Schmitt-Kopplin, P., and Held, A.: **New particle formation above a simulated salt lake in aerosol chamber experiments**, Environmental Chemistry, 12, 489, doi:10.1071/EN14225, 2015.

All different parts of the laboratory experiments were conducted by myself together with J. Ofner in series C and partly A, together with a master student in parts of measurement series A and with support of one bachelor student in series B. All SMPS data processing and analysis was performed by myself. The manuscript was mainly written by myself. J. Ofner and P. Schmitt-Kopplin supplied the data and interpretation of aerosol chemical information and wrote the main paragraph "aerosol chemical information" in the manuscript and helped in editing the manuscript. A. Held gave support in conducting the measurements, interpreting the data, discussing the results and writing the manuscript. B. Lendl helped in editing the manuscript.

Kamilli, K. A., Ofner, J., Krause, T., Sattler, T., Schmitt-Kopplin, P., Atlas, E., Eitenberger, E., Friedbacher, G., Lendl, B., Lohninger, H., Schöler, H. F., and Held, A.: **New particle formation induced by Western Australian salt lakes**, to be submitted 2015.

Field measurement preparation, the performance on-site and the data analysis of the DMPS system was conducted by myself. The manuscript was written by myself with exception of the Raman and SEM-EDX hyperspectral imaging part in the paragraph "chemical characterization of aerosol samples", written by J. Ofner. P. Schmitt-Kopplin, E. Eitenberger, G. Friedbacher, B. Lendl, H. Lohninger and J. Ofner supplied chemical analyses of the particle data and helped editing the manuscript. T. Krause and H. F. Schöler took gas samples during the field measurements and helped editing the manuscript. T. Sattler provided the analyzed VOC data and helped editing the manuscript. A. Held helped to prepare the field campaign, conduct the measurements, helped to interpret the data, discussed the results and helped in writing the manuscript. E. Atlas provided the multi-detector GC/MSD/FID/ECD instrument for the analyses of the canister samples.

Appendix I

Halogen-induced organic aerosol (XOA): A study on ultra-fine particle formation and time-resolved chemical characterization

Johannes Ofner,*[a] Katharina A. Kamilli[b], Andreas Held[b], Bernhard Lendl[a] and Cornelius Zetzsch[c]

DOI: 10.1039/c3fd00093a

[a] *Institute of Chemical Technologies and Analytics, Environmental and Process Analytics Division, Vienna University of Technology, Getreidemarkt 9, 1060 Vienna, Austria; E-mail: johannes.ofner@tuwien.ac.at*
[b] *Junior Professorship in Atmospheric Chemistry, University of Bayreuth, Dr. Hans-Frisch-Strasse 1-3, 95448 Bayreuth, Germany*
[c] *Atmospheric Chemistry Research Laboratory, University of Bayreuth, Dr. Hans-Frisch-Strasse 1-3, 95448 Bayreuth, Germany*

The concurrent presence of high values of organic SOA precursors and reactive halogen species (RHS) at very low ozone concentrations allows the formation of halogen-induced organic aerosol, so-called XOA, in maritime areas where high concentrations of RHS are present, especially at sunrise. The present study combines aerosol smog-chamber and aerosol flow-reactor experiments for the characterization of XOA. XOA formation yields at low and high concentrations of chlorine as reactive halogen species (RHS) were determined using a 700 L aerosol smog-chamber with a solar simulator. The chemical transformation of the organic precursor during the aerosol formation process and chemical aging was studied using an aerosol flow-reactor coupled to an FTIR spectrometer. The FTIR dataset was analysed using 2D correlation spectroscopy. Chlorine induced homogeneous XOA formation takes place at even 2.5 ppb of molecular chlorine, which was photolysed by the solar simulator. The chemical pathway of XOA formation is characterized by the addition of chlorine and abstraction of hydrogen atoms, causing simultaneous carbon chlorine bond formation. During further steps of the formation process, carboxylic acids are formed, which cause a SOA-like appearance of XOA. During the ozone-free formation of secondary organic aerosol with RHS a special kind of particulate matter (XOA) is formed which is afterwards transformed to SOA by atmospheric aging or degradation pathways.

1 Introduction

Secondary organic aerosol (SOA) formation is currently mainly discussed pertaining to reactions of common atmospheric trace-gases like OH, O_3 and NO_x with a large variety of organic precursors. A review by Kroll and Seinfeld[1] summarizes this common understanding of SOA formation initiated by gas-phase oxidation and followed by particle-phase reactions involving the above mentioned atmospheric reactants. The evolution of organic aerosols in the atmosphere and the chemical transformation to aged organic aerosol is generally related to the presence of OH radicals or ozone[2].

Recently, Riipinen et al.[3] proposed that the condensation of low-volatility vapours and the formation of organic salts dominate the first steps in growths of ultra-fine organic particles. Over the open ocean and in marine environments, organic precursor gases such as volatile halocarbons are thought to contribute to marine aerosol formation[4,5].

Apart from this general approach towards SOA formation with a major contribution of ozone and OH radicals, a few publications cover the topic of halogen-induced formation of SOA. The kinetics of the gas-phase reaction of monoterpenes with atomic chlorine have been studied e.g. by Timerghazin and Ariya[6], implying higher reaction rates of chlorine with selected monoterpenes compared to the OH-initiated reaction. They called for further research of the possible impact on the chlorine-initiated oxidation related to aerosol formation. For chlorine-induced aerosol formation from toluene with chlorine and toluene concentrations in the range of several 10^{16} molecules cm^{-3}, particle concentrations up to $3.5x10^{8}$ cm^{-3} are reported[7]. Cai and Griffin[8] report the formation of halogen-induced SOA from different monoterpenes by chlorine atoms using an aerosol smog-chamber. These authors state that the chlorine-induced SOA formation is generally comparable to other scenarios and conclude that the chlorine-initiated oxidation of monoterpenes could be a source of SOA at sunrise. A similar study by these authors arrives at the same conclusion for the chlorine-initiated oxidation of toluene[9]. Kroll and Seinfeld[1] mention the chlorine-initiated SOA formation but conclude that it has a smaller effect on the vapour pressure than caused by OH radicals. A physico-chemical characterization of organic aerosol model substances, processed by reactive halogen species (RHS), considering the difference between halogen-induced organic aerosol and pre-existing SOA, which is processed by RHS during the period of photochemical aging is given by Ofner et al.[10]. This study concludes a similar way of interaction of halogens with organic precursors as found by Kroll et al.[11]. Other halogen species containing bromine and iodine are also suspected to significantly contribute to aerosol formation and processing[12,13,14]. Lifetimes of monoterpenes can be significantly influenced by halogens at dawn, where the reaction of chlorine atoms becomes comparable to the reaction with OH radicals[15].

Halogen-induced organic aerosol formation is strongly dependent on the available concentration of RHS. RHS represent an abundant class of atmospheric oxidants in maritime areas. The importance of chlorine atoms as a tropospheric oxidant in the marine boundary layer was discussed in 1993[16], concluding that the photochemical oxidation of organics by chlorine could exceed the importance of OH under special conditions. Unexpectedly high chlorine concentrations are reported by Spicer et al.[17]. These authors report Cl_2 mixing ratios between 10 and 150 ppt and conclude that an unknown chlorine source must exist, which produces up to 330 ppt Cl_2 per day. A recent review summarizes very high chlorine mixing ratios[18]: 200 ppt for Cl_2, up to 421 ppt for Cl_2 and HOCl, 5.6 ppb for HCl and up to 2.1 ppb for $ClNO_2$. Different sources of RHS are reported in the scientific literature. Early smog-chamber experiments expected a possible release of molecular chlorine by homogeneous and heterogeneous reactions of different halogen sources like salts or acids[19]. The heterogeneous tropospheric chemistry of sea salt aerosol is known as an important source of RHS to the marine boundary layer[20]. The formation of $ClNO_2$ in the night-time and photolysis to Cl radicals and NO_2 during sunrise is reported as a large atomic chlorine source[21].

The abundance of RHS in the marine boundary layer could contribute significantly to organic aerosol formation, especially at dawn and sunrise, when night-time reservoir substances are photolysed and ozone levels are still low. The present study reports aerosol-formation experiments from α-pinene with chlorine atoms. Furthermore, the chemical transformation of the organic precursor was studied using

an aerosol-flow reactor coupled to an FTIR spectrometer and interpreted using 2D correlation spectroscopy[22] to obtain synchronous and asynchronous sequential mechanistic information.

2 Methods

Aerosol smog-chamber setup and experiments

Aerosol formation experiments were performed using a 700 L aerosol smog-chamber. Details on this chamber can be found at Ofner et al.[23]. The smog chamber is equipped with a solar simulator (Osram, HMI, 4000 W). NO_2 actinometry, as reported by Bohn et al.[24], was used to determine the spectral actinic flux, which is shown in Fig. 1 and compared to the solar actinic flux at the Mediterranean Sea in summer. This solar actinic flux was calculated using the STARsci v2.1 software package[25]. The solar simulator allows simulating a comparable solar spectrum compared to the Mediterranean Sea in summer (Fig. 1). Based on the measurement of the spectral actinic flux, the photolysis of molecular chlorine was calculated inside the aerosol smog-chamber with a photolysis rate of $j_{Cl2} = 1.89 \cdot 10^{-3}$ s^{-1}.

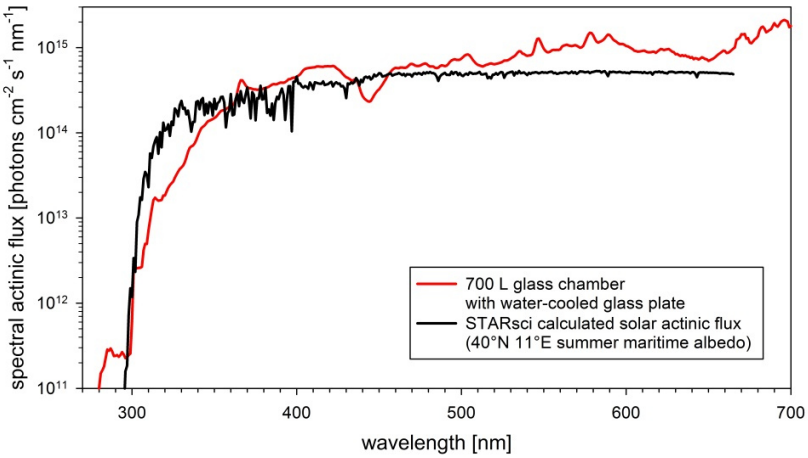

Fig. 1 Spectral actinic flux of the solar simulator of the aerosol smog-chamber compared to the solar actinic flux at the Mediterranean Sea in summer (calculated using STARsci v2.1[25]).

Before the experiments, the chamber was flushed with purified zero-air to avoid contamination of the chamber with aerosols or organic trace gases[23]. Zero air was also used to keep the pressure inside the chamber above ambient conditions during the experiments. Therefore, all experimental data were corrected for dilution and wall-loss. Background measurements determined a dilution rate for the organic precursor of $3.2 \cdot 10^{-3}$ min^{-1}. Ozone concentrations were measured using a chemiluminescence ozone analyser (Bendix-UPK8002; Bad Nauheim, Germany), exhibiting photolytic formed ozone concentrations below 10 ppb. NO_2 and NO concentrations were monitored using a CLD-700-Al analyser (Ecophysics, Dürnten, Switzerland) to ensure low-NO_x conditions (below 10 ppb). A GC-FID system with an RTX resin column and a homemade cryostatic preconcentrator was applied to measure the decay of the organic precursor with a temporal resolution of 10 minutes. The aerosol number and size distribution was measured using a custom-built SMPS (IfT Leipzig, Germany) coupled to a TSI

3772 condensation particle counter (TSI, Shoreview, MN, USA). The aerosol mass formed at time t, M_t, was calculated from the measured aerosol size distributions assuming spherical particles and a particle density of 1.25 g cm^{-3}. Aerosol size distributions were corrected for wall-loss according to Pathak et al.[26] assuming a first-order wall-loss rate determined from plotting $\ln(M_t)$ against time after aerosol mass production has stopped. For size-dependent wall-loss corrections, we adjusted the formulation by Crump and Seinfeld[27] for an arbitrary vessel to our cylindrically shaped smog-chamber, and chose the turbulent energy dissipation parameter k_e in a way that the total aerosol mass derived from the size-dependent wall-loss correction was consistent with the integral wall-loss correction. Figure 2a demonstrates a typical evolution of the aerosol size distribution from a chamber experiment related to XOA formation. The temporal evolution of aerosol mass before and after application of the wall-loss correction is shown in Figure 2b.

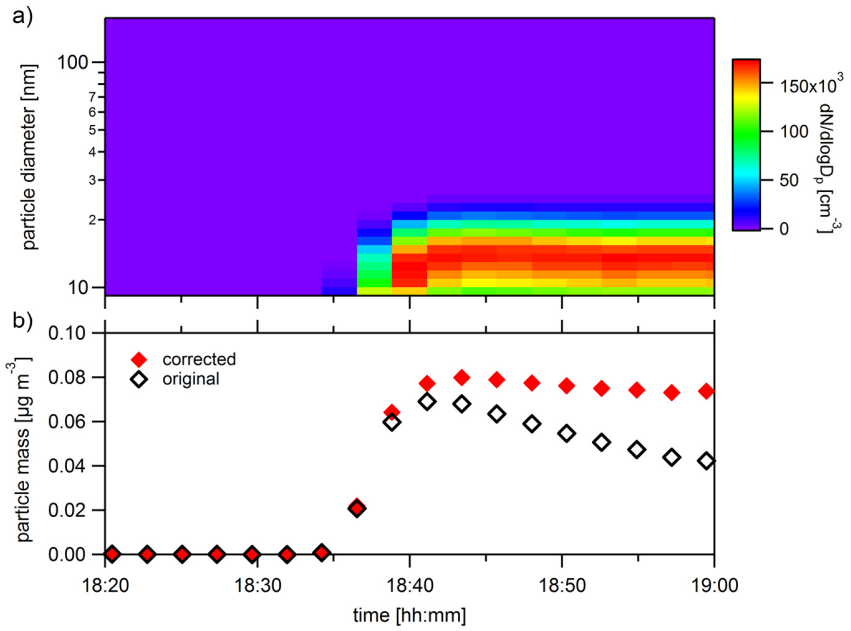

Fig. 2 a) Aerosol size distribution for a chamber experiment with α-pinene and molecular chlorine; b) aerosol mass concentration resulting from the original and corrected SMPS data.

Aerosol formation experiments were started by switching on the solar simulator at zero-air conditions. After establishing a constant spectral actinic flux, α-pinene (Sigma-Aldrich, purity of 98%) was injected into the chamber. The concentration of the organic precursor was adjusted by injecting a known volume of the saturated vapour from the organic species. Two GC background measurements (20 minutes) were performed to monitor the homogeneous distribution of the precursor inside the aerosol smog-chamber and to obviate self-initiated aerosol formation. The aerosol formation was initiated by injection of a known volume of 1% molecular chlorine, diluted in N_2 (Linde, Germany) into the chamber. Table 1 summarizes the experimental conditions of the aerosol smog-chamber runs.

Table 2 Initial conditions, aerosol mass ΔM_0 and aerosol mass yield Y of smog-chamber runs.

Experiment	Cl_2 [ppb]	α-pinene [ppb]	ΔM_0 [µg m^{-3}]	Y
Cl-1	2.5	10	1.3E-03	3.7E-05
Cl-2	5	10	6.0E-02	2.0E-03
Cl-3	5	10	6.4E-02	9.8E-03
Cl-4	20	20	23.7	2.4E-01
Cl-5	100	20	12.4	1.1E-01
Cl-6	200	50	175.7	6.2E-01

Aerosol flow-reactor setup and experiments

To study the chemistry of the halogen-induced organic aerosol formation, an aerosol flow-reactor was set up and coupled to a Bruker IFS 113v FTIR spectrometer, which is equipped with a normal pressure sample compartment. The sample compartment is separated from the vacuum system of the FTIR spectrometer using two KBr windows. A circular multi-reflection cell[28] with path lengths up to 105 cm was installed inside the sample compartment and coupled to the flow reactor. The flow reactor itself is described in detail by Ofner et al., 2010[29]. Additionally, the lamps of a common UV face tanner (Philips UVA Typ HP 3151/A), with an emission characteristic between 270 and 450 nm and a maximum power of 1 W m^{-2} nm^{-1}, were placed around the flow-reactor for photolysis of molecular chlorine. Three mass-flow controllers (MFC) were used to control the flow conditions within the flow reactor. The sheath and reactive gas-flow were mixed using two 2000 sccm MFCs from zero-air and 1% Cl_2 in N_2 and fed to the top of the aerosol flow-reactor itself. Zero-air was saturated with the organic precursor (α-pinene - 500 Pa vapour pressure) and injected into the moveable inlet of the flow reactor. The XOA formation was initiated depending on the position of the moveable inlet, where mixing of the organic vapour and the RHS occurred. The flow conditions and resulting available reaction times are shown in Table 2. The flow reactor was operated at slightly reduced pressure to avoid contamination of the multi-reflection cell and the reactor itself with low-volatile species or aerosol particles. The applied flow rates allowed an operation of the reactor under laminar conditions.

Table 2 Flow conditions and mixing ratios within the aerosol flow-reactor

AFR condition	Cl2 [Vol%]	α-pinene [ppm]	total flow [sccm]	max. reaction time [s]
A	0.44	85	600	8.5
B	0.35	67	750	6.7
C	0.60	116	445	11.5
D	0.84	161	316	16.0

For FTIR spectroscopy, 256 scans with a resolution of 4 cm^{-1} in the range of 4000-600 cm^{-1} were recorded. Spectra were recorded at 5, 10, 20, 30, and 40 cm distance of the inlet to the centre of the multi-reflection cell. Background measurements were performed when the flow reactor was flushed with zero air. The raw spectra were background corrected using the Bruker Opus 7.0 software package because of a strong contribution of Mie scattering of aerosol particles to the absorbance spectra. Further the CO_2 absorbance at 2349 and 667 cm^{-1} were corrected to zero at the lowest stage of the reactor for series A. To allow a clear demonstration of the obtained spectral time-series, 2D correlation spectroscopy[30,31,32] was applied. The software package *2Dshige v1.3* (2Dshige (c) Shigeaki Morita, Kwansei-Gakuin University, 2004-2005) was used to calculate the synchronous and asynchronous 2D correlation plots.

3 Results and Discussion

Halogen-induced ultra-fine particle formation

Aerosol formation experiments were conducted for various concentrations of α-pinene and chlorine radicals (cf. Table 1). After injecting molecular chlorine into the illuminated aerosol smog chamber it took about 2 minutes until the maximum of the particle concentration was reached at low concentrations of the organic precursor and chlorine (Cl-1 to Cl-3, Tab. 1). In the high concentration experiments (Cl-4 to Cl-6, Tab. 1), particle formation started immediately after injection. Chlorine mixing ratios as low as 2.5 ppb were sufficient to induce particle formation. The aerosol yield Y was computed as the mass concentration ΔM_0 ($\mu g\ m^{-3}$) of SOA formed after the organic precursor is completely reacted, divided by the concentration of the reacted organic precursor ΔVOC ($\mu g\ m^{-3}$),

$$\boldsymbol{Y = \frac{\Delta M_0}{\Delta VOC}} \qquad (1).$$

Following Pandis et al.[33], in most aerosol formation experiments, Y is evaluated after the organic precursor is completely reacted, gas-particle equilibrium is established, and aerosol growth has stopped. However, several studies have investigated time-dependent aerosol formation[34,35], i.e. ΔM_0 and ΔVOC are evaluated frequently in one individual experiment.

In Fig. 3 and 4, we present both the traditional aerosol yield derived from Eq. 1 after α-pinene is completely reacted (large symbols), and the time-dependent yield curves (small symbols). For comparison, the yields from Cai and Griffin[8] resulting from six α-pinene and chlorine experiments are also included in Fig. 3. Finally, we compare our yields with the yield curve from a two-product model (2P-M) after Odum et al.[36] parameterized by Cai and Griffin[8].

We consider the precursor mixing ratios of several ppb of α-pinene and chlorine in the experiments Cl-1 to Cl-3 to be within one or two orders of magnitude of typical ambient conditions in coastal environments with biogenic emissions of volatile organic compounds. In any case, these experiments extend previous studies to aerosol mass concentrations almost four orders of magnitude lower than the work by Cai and Griffin[8]. The yields ranging from 0.0013 to 0.065 are in reasonable agreement with the two-product model shown in Fig. 3 and 4.

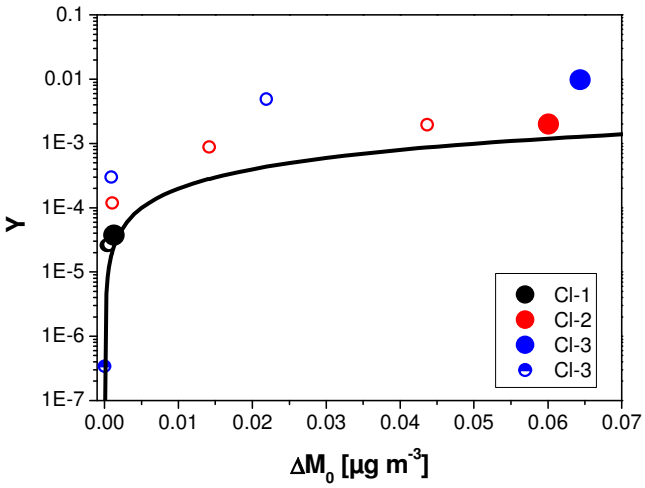

Fig. 3 Yield curves of α-pinene and chlorine from six smog-chamber experiments, and yields of six experiments and the yield curve from a two-product model by Cai and Griffin[8]. For clarity, the lowest yield from Cl-3 is not shown.

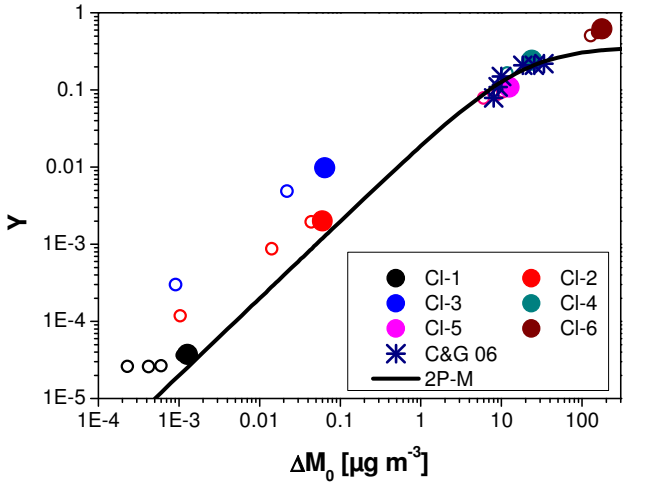

Fig. 4 Closeup of the low concentration experiments Cl-1 to Cl-3.

Precursor mixing ratios in experiments Cl-4 and Cl-5 are similar to the concentration range covered by Cai and Griffin[8]. Our experiments confirm their results. Higher mixing ratios of α-pinene and chlorine in experiment Cl-6 give an aerosol yield higher than expected from the two-product model by Cai and Griffin[8].

Overall, the observed yields are lower than the yields reported for ozone oxidation of α-pinene but larger than yields reported for photooxidation of α-pinene (e.g. Griffin et al.[37]). Therefore, the chlorine oxidation mechanism cannot be neglected in environments with high ambient chlorine concentrations.

Halogen consumption and organic precursor decays

By calculating the decay of available molecular chlorine (based on the chamber actinometry and calculation of the photolysis rate) and subsequently the availability of chlorine atoms, the maximum decay of the organic precursor was calculated. The calculation is based on the simple assumption that every chlorine atom promptly reacts with a molecule of the organic precursor and is not recovered to react with other unprocessed precursor molecules. This maximum decay is compared to the real observed decays of α-pinene, obtained from gas chromatography, for the low-concentration experiments (Figure 5).

As indicated in Figure 5, the maximum decay consuming all chlorine atoms for the experiments with 2.5 ppb of molecular chlorine would only allow decays from 10 down to 5 ppb. The real measured decays are much higher. Tens to hundreds of ppt are reached after 60 minutes, thus, indicating that the basic assumption that chlorine atoms are fully consumed by the same equivalent of organic precursor and not regenerated is not according to the observed reaction mechanism. The formation of XOA appears to be mainly driven by a radical-chain-reaction like mechanism.

For the aerosol smog-chamber experiments, the best agreement of the calculated decay and the measured decay is at 5 ppb of molecular chlorine and 10 ppb of organic precursor. At higher concentrations, the diffusion of the organic precursor and the RHS becomes limiting. XOA formation at low chlorine concentrations appears to be driven by a radical-chain-like reaction. This is consistent with an initial Cl addition pathway to alpha-pinene and subsequent opening of the ring leading to pinonaldehyde and release of Cl as proposed by Cai and Griffin[8]. A major limiting factor is the diffusivity of the gaseous species.

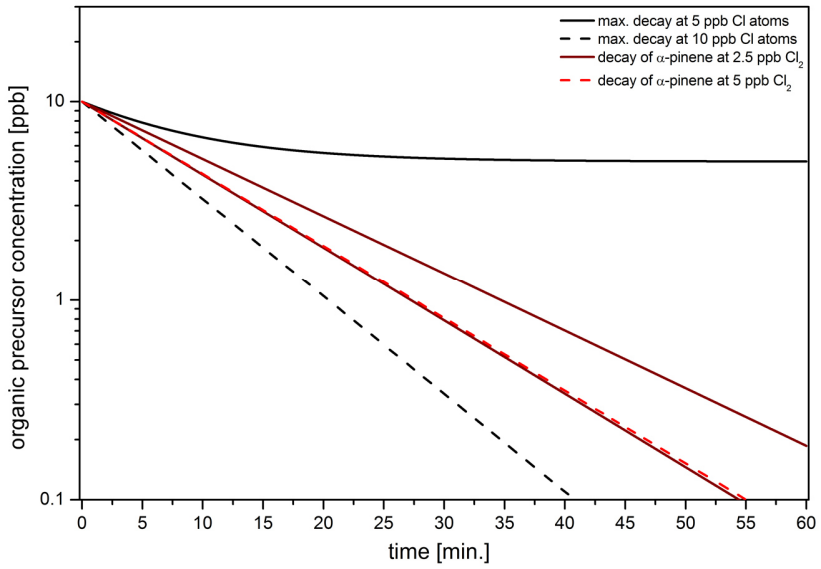

Fig. 5 Calculated maximum and measured decays of the organic precursor based on the available chlorine concentration.

Chemical transformation of XOA during the formation and aging process

Chemical details on XOA formation were obtained from the aerosol flow-reactor experiments, where each series is represented by 5 single experiments at different times of the reaction. The general interpretation of the FTIR spectra and 2D correlation plots is related to the FTIR spectrum of pure α-pinene[38]. Spectra of the AFR conditions A and C (Table 2) represent the highest spectral changes, thus these two time series were interpreted in detail. Condition A allows temporal steps of 1.1, 2.1, 4.2, 6.3 and 8.5 seconds (related to the distance of the inlet to the centre of the multi-reflection cell – see section 2 Methods), condition C of 1.4, 2.9, 5.8, 8.7 and 11.5 seconds. The 2D correlation of the fast condition A is more sensitive towards changes related to the gaseous species like HCl and CO_2. The slower condition C exhibits significant changes related to the aerosol particle phase like changes of the ν(C=O), ν(C=C), ν(C-H) and the ν(C-Cl) stretch vibrations. While the temporal starting point of both series should be rather similar, significant differences (e.g. in the ν(C=O) spectral region) are visible. These differences can be explained by changing flow conditions, different concentration profiles and a different behaviour of the laminar flow profile and the related mixing inside the flow reactor.

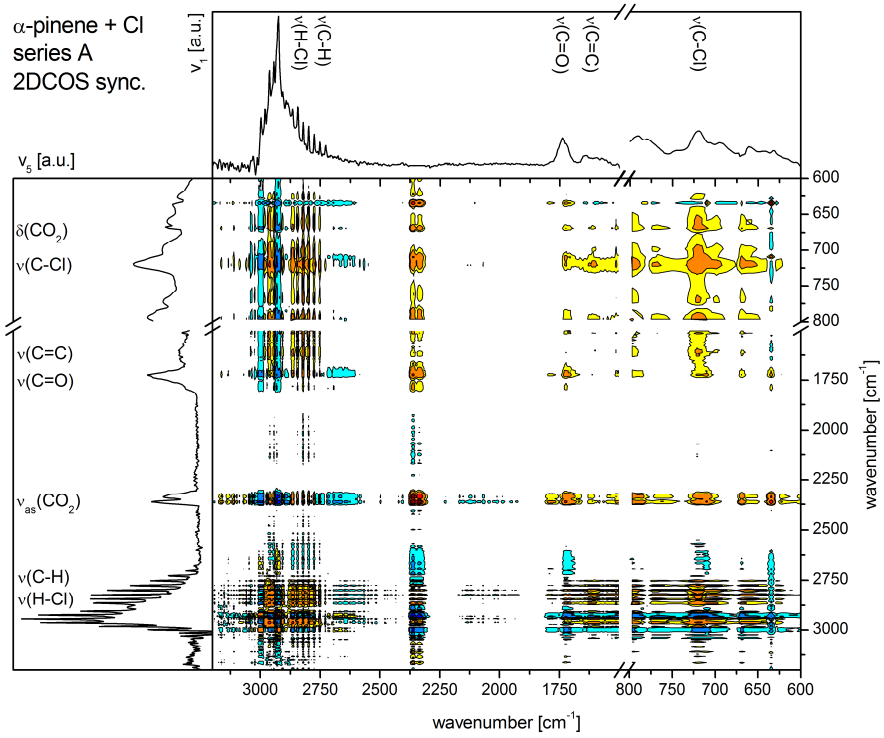

Fig. 6 Synchronous 2D correlation spectroscopy plot of photochemical XOA formation from α-pinene with chlorine at condition A, where ν1 is the first obtained spectrum at 1.1 second and ν5 is the last obtained spectrum at 8.5 seconds – yellow to red contours indicate a synchronized change of the signals in the same direction, whereas blue contours indicate a synchronized change of the signals in opposite directions.

As mentioned above, the 2D correlation spectroscopy plots (Figures 6 and 7) of the photochemical XOA formation from α-pinene with chlorine at aerosol flow-reactor condition A appear to be more sensitive to the gaseous species. The synchronous plot (Figure 6) indicates a coupling of CO_2 (ν_{as}(C=O) at 2349 cm^{-1}) and HCl (narrow absorptions between 2700-3100 cm^{-1}) formation. The aerosol formation itself is also correlated with the formation of carbon chlorine bonds (ν(C-Cl) at 720 cm^{-1}), by addition of chlorine to the C=C double bond or to a radical site, and of carbonyls and/or carboxylic acids (ν(C=O) at 1700-1750 cm^{-1}). The synchronous plot exhibits an anti-correlation of the aliphatic ν(C-H) of the $-CH_3$ groups of α-pinene[38] at 2995 cm^{-1} and 2925 cm^{-1} with the overall aerosol formation (which is caused by a halogen-induced abstraction of hydrogen atoms).

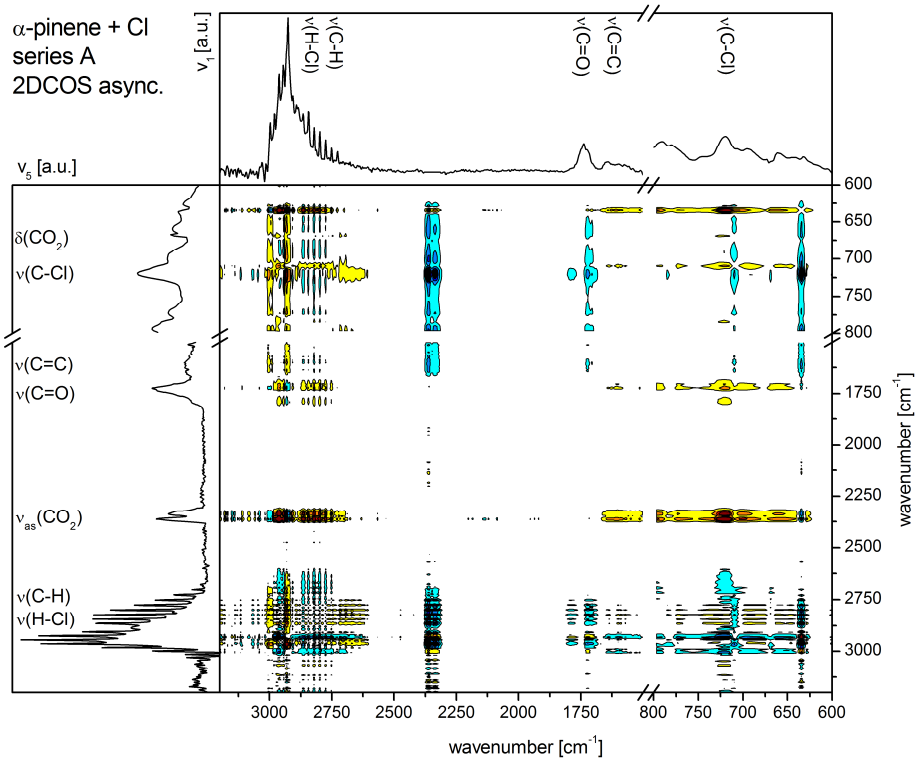

Fig. 7 Asynchronous 2D correlation spectroscopy plot of XOA formation from photochemical reactions of α-pinene with chlorine at condition A, where ν1 is the first obtained spectrum at 1.1 second and ν5 is the last obtained spectrum at 8.5 seconds – yellow to red contours indicate a change of absorption in ν1 before ν2, whereas blue contours indicate the other way round.

Details on the sequence of transformation of single absorptions and species are given by the 2D asynchronous plot (Figure 7). The sequential order was interpreted according to the so-called "Noda" rules[22]. No asynchronous cross-peaks exist in case of the absorptions of the C-Cl bond formation and the HCl release (which is indicated in the synchronous plot by positive cross-peaks). The formation of halogenated species in the aerosol phase is synchronous and thus coupled to the release of HCl to the gas phase. Due to the fact, that the synchronous cross-peaks between CO_2 and the C-Cl formation are positive and asynchronous cross-peaks exist, the CO_2 release is following the C-Cl formation and HCl release. Missing asynchronous cross-peaks between the ν(C=O) and the release of CO_2 indicate a

synchronous coupling of the formation of carbonyls or carboxylic acids and the release of CO_2. The sequence of ν(C-Cl) formation with HCl release and following C=O bond formation is also indicated by the asynchronous cross-peaks between HCl and ν(C=O) and ν(C-Cl) and ν(C=O).

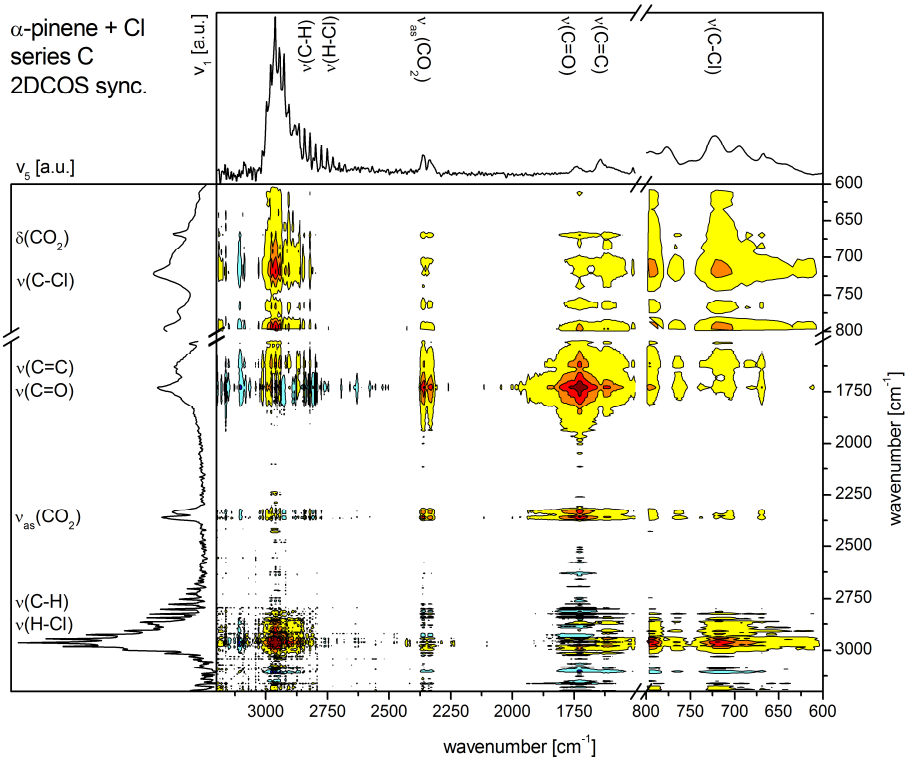

Fig. 8 Synchronous 2D correlation spectroscopy plot of photochemical XOA formation from α-pinene with chlorine at condition C; ν_1 at 1.4 s and ν_5 at 11.5 s.

In contrast to series A, plots from series C appear to be more sensitive towards changes of the formed aerosol phase. The synchronous plot of 2D correlation spectroscopy in Figure 8 exhibits strong auto-correlation peaks related to the formation of carbonyls and/or carboxylic acids (ν(C=O) at 1700 to 1750 cm^{-1}) and to the formation of carbon chlorine bonds at 720 cm^{-1}. Further changes are visible in case of the olefinic ν(C=C) stretch vibration which appears to broaden, caused by the formation of oligomers and more complex species. While the degradation of the well-defined ν(C-H) stretch vibration in Figure 8 is not visible like in Figure 6, a general broadening of the aliphatic carbon hydrogen bond regime is observed. This broadening, which appears like carbon-hydrogen bond formation, can be related to the formation and aging of particulate matter.

The sequence of the gaseous species is similarly demonstrated in the asynchronous plot of series C (Figure 9). The formation of carboxylic acids or carbonyls follows after C-Cl formation. Also the transformation of the sharp ν(C=C) stretch vibration of the organic precursor (around 1650 cm^{-1}) to the broad absorption of various olefinic structures within the particulate phase takes place before ν(C=O) formation. The broad asynchronous cross-peaks between 600 and 800 cm^{-1} indicate the formation of a broad finger-print region. This can be related to the formation of oligomers and high-molecular structures or a large variety of different organic species.

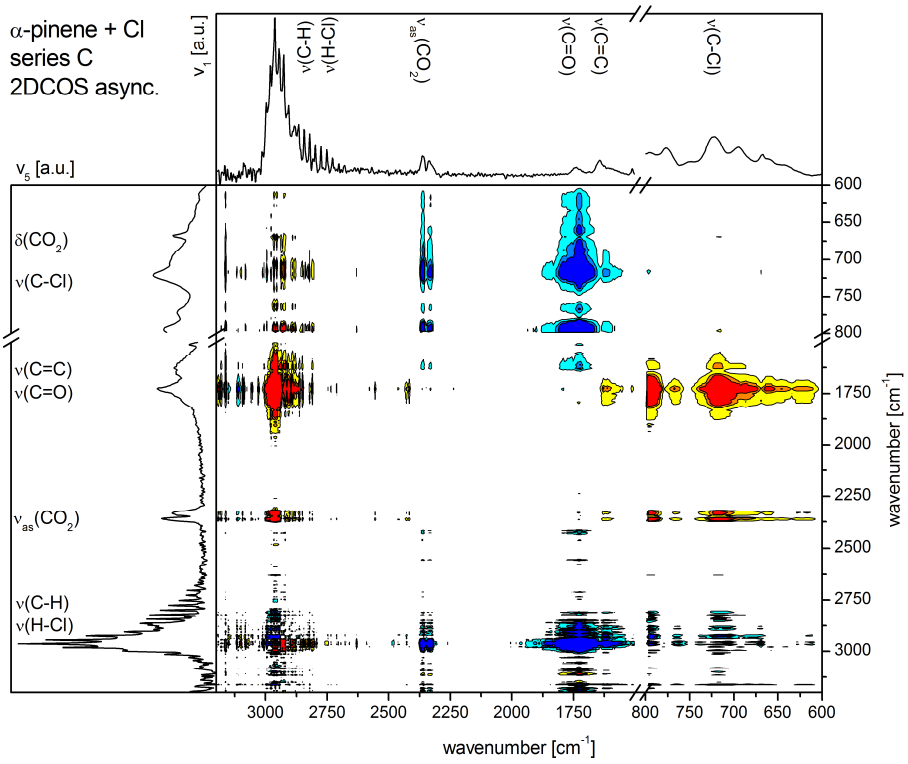

Fig. 9 Asynchronous 2D correlation spectroscopy plot of photochemical XOA formation from α-pinene with chlorine at condition C; ν_1 at 1.4 s and ν_5 at 11.5 s.

The general roadmap of XOA formation, initiated by addition of chlorine and H atom abstraction, forming HCl and chlorine carbon bonds is in good agreement with the studies by Cai and Griffin[8] and Karlsson et al.[7]. Also, the subsequent addition of oxygen to the so formed radical sites of the organic structure and the coupled formation of carbonyls and carboxylic acids as well as the concurrent release of CO_2 is according to the suggestions made by these authors. During further processing, the freshly formed XOA appears to degrade and becomes more SOA-like, losing the halogen-induced characteristics and appearing more "common".

Conclusions

Reactive halogen species releasing Cl radicals can induce organic aerosol formation by reaction with organic precursor gases such as α-pinene. From the experiments in this work evidence is found both for a Cl addition pathway to α-pinene as well as an H-atom abstraction pathway. On one hand, the formation of C-Cl bonds in the FTIR spectra as well as indirect evidence for a radical-chain mechanism (cf. Fig. 5) is consistent with Cl addition. On the other hand, the formation of HCl observed in the flow-reactor experiments is consistent with H-atom abstraction in the reaction between Cl and α-pinene[15]. However, it is difficult to quantify the respective contributions of these pathways to the overall reaction.

The aerosol yield found in low and high concentration experiments is in general agreement with previous experimental data by Cai and Griffin[8] as well as a parameterization of the yield curve presented by the same authors. Even at precursor concentrations almost four orders of magnitude lower than the previous experiments, a reasonable agreement with the two-product parameterization is found. With a broad range of mixing ratios of α-pinene and chlorine in six experiments we could extend the data from these authors and obtaining aerosol formation yields even at close-to-ambient conditions.

The chemical formation of this type of organic aerosol is halogen driven as demonstrated by the aerosol flow-reactor experiments. The formation process occurs in the absence of ozone but also even without oxygen. Thus, the formation of halogen-induced organic aerosol represents an aerosol formation process apart from the commonly considered formation pathways. The further processing of XOA with oxygen and oxygen-containing reactants causes a transformation of XOA to the common SOA, which is dominated by oxygen-containing functional groups. This XOA-born SOA still exhibits carbon chlorine bonds, thus indicating the XOA-like source of the organic aerosol. With further chemical aging and processing by atmospheric reactive species, the XOA-like character of the organic aerosol from monoterpenes and RHS is lost.

The formation of XOA from monoterpenes or other organic volatile species with RHS must not be neglected for e.g. maritime areas, where high RHS and VOC concentrations occur at dawn or sunset simultaneously. Although XOA appears to transform to SOA by aging and processing, this special type of organic aerosol might exhibit different features not commonly related to SOA or the organic aerosol in general. The halogen-driven formation and the coupled formation of solid halogen species in the particle phase significantly influences physico-chemical parameters like water-solubility, the potential to act as CCN or IN, the adsorption behaviour with respect to gas-phase species as well as the interaction with sunlight (or the UV/VIS absorption spectrum[10]). This changes the influence on radiative forcing and thus, modifies the influence of XOA on global warming compared to commonly considered SOA.

Acknowledgement

The authors like to thank the German research foundation for funding within the research unit HaloProc (HE5214/5-1 and ZE792/5-2). Further the authors thank Georg Ramer from the Institute of Chemical Technologies and Analytics, Vienna University of Technology for his assistance for 2D correlation spectroscopy.

References

1. J. H. Kroll and J. H. Seinfeld, *Atmos. Environ.*, 2008, **42**, 3593–3624.

2. J. L. Jimenez, M. R. Canagaratna, N. M. Donahue, A. S. H. Prevot, Q. Zhang, J. H. Kroll, P. F. DeCarlo, J. D. Allan, H. Coe, N. L. Ng, A. C. Aiken, K. S. Docherty, I. M. Ulbrich, A. P. Grieshop, A. L. Robinson, J. Duplissy, J. D. Smith, K. R. Wilson, V. A. Lanz, C. Hueglin, Y. L. Sun, J. Tian, A. Laaksonen, T. Raatikainen, J. Rautiainen, P. Vaattovaara, M. Ehn, M. Kulmala, J. M. Tomlinson, D. R. Collins, M. J. Cubison, E. J. Dunlea, J. A. Huffman, T. B. Onasch, M. R. Alfarra, P. I. Williams, K. Bower, Y. Kondo, J. Schneider, F. Drewnick, S. Borrmann, S. Weimer, K. Demerjian, D. Salcedo, L. Cottrell, R. Griffin, A. Takami, T. Miyoshi, S. Hatakeyama, A. Shimono, J. Y. Sun, Y. M. Zhang, K. Dzepina, J. R. Kimmel, D. Sueper, J. T. Jayne, S. C. Herndon, A. M. Trimborn, L. R. Williams, E. C. Wood, A. M. Middlebrook, C. E. Kolb, U. Baltensperger, and D. R. Worsnop, *Science (New York, N.Y.)*, 2009, **326**, 1525–9.

3. I. Riipinen, T. Yli-Juuti, J. R. Pierce, T. Petäjä, D. R. Worsnop, M. Kulmala, and N. M. Donahue, *Nature Geoscience*, 2012, **5**, 453–458.

4. C. O'Dowd, M. Facchini, F. Cavalli, D. Ceburnis, M. Mircea, S. Decesari, S. Fuzzi, Y. J. Yoon, and J.-P. Putaud, *Nature*, 2004, **431**, 676–680.

5. L. J. Carpenter, S. D. Archer, and R. Beale, *Chem. Soc. Rev.*, 2012, **41**, 6473–506.

6. Q. K. Timerghazin and P. A. Ariya, *Phys. Chem. Chem. Phys.*, 2001, **3**, 3981–3986.

7. R. S. Karlsson, J. J. Szente, J. C. Ball, and M. M. Maricq, *J. Phys. Chem. A*, 2001, **105**, 82–96.

8. X. Cai and R. J. Griffin, *J. Geophys. Res.*, 2006, **111**, D14206.

9. X. Cai, L. D. Ziemba, and R. J. Griffin, *Atmos. Environ.*, 2008, **42**, 7348–7359.

10. J. Ofner, N. Balzer, J. Buxmann, H. Grothe, P. Schmitt-Kopplin, U. Platt, and C. Zetzsch, *Atmos. Chem. Phys.*, 2012, **12**, 5787–5806.

11. J. H. Kroll, N. M. Donahue, J. L. Jimenez, S. H. Kessler, M. R. Canagaratna, K. R. Wilson, K. E. Altieri, L. R. Mazzoleni, A. S. Wozniak, H. Bluhm, E. R. Mysak, J. D. Smith, C. E. Kolb, and D. R. Worsnop, *Nature chemistry*, 2011, **3**, 133–9.

12. T. Moise and Y. Rudich, *Geophys.Res. Lett.*, 2001, **28**, 4083–4086.

13. R. C. Sullivan and K. A. Prather, *Anal. Chem.*, 2005, **77**, 3861–85.

14. D. Vione, V. Maurino, S. C. Man, S. Khanra, C. Arsene, R.-I. Olariu, and C. Minero, *ChemSusChem*, 2008, **1**, 197–204.

15. B. J. Finlayson-Pitts, C. J. Keoshian, B. Buehler, and A. A. Ezell, *Int. J. Chem. Kinet.*, 1999, **31**, 491–499.

16. B. J. Finlayson-Pitts, *Res. Chem. Intermed.*, 1993, **19**, 235–249.

17. C. Spicer and E. Chapman, *Nature*, 1998, **1996**, 1996–1999.

18. A. Saiz-Lopez and R. von Glasow, *Chem. Soc. Rev.*, 2012, **41**, 6448–72.

19. C. Zetzsch and W. Behnke, *NATO ASI Ser., Ser. I*, 1993, **7**, 291–306.

20. B. J. Finlayson-Pitts, *Chem. Rev.*, 2003, **103**, 4801–22.

21. J. A. Thornton, J. P. Kercher, T. P. Riedel, N. L. Wagner, J. Cozic, J. S. Holloway, W. P. Dubé, G. M. Wolfe, P. K. Quinn, A. M. Middlebrook, B. Alexander, and S. S. Brown, *Nature*, 2010, **464**, 271–4.

22. I. Noda, *Generalized Two-Dimensional Correlation Spectroscopy in Frontiers of Molecular Spectroscopy (Jaan Laane, Editor)*, Elsevier, ISBN: 978-0-444-53175, 2009.

23. J. Ofner, H.-U. Krüger, H. Grothe, P. Schmitt-Kopplin, K. Whitmore, and C. Zetzsch, *Atmos. Chem. Phys.*, 2011, **11**, 1–15.

24. B. Bohn, F. Rohrer, T. Brauers, and A. Wahner, *Atmos. Chem. Phys.*, 2005, **5**, 493–503.

25. A. Ruggaber, R. Dlugi, and T. Nakajima, *J. Atmos. Chem.*, 1994, **18**, 171–210.

26. R. K. Pathak, C. O. Stanier, N. M. Donahue, and S. N. Pandis, *J. Geophy. Res.*, 2007, **112**, D03201, doi:10.1029/2006JD007436.

27. J. G. Crump and J. H. Seinfeld, *J. Aerosol Sci.*, 1981, **12**, 405–415.

28. J. Ofner, H.-U. Krüger, and C. Zetzsch, *Appl. Optics*, 2010, **49**, 5001.

29. J. Ofner, H.-U. Krüger, and C. Zetzsch, *Z. Phys. Chem.*, 2010, **224**, 1171–1183.

30. I. Noda, *Appl. Spectrosc.*, 1993, **47**, 1329–1336.

31. I. Noda, A. Dowrey, and C. Marcott, *Appl. Spectrosc.*, 2000, **54**, 236A–248A.

32. B. Muik, B. Lendl, A. Molina-Diaz, M. Valcarcel, and M. J. Ayora-Cañada, *Anal. chim. acta*, 2007, **593**, 54–67.

33. S. N. Pandis, R. A. Harley, G. R. Cass, and J. H. Seinfeld, *Atmos. Environ. A*, 1992, **26**, 2269–2282.

34. T. Hoffmann, J. Odum, F. Bowman, D. Collins, D. Klockow, R. C. Flagan and J. H. Seinfeld, *J. Atoms. Chem.*, 1997, **26**, 189–222.

35. N. L. Ng, J. H. Kroll, M. D. Keywood, R. Bahreini, V. Varutbangkul, R. C. Flagan, J. H. Seinfeld, A. Lee, and A. H. Goldstein, *Environ. Sci. Technol.*, 2006, **40**, 2283–2297.

36. J. R. Odum, T. Hoffmann, F. Bowman, D. Collins, R. C. Flagan, and J. H. Seinfeld, *Environ. Sci. Technol.*, 1996, **30**, 2580–2585.

37. R. J. Griffin, D. R. Cocker, R. C. Flagan, and J. H. Seinfeld, *J. Geophys. Res.*, 1999, **104**, 3555.

38. H. W. Wilson, *Appl. Spectrosc.*, 1976, **30**, 209–212.

Appendix II

New particle formation induced by Western Australian salt lakes

K. A. Kamilli[1], J. Ofner[2], T. Krause[3], T. Sattler[3], P. Schmitt-Kopplin[4], E. Atlas[5], E. Eitenberger[2], G. Friedbacher[2], B. Lendl[2], H. Lohninger[2], H. F. Schöler[3], A. Held[1,6]

[1]{Atmospheric Chemistry, University of Bayreuth, Bayreuth, Germany}

[2]{Institute of Chemical Technologies and Analytics, TU Wien, Vienna, Austria}

[3]{Institute of Earth Science, University of Heidelberg, Germany}

[4]{Research Unit Analytical BioGeoChemistry, Helmholtz Centre Munich, Germany, Oberschleißheim, Germany}

[5]{Marine and Atmospheric Chemistry, Rosenstiel School of Marine and Atmospheric Science, University of Miami, Miami, Florida, USA}

[6]{Bayreuth Center of Ecology and Environmental Research BayCEER, Bayreuth, Germany}

Correspondence to: K. A. Kamilli (katharina.kamilli@uni-bayreuth.de)

Abstract

New particle formation directly induced by gaseous precursors emitted from salt lakes in Western Australia was investigated in field experiments in 2013. A mobile Teflon chamber was set up above the transition zone between the salt crust and organic-enriched mud layers of seven different salt lakes on eleven measurement days. The mobile chamber setup made it possible to relate particle formation directly to the salt lakes surfaces. Particle size distributions, ozone and volatile organic compound mixing ratios, air temperature, global radiation, relative humidity, and lake water chemistry were analyzed at four different lakes in detail. The main particle formation events were typically related to an enhanced air temperature and enhanced irradiance. The four considered lakes showed particle growth rates from 2.9 to 25.4 nm h^{-1}. Obviously, the enrichment in the mobile chamber led to high mixing ratios of potential organic precursor gases which might explain the observed particle growth. Raman spectroscopy combined with scanning electron microscopy gave evidence for a strong contribution of inorganic salts to the pre-existing coarse mode, while the organic aerosol was chemically diverse and included organosulfates. These organic compounds both have coated the existing inorganic particles of the coarse mode and are suggested to serve as precursor gases for new particle formation.

1 Introduction

In the mid-19th century, Western Australia was covered with Eucalyptus trees before large-scale deforestation for agricultural purposes led to decreased mean evapotranspiration in this region. Thus, the groundwater formation from precipitation increased and the groundwater table rose. The rising groundwater passed mineral-rich layers and brought dissolved salts and minerals to the surface, causing secondary salinization (Addison, 2001; Ghauri, 2004). Nowadays, Western Australia is covered by a large number of salt lakes with pH levels from 2.4 to 8.7 (Krause, 2014). The land is mainly used for wheat farming and livestock and becomes drier due to a lack of precipitation. The decrease in precipitation has been explained by the formation of ultrafine particles from salt lakes, which increases the number of cloud condensation nuclei (CCN), and thus potentially suppresses precipitation. Junkermann et al. (2009) found an increased CCN number concentration over the agricultural land linked to the salt lakes where the precipitation decreased by about 30 % in Australian winter since the 1970s (Hope et al., 2010). In a case study along the State Barrier Fence of Western Australia, which is the border between agricultural land and native vegetation, Esau and Lyons (2002) found a change of turbulent fluxes and cloud formation over the agricultural areas. Clouds develop more often over regions with natural vegetation (Lyons, 2002), and seem to dissipate over the agricultural and salt lake areas. Junkermann et al. (2009) determined a regional feedback in land use change and aerosol production and proposed that different land covers evoke distinct particle populations affecting cloud formation. Secondary aerosols from natural sources becoming CCNs have been observed above forests, where mainly sulfuric acid in combination with biogenically emitted organic compounds (e.g. Kavouras et al., 1998) act as key reactants (e.g. Kulmala et al., 2004). Depending on the type of vegetation, a mixture of volatile organic compounds is emitted. After oxidation in the atmosphere, the VOC oxidation products may contribute to aerosol growth (e.g. Andreae and Crutzen, 1997; O'Dowd et al., 2002). Besides oxidants like OH, O_3 and NO_3 (e.g. Nunes and Pio, 2001), the reaction of organic precursor gases with reactive halogen species (RHS) may also contribute to secondary organic aerosol (SOA) formation. Recently, salt lakes have been identified as a natural source for reactive halogen species (Buxmann et al., 2012). Also, in simulation experiments under laboratory conditions using simulated sunlight, particle formation was observed from the reaction of terpenes with chlorine (Cai and Griffin, 2006; Cai et al., 2008; Ofner et al., 2013) and bromine. Therefore, reactions of volatile organic compounds with RHS may extend the possible formation pathways and the chemical diversity of SOA.

In the present study, particle formation was identified directly above various salt lakes. Particle growth rates will be quantified and the chemical composition of representative aerosol samples collected directly above the salt lakes will be characterized.

2 Field campaign and experimental setup

2.1 Field campaign and measurement sites

Measurements were conducted in the Lake King (33.09°S, 119.69°E) area about 450 km east of Perth in Southwest Australia in the so-called Australian Wheatbelt region. Wheat farming and livestock is the predominant agricultural use in this region. The land has been considerably changed in the 1980ies, when large-scale deforestation took place, and the originally deep-rooted native vegetation called mallee, mainly

eucalyptus species, was cut for pastures and winter growing annual crops, mainly wheat. Clearance of the deep-rooted plants led to a rising ground water table, and dissolved salts and minerals rose to the surface. Consequently, the soil surface in this area became widely spread with salt lakes.

The field measurements took place in March 2013, in the southern hemisphere autumn. Temperatures, measured at the Newdegate Research Station (33.11°S, 118.84°E), ranged between 14.6 and 32.4 °C during the field campaign. In March 2013, 3 days with rain occurred in Lake King with a total precipitation of 38.4 mm. The daily solar exposure in Lake King was between 4.6 and 26.6 MJ/m^2. The general meteorological data was obtained from the Australian Government, Bureau of Meteorology (www.bom.gov.au).

Seven salt lakes were chosen for detailed characterisation. An overview of the Lake King area and the location of the seven salt lakes are given in Figure 1. These salt lakes were chosen based on their accessibility, water content, pH value and surrounding. The geographic coordinates of the salt lakes can be found in Table 1. Detailed maps of the chosen salt lakes are displayed in Figure 2 with indication of the position of the mobile observational chamber OzCa. Measurement days were chosen to have low cloud coverage, to enhance photochemical particle formation, and to have low wind speeds, to reduce external mixing of air masses into the chamber.

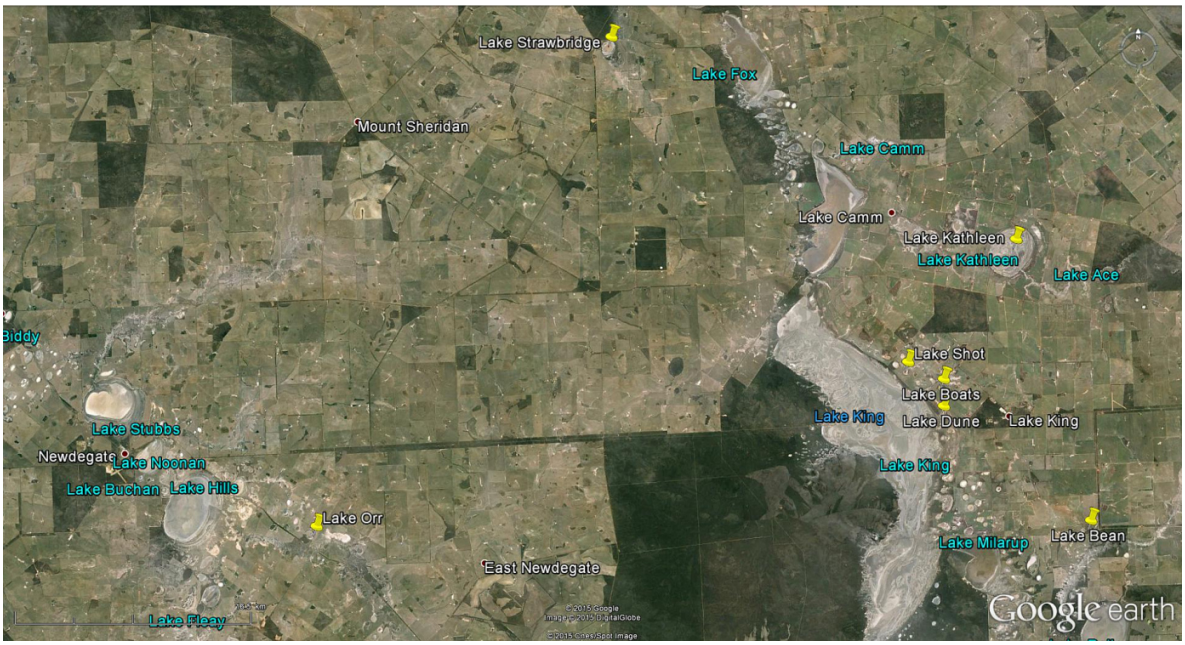

Figure 1. Map of the Lake King area and the location of the seven chosen salt lakes (© 2015 Google; Image © 2015 DigitalGlobe; © 2015 Cnes/Spot Image).

Table 1. Overview of the salt lakes with geographic coordinates, measurement date, daily mean pH value, new particle formation (NPF) (x/-), and daily maximum of particle concentration (N), iron (II), iron (III) and H_2O_2 concentration. [a] CPC measurement

Lake	Geographic coordinates	Measurement date	pH	NPF	N [cm^{-3}]	Iron (II) [mg/l]	Iron (III) [mg/l]	H_2O_2 [mg l^{-1}]
Dune	33.08 S / 119.64 E	13/03/2013	2.9	x	191 000	8.9	2.9	2
Boats	33.07 S / 119.64 E	18/03/2013	2.8	x	141 000	38.6	7.3	0
Shot	33.05 S / 119.61 E	21/03/2013	3.5	x	40 000	1.9	0.5	7.5
Bean	33.16 S / 119.74 E	29/03/2013	7.1	x	23 000	0.2	1.7	2
Boats	33.07 S / 119.64 E	08/03/2013	2.5	x	117 000	213.2	10.6	0
Strawbridge	32.84 S / 119.40 E	09/03/2013	7.0	x	51 000[a]	N.A.	N.A.	5
Dune	33.08 S / 119.64 E	14/03/2013	2.9	x	45 000	N.A.	N.A.	N.A.
Orr	33.15 S / 119.17 E	19/03/2013	4.2	-	7 000	0.34	0.04	3.5
Shot	33.05 S / 119.61 E	22/03/2013	3.5	x	25 000	1.4	0.6	3.5
Dune	33.08 S / 119.64 E	23/03/2013	3.2	x	247 000	4.1	0.6	1.25
Kathleen	32.98 S / 119.68 E	24/03/2013	7.0	-	7 000	0.1	0.4	2

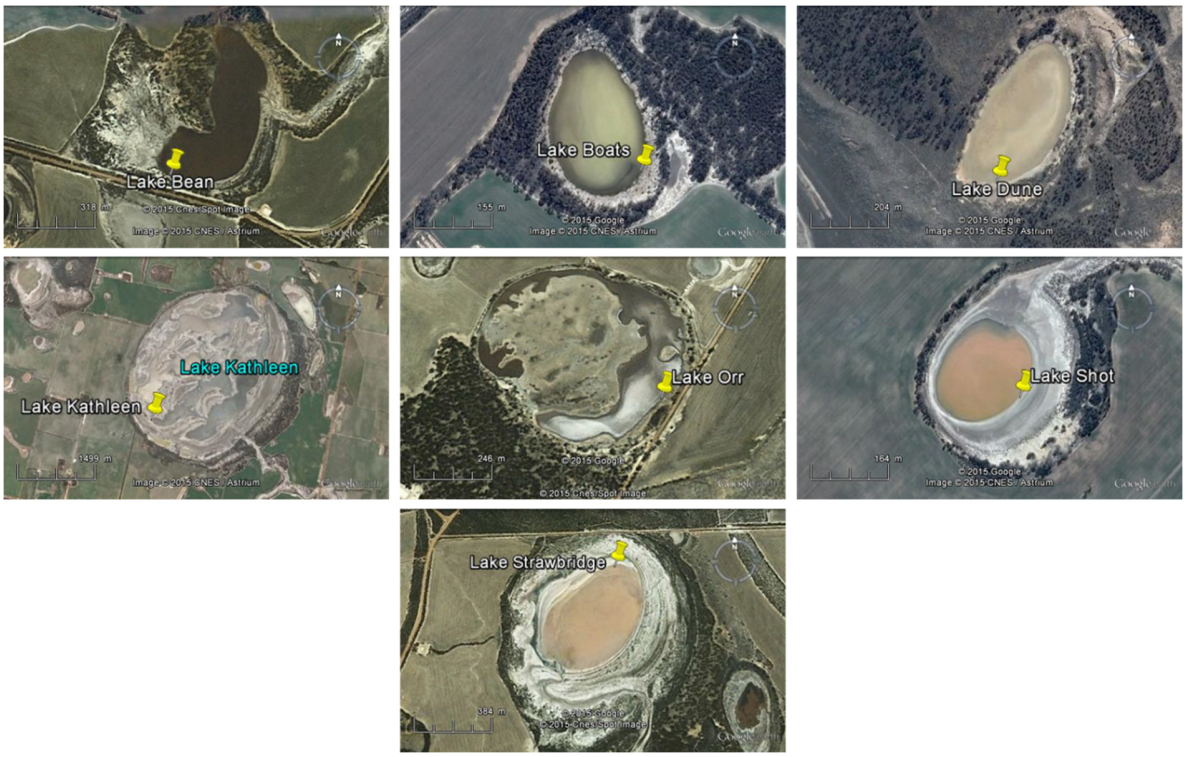

Figure 2. Detailed maps of the seven salt lakes with indication of the position of the mobile observational chamber OzCa (© 2015 Google).

2.2 Mobile observational chamber OzCa

A mobile observational chamber with a volume of about 2.3 m^3 has been designed and successfully applied to study gas emissions and new particle formation in-situ above Western Australian salt lakes (Fig. 3). The mobile chamber OzCa is made from Teflon (FEP 200A, DuPont) with almost cubical dimensions of 1.4 m x 1.4 m x 1.2 m. The four side walls and the top wall are stabilized with metal rods at the four lateral edges and the four top edges, while the bottom of the chamber is left open to the ground.

The chamber can be set up within 10 min, and was typically put above the transition zone between salt crust and organic-enriched mud layers at different salt lakes. The transition zone was chosen to reflect all major parts of the salt lakes, including the liquid water phase, the salt crust, the mud layer and the silica soil. Solar radiation can penetrate through the Teflon walls, whereas mixing of the chamber air with air masses from outside is minimized. For example, the advection of previously formed particles from unknown sources is prevented at moderate wind speeds up to about 5 m s^{-1}. Thus, the mobile chamber OzCa made it possible to relate particle formation directly to salt lake emissions.

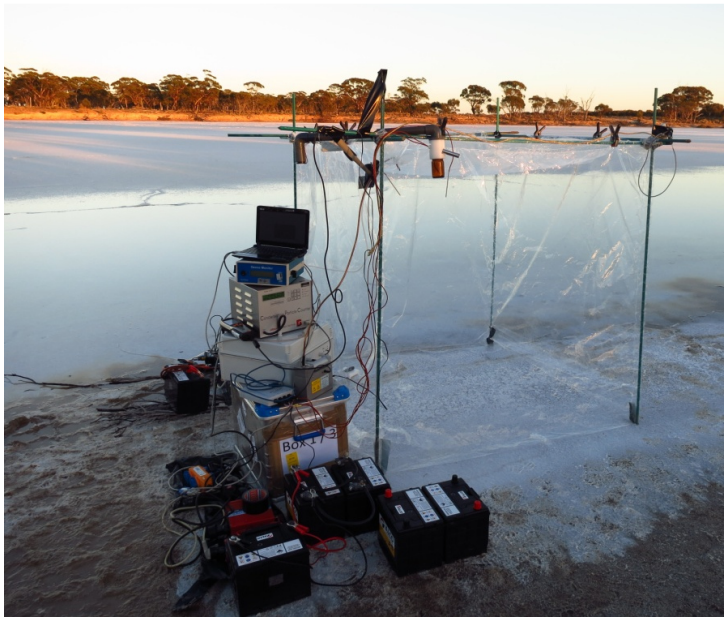

Figure 3. Setup of the mobile observational chamber OzCa above the transition zone between salt crust and organic-enriched mud layers at Lake Dune.

To evaluate the possibility of particle formation from contamination of the Teflon walls of the mobile chamber, a reference measurement has been carried out. Here, an entirely closed chamber has been set up during a bright and sunny day in an area with many eucalyptus trees in Lake King. When starting the experiment, the chamber was set up as usual with metal rods at the four top edges, but closed at the bottom. Thus, the chamber was filled with ambient air that had background concentrations of about 940 particles cm^{-3} measured in the diameter range of interest between 5 nm and 220 nm. During the experiment, the particle concentration decreased continuously due to particle deposition, coagulation and wall losses. This behaviour can be generally described by an exponential function, which can be interpreted as the efficient first-order particle loss function of the chamber setup (e.g. Pathak et al., 2007). The first-order time constant was found to be τ = 325 min, i.e. the aerosol number concentration decreases to 1/e of its initial value in about 5.5 hours. Overall, this reference experiment showed that new particle formation due to contamination of the Teflon chamber walls can be excluded for our measurements.

On a typical measurement day, the assembly of OzCa and the instruments started early in the morning before 06:00 (all time designations are made in local time; UTC +8) in order to begin measuring before sunrise. In the field, all instruments were powered by 12 V car batteries.

The water layer at the bottom of the mobile observational chamber was periodically analyzed. The H_2O_2 content of the water layer was determined with test strips (Quantofix, Peroxyde 25, Macherey-Nagel, Germany). Additionally, pH values, the redox potential Eh, the water temperature, and the concentration of dissolved oxygen of the salt lake water were measured with a flow cell driven by a peristaltic pump (TP 3005, Thölen Pumpen, Germany), while the data were logged by a WTW 3430 multimeter (WTW, Germany). These parameters, especially the H_2O_2 concentrations, were recorded to evaluate the potential influence of a Fenton reaction of dissolved iron species on the formation of organic species, which may contribute to the formation of nucleation mode particles (details are discussed in section 4.4).

2.3 Online instrumentation at the chamber

In order to measure particle number size distributions in a remote environment, a field portable differential mobility particle sizer (DMPS) was custom-built. The DMPS, which is installed in a rugged box (36 cm x 36 cm x 21 cm), consists of a Minispiral blower (Model SE12RE21SA, Ametek, USA) to provide the sheath flow; two HEPA filters (CAP36, Whatman) to remove particles in the sheath flow; one air mass flow sensor (AWM 5104 VN, Honeywell, USA) to control the sheath flow loop; a custom-built radial differential mobility analyzer (rDMA) following the design of Zhang et al. (1995) with modifications by Gonser and Held (2013); a humidity and temperature sensor (GE ChipCap, CC-R); a custom-built control board; a positive high voltage supply from 7 to 12 500 V to control the rDMA (HCE7-12500 POS, fug, Germany); and a National Instruments USB-6008 data acquisition device. Aerosol particles were counted with a condensation particle counter CPC Series 5.400 (GRIMM Aerosol Technik, Germany).

Aerosol was sampled from the chamber through 0.8 m of copper tubing (1/4 inch outer diameter). Before entering the DMPS system, the aerosol was brought into charge equilibrium with an annular dielectric barrier discharge (aDBD) neutralizer (GRIMM Aerosol Technik; Pesch et al., 2013). The aDBD was operated with an AC current at a frequency of 20 kHz and a voltage of 7.4 kV. The aDBD sample flow rate of 0.3 l min^{-1} corresponds to the flow rate of the CPC. The size distribution was measured with a time resolution of 5 minutes for one up- and downscan, corresponding to a 10 minute total scan time, within a diameter range between 5 and 220 nm in 18 size bins. Positively charged particles were selected in the rDMA. The measured mobility distributions were inverted by taking into account the diffusing transfer function of the rDMA (Zhang and Flagan, 1996) and the bipolar charge distribution (Wiedensohler, 1988).

Additionally, ozone mixing ratios inside of the chamber were measured with an ozone analyzer Model 205 (2B Technologies, USA). Further, the air temperature was measured inside the chamber with a PT-100 sensor. Outside of the chamber, global radiation was measured with a calibrated Siemens BPW21 photodiode. Air temperature and relative humidity were measured with a ventilated and radiation-shielded psychrometer using PT-100 sensors.

2.4 Sampling for offline analysis

Inside of the mobile observational chamber, aerosol samples were collected on aluminium substrates with a Sioutas cascade impactor (SKC, USA) at a flow rate of 9 liters per minute on four stages covering the diameter range from 250 nm to 10 µm. Particles smaller than 250 nm in diameter were collected on a PTFE backup filter. Additionally, open filter holders were loaded with polycarbonate, silica and PTFE filters in order to collect aerosol particles formed directly above salt lakes for subsequent analysis of the chemical composition. At one specific lake, filter samples were also collected from a smaller PTFE chamber (Mini OzCa; 50 x 50 x 60 cm) over a period of 82 hours.

Gas samples were taken hourly with 2 L electropolished stainless steel canisters that were evacuated with a rotary vane pump and a turbomolecular high vacuum pump to less than 10-3 mbar. At the sampling site, valves were opened for gas to flow into the evacuated canister, and a compressor pump (N814KTDC, KNF Neuberger, Germany) was connected to fill the canister.

3 Chemical characterization of sampled aerosols and vapours

For a general chemical characterization, the following offline methods were used in addition to the in-situ measurements to analyze the composition of the aerosol and gas phase samples collected in the field:

Multisensor hyperspectral imaging for an image-based chemical analysis of precipitated coarse mode particles (Lohninger and Ofner, 2014; Ofner et al., 2015) combines Raman and elemental imaging. Due to the fact that confocal Raman micro-spectroscopy is a surface-sensitive technique, thin layers of organic material can be analyzed. To enhance the spectral information related to organic layers and to allow the allocation of single vibrational features, single-spot Raman micro-spectroscopy was applied to selected coarse-mode particles focusing on the organic layer.

Furthermore, the organic particle phase was characterized in detail by high-resolution mass spectrometry. Due to the benefit of a high-resolution Fourier-transform mass spectrometer, molecular formulas were directly obtained, allowing a classification of halogen-, nitrogen-, sulfur-, and oxygen-containing organic species.

Gas-chromatography for the chemical analysis of gas phase samples yields information about organic precursor species, which may contribute to SOA formation.

3.1 Multisensor Hyperspectral imaging and Raman spectroscopy

Particles in the aerodynamic diameter range between 250 nm and 10 µm collected with the Sioutas impactor on aluminium foils were analyzed using chemical imaging and electron microscopy. Because particle collection by impaction on aluminum foils was limited to the size range from 250 nm to 10 µm, only the accumulation and coarse mode were chemically characterized. However, we suggest that organic coatings found on coarse-mode particles are similar to compounds contributing to nucleation mode SOA. The combination of hyperspectral confocal Raman microscopy (Dieing et al., 2011) and scanning electron microscopy with energy-dispersive x-ray spectroscopy (SEM-EDX) imaging allows for a detailed characterization of the collected aerosol particles (Batonneau et al., 2006).

For hyperspectral Raman imaging, a LabRam 800HR Raman microscope (HORIBA Jobin Yvon GmbH) was used. The images were acquired using a 532 nm frequency-doubled NdYAG DPSS laser (nominal power 50 mW; operated at 25 %) at an acquisition time of 0.2 s per spot. An area of 100 x 100 μm^2 at a step-size of 1 µm was mapped using a 50-times Olympus objective lens (NA 0.75). Rayleigh scattering of the laser was filtered using a holographic super notch plus filter (Kaiser Optical Systems, Inc.). Spectra were recorded using an Open-Electrode-CCD (HORIBA Jobin Yvon GmbH, Synapse OE-CCD) and the software package LabSpec 6 (HORIBA Jobin Yvon GmbH). The aluminium foils were analysed afterwards with a FEI Quanta 200 scanning-electron microscope, equipped with an energy-dispersive x-ray (EDX) detector for imaging (EDAX Phoenix), operated at an acceleration voltage of 20 kV. Both instruments examined the same area of the foils.

Both hyperspectral datasets were analysed using the software package Imagelab (Epina Software Labs – www.imagelab.at). The single hyperspectral datasets were combined to one multisensor hyperspectral

dataset and subsequently analysed (Lohninger and Ofner, 2014; Ofner et al., 2015). By combining vibrational imaging and electron microscopy with energy-dispersive x-ray spectroscopy, molecular information as well as elemental composition at a high lateral resolution is provided.

3.2 High-resolution mass spectroscopy

Aerosol samples collected with open-faced filter holders were analyzed by ultrahigh resolution mass spectrometry using a SOLARIX Fourier transform ion cyclotron resonance mass spectrometer (FT-ICR/MS; Bruker; Bremen, Germany). The FT-ICR/MS was operated with a 12 Tesla superconducting magnet and an Apollo II electrospray source in negative mode (Schmitt-Kopplin et al., 2010). Before the analysis, the sample filters were desalted by extraction with water to eliminate the high salt concentrations in the sample. Without this step, it may be impossible to distinguish between chlorine-adducts (Boutegrabet et al., 2012) and organohalogens contained in the deposited SOA. Also, some signals of nitrogen-containing and sulfur-containing compounds may be suppressed otherwise. The organic matter deposited onto the filter was enriched by solid phase extraction (SPE) using C18 cartridges (Schmitt-Kopplin et al., 2012).

Analysis results are presented in van Krevelen diagrams showing the hydrogen/carbon (H/C) and oxygen/carbon (O/C) ratios of the individual compounds, which allows a detailed analysis of the oxidation state of organic species, especially in combination with the averaged carbon oxidation state (Ofner et al., 2012).

3.3 Analysis of the gaseous samples

Whole air canister samples were analyzed using a multi-detector GC/MSD/FID/ECD instrument (Agilent 7890 GC/5973 MSD) interfaced to a Markes Unity II Thermal Desorption Unit. Quantitation of the samples was performed by comparison to a working whole air standard that was calibrated against known mixtures, either directly or by dynamic dilutions. Every canister was measured twice and the multi-detector GC/MSD/FID/ECD was run with an internal standard to confirm the steadiness of the measurements. The detected differences were lower than 7 % for all compounds. Besides reduced sulfur compounds and halogenated VOCs, the samples were analyzed for monoterpenes to asses the role of certain VOCs for particle formation. The analysis included α-pinene, limonene, delta-3-carene and 1,8-cineole.

4 Results and Discussion

4.1 Characterization of measurements outside and inside the chamber

In order to identify new particle formation (NPF) events above the salt lake of interest, particle size distributions were measured inside of OzCa. Every full hour, the aerosol inlet was changed from chamber air to ambient air for one up- and downscan of the particle size distribution, and for about 2 min measuring the total particle number concentration outside and inside the chamber. Thus, the measurement of the evolution of the particle size distribution inside the chamber was disrupted for a total of approximately

12 minutes. For visualization of the temporal evolution of the particle number size distributions inside the chamber, the gaps due to ambient measurements were linearly interpolated. The ambient measurements were conducted in order to compare the development of aerosol concentrations both inside and outside of the chamber, and thus, the enrichment of particles in the chamber.

As an example, a comparison of measurements outside and inside the mobile chamber is shown in Fig. 4 for Lake Bean on 29 March. The measurements started at 06:30 under foggy conditions.

The comparison of particle number concentrations from hourly ambient measurements and the chamber measurements initially shows a similar evolution inside and outside the chamber (Fig. 4a-b). The background concentration was higher outside the chamber before the NPF started. During NPF (Fig. 4c), the particle concentration inside the chamber increased strongly. Due to prevented mixing and dilution, newly formed particles were enriched in the 2.3 m³ volume of the chamber compared to the outside air.

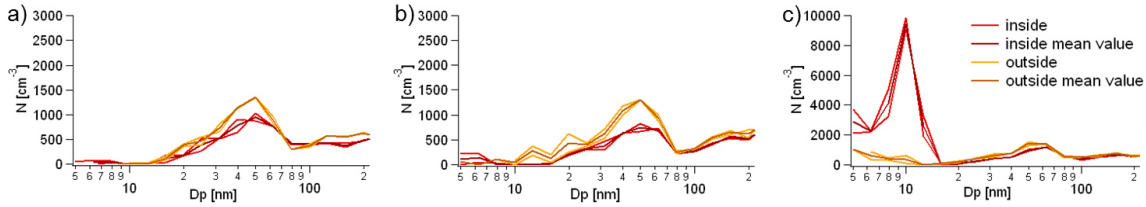

Figure 4. Comparison of chamber and ambient air measurements on 29 March at Lake Bean: the evolution of particle size distributions inside (red lines) and outside (yellow lines) the chamber are shown for a) 08:00, b) 09:00 and c) 10:00. The light red/yellow line denote the up- and downscan of the particle size distribution and the dark red/yellow line the mean value of the scan, respectively.

4.2 Evolution of particle size distributions during chamber experiments

We measured the evolution of the particle number size distribution directly above various salt lakes inside of the mobile chamber OzCa on eleven days between 8 and 29 March, 2013. The salt lakes are listed in Table 1 with geographical coordinates, measurement date, as well as pH value, H_2O_2 concentration and iron content of the lake water, which may be controlling factors of particle formation and explain increased particle number concentrations. New particle formation events were identified according to the three following criteria modified after Dal Maso et al. (2005):

1. particles in the diameter range from 5 nm to 20 nm (nucleation mode) must be present
2. the nucleation mode persists for at least one hour
3. the nucleation mode shows continuous growth

The geometric mean diameter between 5 and 20 nm ($GMD_{5\text{-}20\ nm}$) was calculated to identify NPF events. Only if the $GMD_{5\text{-}20\ nm}$ showed a clear drop and increase afterwards, an NPF event was identified and selected for further analysis. This procedure excludes brief periods of concentration maxima in the nucleation mode.

On every measurement day, particles were observed in the diameter range between 5 nm and 20 nm. However, two measurement days were excluded from further analysis and were not classified as NPF event days. On these two non-event days at Lake Orr (19 March) and Lake Kathleen (24 March), the particle background above 40 nm was as high as or even higher than the concentration of particles smaller than 20 nm, and the maximum total particle number concentration was much lower than for the other nine days of measurement (see Tab. 1).

Five days of measurement were also not evaluated in detail, even though NPF was observed. Those measurements were conducted at Lake Boats on 8 March, Lake Strawbridge on 9 March, Lake Dune on 14 March, Lake Shot on 22 March and Lake Dune on 23 March. Most of these lakes were highly acidic with a pH < 3.5 except for Lake Strawbridge with a pH value of 7.0 (Tab. 1). The measured maximum particle number concentrations ranged from 25 000 cm^{-3} (Lake Shot) to 247 000 cm^{-3} (Lake Dune; setup above aged eucalyptus leaves).

Four observational days at four different lakes were chosen for a detailed analysis of the number size distribution evolution (Fig. 5). The pH values of the four lakes ranged from acidic to neutral with pH 2.8 at Lake Boats on 18 March, pH 2.9 at Lake Dune on 13 March, pH 3.5 at Lake Shot on 21 March, and pH 7.1 at Lake Bean on 29 March. Usually, Lake Bean is also an acidic lake but it had been diluted due to heavy rainfalls just before the measurements.

The starting time of a NPF event was directly identified from a sudden drop of the $GMD_{5\text{-}20\ nm}$. On 13 March at Lake Dune, the first NPF event phase was observed starting at 8:00, when the temperature was about 22 °C and solar irradiance reached a value of almost 400 W m^{-2} (Fig. 5a). The hourly measurements of H_2O_2 concentrations in the lake water showed a value between 0.5 and 2 mg l^{-1} at 8:00, while H_2O_2 had not been detected before. About one hour later, the main NPF event began. It is striking that the irradiance increased distinctly to a value of 550 W m^{-2} just before this event phase. The temperature was 25 °C, and the pH value of the lake water clearly decreased before the event started. Similar drops or local minima of the pH value were also found after 10:30, when nucleation mode particles showed growth. At 10:00, H_2O_2 concentrations rose to 2 mg l^{-1} and remained constant until 14:00. Subsequently, H_2O_2 decreased below the detection limit (0.5 mg l^{-1}) within three hours.

On 18 March at Lake Boats, a first weak NPF event phase started at 07:16 without any remarkable changes in meteorological parameters (Fig. 5b). The main event started at 09:17 coincident with a rise of temperature and solar radiation. Later, periods with very low particle concentrations were observed. H_2O_2 concentrations were below the detection limit at this lake.

On 21 March at Lake Shot, there was one clear NPF event at 09:30 (Fig. 5c). Temperature and irradiance increased strongly before the start of the event, and fluctuated between 25 and 30 °C and 350 to 700 W m^{-2} during the NPF event. The H_2O_2 concentration was 2 mg l^{-1} when the event started, and increased to 5 mg l^{-1} at noon, when the particle number concentration reached its maximum.

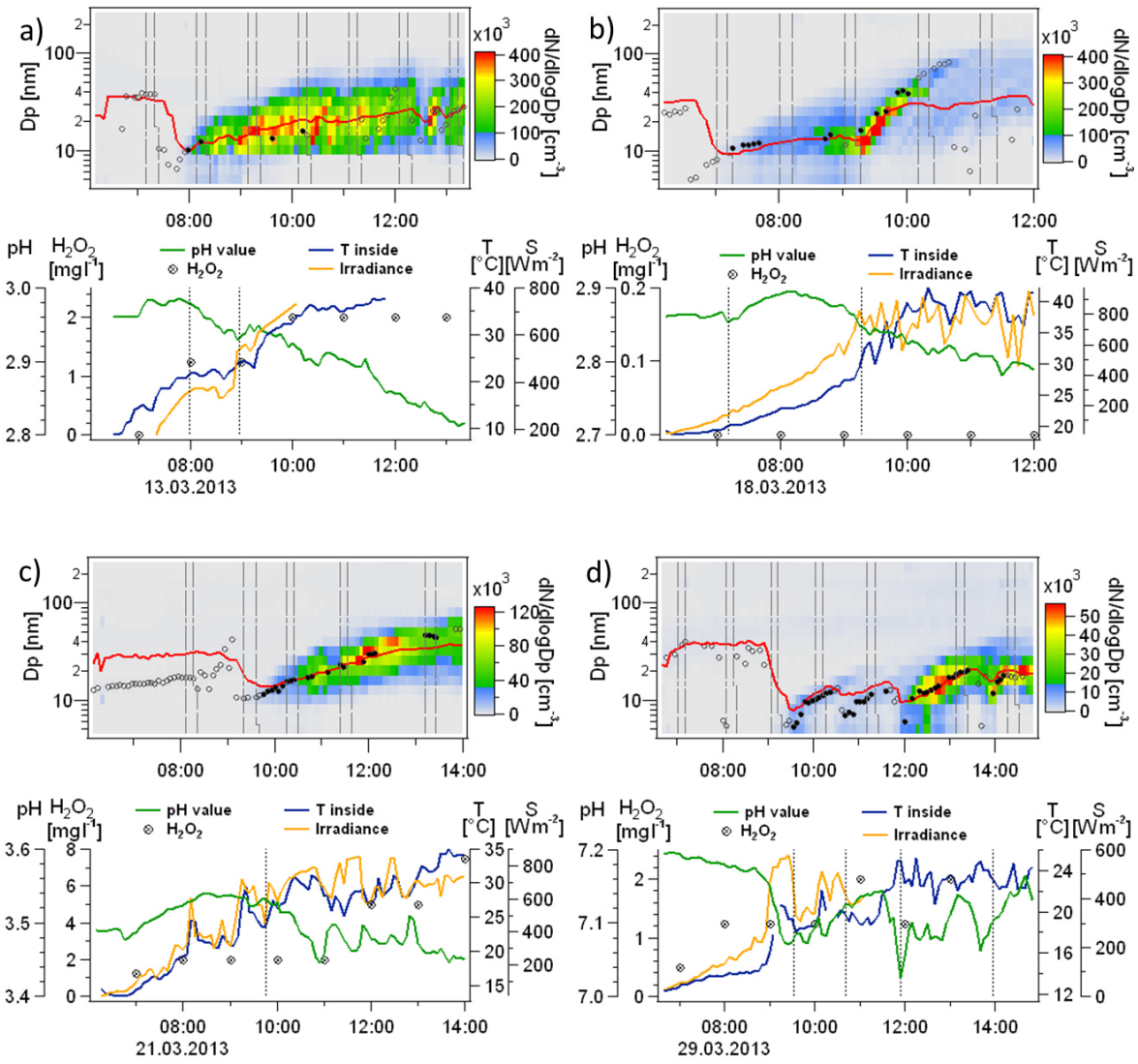

Figure 5. Particle size distributions with geometric mean diameter $GMD_{5\text{-}60\ nm}$ (red line) and mode diameter determined by the mode-fitting method (circles), pH values and H_2O_2 concentrations of lake water, air temperature T and irradiance S a) on 13 March at Lake Dune, b) on 18 March at Lake Boats, c) on 21 March at Lake Shot, and d) on 29 March at Lake Bean. Interpolated periods due to hourly ambient measurements are indicated by grey broken lines in the image plots. Starting times of NPF events are indicated by vertical dotted lines in the lower figure parts, respectively.

On 29 March at Lake Bean (Fig. 5d), the air temperature was below 15 °C until 09:00 due to foggy conditions. On all other days, the temperature rose quickly beyond 15 °C before 08:00. Particle formation was not expected under these cold and humid conditions. At 09:00, the cloud cover suddenly disappeared and the irradiance increased from 250 to nearly 600 W m^{-2}. Obviously, the first and second NPF event phases are directly related to changes in irradiance. The start of these weak events coincides with distinct maxima of irradiance, respectively. These event phases exhibit lower particle concentrations than the two following stronger NPF event phases. The main event of this day started around noon, lasted about 2 hours

and merged into the fourth, final event phase. Again, the lake water pH exhibits pronounced local minima directly before NPF.

Inside the chamber, ozone mixing ratios (not shown) typically ranged from 20 to 30 ppb with little variation and no strong increase or decrease before or during NPF events. It is striking that the maximum particle number concentrations (cf. Tab. 1) are much higher on 13 and 18 March compared to 21 and 29 March. This is consistent with a higher air temperature and irradiance on those two days.

Obviously, the main NPF events do not start at air temperatures below 25 °C. At lower temperatures, brief events may start which are either masked by weaker NPF event phases (e.g. on 18 March before 09:00, and on 29 March before noon) or do not show distinct particle growth like on 18 March before 9:00. On the other hand, in all four cases the temperature showed a distinct increase directly before the main event started. Also, the irradiance was always greater than 500 W m^{-2} and started to rise before or when the daily main event was initiated. A decline in the pH value of about 0.1 was observed directly before the main NPF event at three of the four analyzed dates (13, 18, 29 March). This suggests that NPF may be related to pH-dependent aqueous-phase chemistry. A direct relation of NPF and H_2O_2 concentrations was not found.

4.3 Particle growth rates

We determined the particle growth rate (GR) by applying a linear regression analysis to the temporal evolution of the geometric mean diameter from the lowest diameter, i.e. 5 nm, to 60 nm ($GMD_{5\text{-}60nm}$) similar to Place Jr. et al. (2010) and Held et al. (2004). For all linear regression analyses, the coefficient of determination R^2 was greater than 0.9, indicating a good linear relationship, and thus, constant growth rates. The GMD-derived growth rates were compared with growth rates determined by the mode-fitting method (MFM; cf. Tab. 2) as suggested in Hussein et al. (2005). Here, a maximum of three modes were fitted to the original number size distributions. In the MFM, the particle growth rate was determined by tracking the growth of the nucleation mode fitted to the diameter range from 7 to 20 nm. In some cases, the growing nucleation mode may grow into a larger mode. Therefore, the growth rates determined by the mode-fitting method have been manually validated.

Table 2. Comparison of growth rates during NPF events derived from the $GMD_{5\text{-}60nm}$ and the mode-fitting method (MFM).

date	event number	starting time	$GMD_{5\text{-}60\ nm}$ [nm h^{-1}]	MFM [nm h^{-1}]
13 March	1	07:59	8.4	8.7
	2	08:58	6.5	4.1
18 March	1	07:16	2.9	2.2
	2	09:17	25.4	36.4
21 March	1	09:46	6.5	9.6
29 March	1	09:33	8.1	8.0
	2	10:42	4.7	6.4
	3	11:55	7.4	10.0
	4	13:57	18.6	24.5

In Fig. 5, black circles represent the nucleation mode derived from the mode-fitting method, and red lines represent the $GMD_{5\text{-}60nm}$. Growth rates were compared from the start of an event phase as indicated in Table 2. On 13 March, the first nucleation event starting at 7:59 showed a GR = 8.4 nm h^{-1} derived by $GMD_{5\text{-}60nm}$, and 8.7 nm h^{-1} derived by MFM (Fig. 5a; Tab. 2). The main event on 13 March occurred directly after the end of the first event, with a GR of 6.5 nm h^{-1} ($GMD_{5\text{-}60nm}$) compared to 4.1 nm h^{-1} (MFM).

The first nucleation event on 18 March showed a growth rate of 2.9 nm h^{-1} derived by the $GMD_{5\text{-}60nm}$ between 07:30 and 09:00. In comparison, the MFM growth rate is slightly smaller (Fig. 5b; Tab. 2) with a value of 2.2 nm h^{-1}. The main event starting after 09:00 exhibited a growth rate of 25.4 nm h^{-1}. In the beginning, the GMD follows the number concentration maximum, but after 10:00, the slope is obviously too small. This indicates that the concentration maximum rises above the 60 nm limit used for computation of the $GMD_{5\text{-}60nm}$. Overall, it seems that the MFM better reflects the growth of this event.

On 21 March, the growth rates derived from MFM and $GMD_{5\text{-}60nm}$ are also in good agreement (Fig. 5c; Tab. 2). From 10:00 until the end of the measurement, MFM diameters and $GMD_{5\text{-}60nm}$ show a similar behavior. Only at the end of the event after 13:00, the mode-fitting method yields larger diameters than the GMD. Therefore, the GRs differ by a factor of 1.5 with values of 6.5 nm h^{-1} (GMD) and 9.6 nm h^{-1} (MFM).

On 29 March, the agreement between GMD and MFM is best during the first event (Fig. 5d; Tab. 2). The second and later events are influenced by larger particles formed during the previous event. Therefore, the growth rate derived from $GMD_{5\text{-}60nm}$ is smaller than the GR derived from MFM.

4.4 Hydrochemistry and organic precursor gases

Comparing the four measurement days with respect to the pH value (Tab. 1), it is striking that the lakes with the lowest pH values, Lake Boats and Dune, show the highest particle number concentrations during the course of the day while Lake Bean, the lake with almost neutral pH values, shows the lowest particle number concentration (Tab. 1). This is consistent with the general finding that neutral lakes tend to produce fewer particles or do not show new particle formation at all (cf. Lake Kathleen, Tab. 1). Besides the lowest pH value, Lake Boats also shows the earliest start of NPF compared to the other three days, the highest particle growth rate and the highest concentrations of Fe(II) and Fe(III) in the lake water. Fe(II) concentrations in Lake Boats reached 213 mg l^{-1} while Fe(II) concentrations in all other lakes were below 10 mg l^{-1}. Similarly, the Fe(III) concentration in Lake Boats was up to 11 mg l^{-1} compared to a maximum of 3 mg l^{-1} in all other lakes. Because H_2O_2 was not detected in the waters of Lake Boats, one might speculate that H_2O_2 was converted to OH radicals, and Fe(II) was oxidized to Fe(III) in a Fenton reaction. OH radicals might oxidize VOCs, react with sulfuric acid in the aqueous phase to form sulfate radicals (Tang et al., 1988), or activate halogens that react with organic matter to form halogenated volatile organic carbons (VOX) already in the aqueous phase. VOX and VOC could then act as SOA precursors. The lowest particle number concentration of the four lakes of interest was observed at Lake Bean. Here, the concentration of Fe(III) was higher than Fe(II) (Tab. 1). This was also visible in the orange-brownish color of the lake water. Comparing all lakes, only Lake Bean and Lake Kathleen, which is also a pH neutral lake, showed this unique feature of higher Fe(III) than Fe(II) concentrations. The conversion of Fe(II) to Fe(III) in the presence of organic matter indicates a Fenton reaction. In laboratory experiments above a simulated salt lake mixture, Kamilli et al. (2015) found a key role of the Fe(II) concentration for particle formation. With increasing

Fe(II) concentrations, an increasing chemical diversity of the organic aerosol was observed, while the formed particle number and volume concentrations decreased. In these experiments, Fe(II)-controlled reactions in the aqueous phase competed with SOA formation in the gas phase, thus decreasing the new particle formation potential (Kamilli et al., 2015). Even though the laboratory experiments were performed under acidic conditions, these observations suggest a coupling of aqueous-phase chemistry and particle formation. Therefore, we suggest an influence of aqueous-phase chemistry on aerosol formation related to natural salt lakes as well. Organic aerosol compounds resulting from halogenation or sulfonation of oxygenated organics (cf. section 4.5) give additional evidence for the relevance of aqueous-phase reactions for particle formation. While the role of Fe(II) in natural particle formation cannot be quantified from our observations due to the complexity of the natural system, the onset of the main particle formation event just after a decline of the pH value is consistent with the proceeding of a Fenton reaction, favored at low pH values. In acidic waters, the oxidation of Fe(II) leading to the formation of reactive oxidants is believed to be one of the main mechanisms through which organic compounds are oxidized (Southworth and Voelker, 2003). However, under neutral and basic pH conditions, Fe(II) is quickly oxidized to form Fe(III) hydroxides in the presence of oxygen (O_2), and Fe(II) is therefore no longer available for the redox cycle (Remucal and Sedlak, 2011).

Many different volatile organic compounds were found in gas samples taken from the mobile chamber. These VOCs do not originate from direct plant emissions since the chamber is only open to the lake water and soil. We propose that VOCs are released from the organic-enriched layer located below the salt crust of the salt lakes, where eucalyptus litter is decomposed. The most abundant monoterpene found in the gas samples taken from the mobile chamber was 1,8-cineole with daily maximum mixing ratios ranging from <0.5 to 23.1 ppb.

Obviously, VOCs are enriched in the mobile chamber, leading to high mixing ratios of potential organic precursor gases which could explain the observed particle growth. A detailed analysis of the particle growth dynamics and its relation to organic precursor concentrations is not possible due to the 1-hr time resolution of the gas sampling, the lack of oxidant concentration data other than ozone, and the limited information about the detailed chemical reaction mechanisms. Co-condensation of a variety of oxidation products of the abundant organic precursor gases may fully explain the observed particle growth. However, we do not find a simple correlation of individual organic precursor gas concentrations and observed growth rates. For example, Lake Shot shows the highest mixing ratios of 1,8-cineole but only moderate particle growth rates. This may indicate that particle growth is promoted by many different precursor species which may have not been fully taken into account. Overall, we hypothesize that organic precursor gases are available in sufficient concentrations to explain the observed particle formation events, however, the production of condensable vapors for new particle formation and growth is dependent on additional factors such as oxidant concentrations and meteorological conditions.

4.5 Chemical characterization of aerosol samples

4.5.1 Multisensor hyperspectral imaging of coarse mode particles

Particles collected with the Sioutas impactor were analyzed by combined multisensor Raman and SEM-EDX hyperspectral imaging. The hyperspectral image obtained from the Raman mapping system exhibits typical Raman bands for inorganic species as well as organic compounds. The hyperspectral EDX data was used to characterize non-Raman active species and further allocate elemental distributions to Raman active areas of the images.

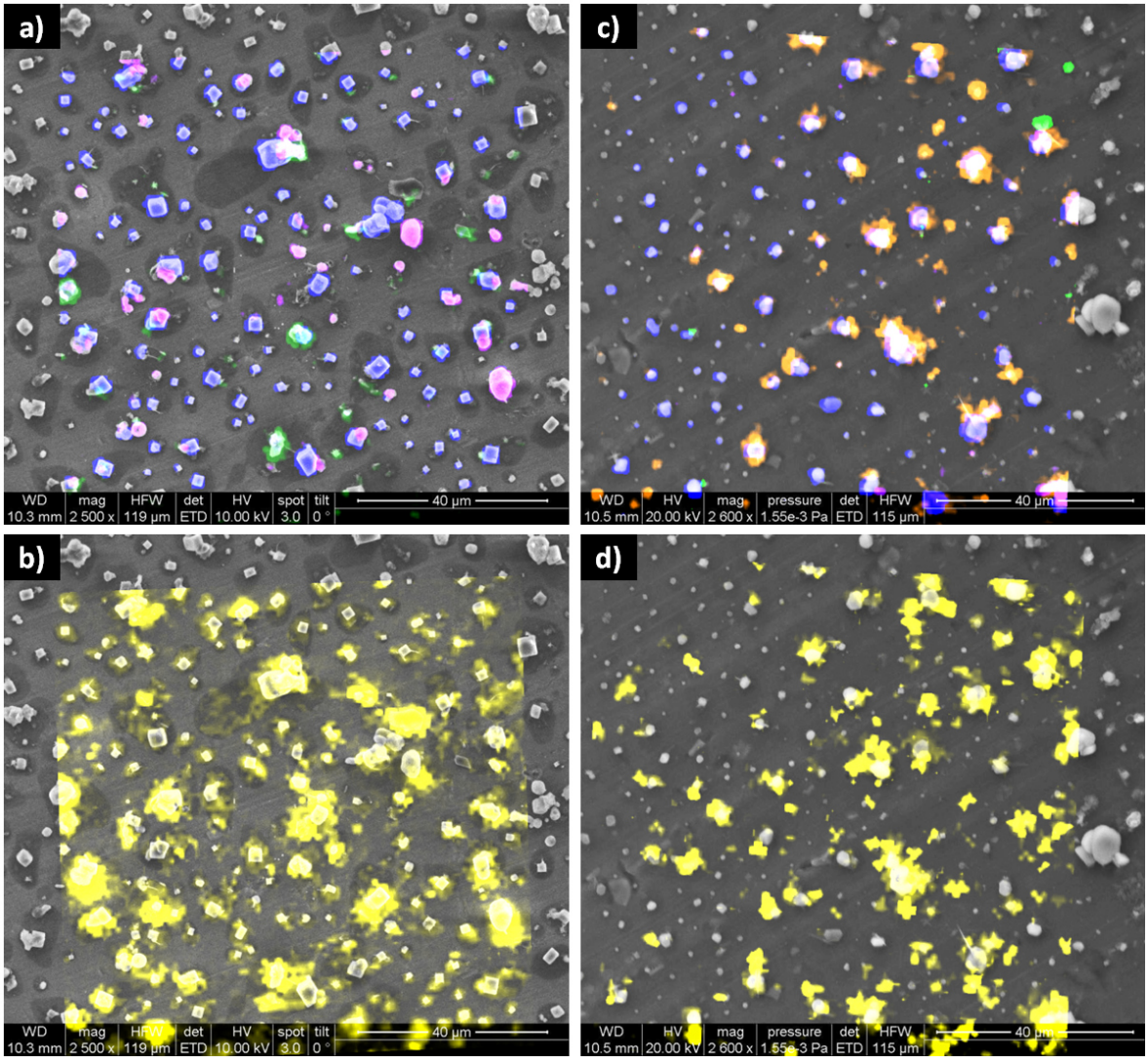

Figure 6. Hyperspectral images (Raman combined with SEM-EDX) of coarse-mode aerosol (Sioutas impactor stage B (>1 µm)) above Lake Dune (a, b) and Lake Shot (c, d): inorganic species implying NaCl (blue), silicates (violet), $CaSO_4$ (green) and $NaNO_3$ (orange) are depicted on top (a, c); organic species in yellow below (b, d).

The chemical composition of the coarse-mode particle fraction with diameters > 1 µm collected at Lake Dune (13 March) and Lake Shot (Mini OzCa; 22 to 24 March) is shown in Fig. 6. The main components are sodium chloride (obtained from EDX as chemical maps of Na and Cl; Fig. 6a, c: blue), silicates (obtained from EDX as chemical maps of Si and O; Fig. 6a, c: violet), $CaSO_4$ (Fig. 6a, c: green) and $NaNO_3$ (Fig. 6a, c: orange). $CaSO_4$ and $NaNO_3$ were identified by the characteristic Raman spectra and chemical maps from the EDX data containing Ca, S and O (calcium sulfate), or Na and O (sodium nitrate), respectively. For the Raman allocation, reference spectra from pure chemicals were compared to extracted spectra from the Raman hyperspectral data. Samples from all investigated lakes exhibit a strong contribution of NaCl to the coarse mode. Lake Dune is additionally characterized by silicates and $CaSO_4$. Lake Shot coarse-mode aerosol is composed of NaCl, $NaNO_3$, silicates and $CaSO_4$ (in descending importance). The Raman hyperspectral data further reveals a strong coating of almost all coarse-mode particles with an organic layer at the two lakes. To obtain the image of the organic compounds (Fig. 6b, d: yellow), the hyperspectral data were analyzed according to the C-H stretch vibration spectral region (2750-3000 cm^{-1} Raman Stokes shift). Further, soot (characterized by a significant Raman spectrum; D and G band of graphene at 1350 and 1600 cm^{-1}) was allocated to the organic species. This allocation is based on the formation of soot by burning of organics caused by the high Raman laser power. The fact that soot spectra were also correlated to coarse-mode particles exhibiting coating of the coarse-mode with burned organics, and no single soot particles could be found, supports the interpretation of soot as organics burned by the Raman laser. The organic material found on coarse-mode particles is probably due to condensation of secondary organic compounds, which may also contribute to the observed formation of the nucleation mode. The presence of the coarse mode itself might be explained by preexisting coarse-mode particles, and a slight exchange of chamber and ambient air, since the chamber was not supposed to be a hermetically sealed system like an aerosol chamber in a laboratory environment.

4.5.2 Raman microspectroscopy of the organic phase

To analyze the chemical signature of the organic species in more detail, single Raman micro-spectra of organic spots were recorded. Two spectra were analyzed according to characteristic Raman group frequencies (Socrates, 2001) both for Lake Dune and Lake Shot. The interpretation of the Raman spectra is based on potential chemical functional groups according to the chemical composition of the salt lakes. Thus, sulfuric and nitrogen containing functional groups were taken into account. Further, Raman spectra were analyzed according to biological fingerprints. The allocation of spectral features to functional groups is shown in Fig. 7. The spectral region of the $\nu_{aliphatic}$(C-H) vibration is very prominent in all samples. Correlated with the stretch vibration, the deformations $\delta(CH_2)$ and $\delta(CH_3)$ can also be found in the spectra at about 1450 cm^{-1}. Only spectrum 2 of Lake Dune exhibits an aromatic $\nu_{aromatic}$(C-H) stretch vibration. Also, the ν(C=O) vibration, which is weak in Raman spectra, was found in spectrum 2 of Lake Dune. Raman bands at 1600 cm^{-1} are characteristic for ν(C=C) vibrations, e.g. of terpenes, carboxylates ($\nu_{as}(CO_2^-)$) and nitrates ($\nu_{as}(NO_2)$ and ν(C=N)). The $\nu_s(CO_2^-)$ vibration at 1400 cm^{-1}, indicating carboxylates, is overlapped by the $\nu_{as}(SO_2)$ vibration of covalent sulfonates. These bands are only present in Lake Dune spectrum 1, and Lake Shot spectrum 2. Thus, carboxylates are likely species in these two samples. $\nu_{as}(SO_2)$ and $\nu_s(NO_2)$ bands are present in all spectra. Symmetric $\nu(SO_2)$ bands could be found for all samples, especially as sulfones for Lake Dune spectrum 2. $\nu_s(SO_2)$ vibrations of sulfones and organic sulfate salts are present in all spectra.

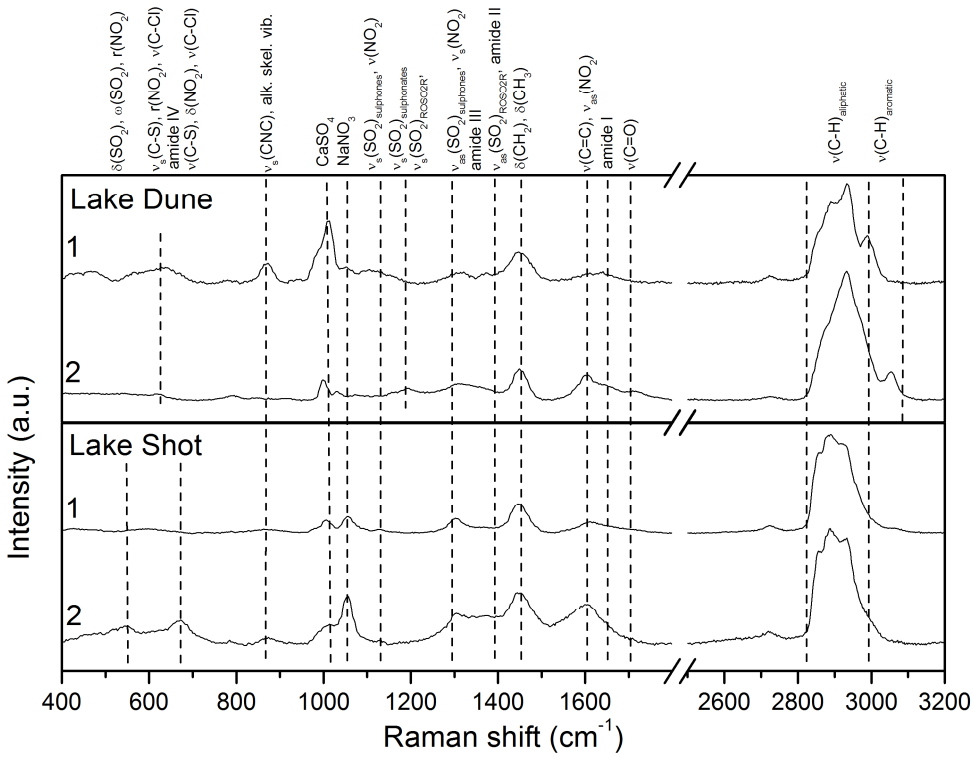

Figure 7. Raman spectra of organic species found in the coarse-mode samples of Lake Dune and Lake Shot. The spectral region of the $\nu_{aliphatic}$(C-H) vibration is very prominent in both samples, whereas only spectrum 2 of Lake Dune exhibits an aromatic C-H stretch vibration. Contribution of $NaNO_3$ to the spectra is more pronounced at Lake Shot.

Due to a contribution of $CaSO_4$ and $NaNO_3$ to the spectra, bands between 1000-1100 cm^{-1} Raman shift were not analyzed. Hence, the interpretation of possibly existing aliphatic ethers ν_s(C-O-C) (1140-820 cm^{-1}) is hampered. Lake Dune spectrum 1 and Lake Shot spectrum 2 exhibit a band at about 880 cm^{-1}. This band can be related to the ν_s(CNC) vibration of proteins or to skeleton vibrations of saturated aliphates. In these spectra, also the other amide bands can be found (amide 1 at 1655, amide II at 1400, amide III at 1300, and amide IV at 625 cm^{-1} (only Lake Dune)). Hence, a contribution of degraded biogenic material to the organic aerosol phase is likely. Lake Dune spectrum 1 and Lake Shot spectrum 2 also exhibit Raman bands below 700 cm^{-1}. Fundamental vibrations related to ν(C-S) and ν(C-Cl) but also NO_2 deformations and wagging vibrations could be found. While some spectra exhibit vibrations related to carboxylates or carbon-chlorine bonds, Raman bands related to organosulfates, organosulfate salts and organonitrates are present, and a contribution of these species to the organic phase is likely. The organic film on the coarse-mode particles is characterized by oxidized organic species with contributions of sulfates and nitrates. Overall, the formation of organosulfates and organonitrates both as covalent species and salts by degradation pathways caused by biological activity, temperature, pH and redox reactions of biogenic and biological material is proposed as the main formation pathway for the organic particle phase.

4.5.3 High-resolution spectrometry of the organic phase

In order to investigate the nature and origin of the organic particle phase in more detail, four filter samples from three lakes were analyzed by ultrahigh resolution FT-ICR/MS comprising (oxygenated) organics (CHO), chlorinated organics (CHOCl), sulfur-containing organics (CHOS), and nitrogen-containing organics (CHON). Figures 8a-d show the H/C and O/C ratios (van Krevelen diagrams) of the individual organic compounds (left panels), and the average carbon oxidation state (OS_c) as a function of carbon number n_c (right panels). Figure 8e shows the total number of individual CHO, CHOS, CHON, and CHOCl compounds found in the four samples (left), and the relative contribution of these four compound groups in the four samples (right). A night-time sample collected at Lake Dune (Fig. 8a) and a daytime sample collected at Lake Shot (Fig. 8b), both taken in the chamber OzCa, show a similar distribution of CHO, CHOS, and CHON compounds in the van Krevelen diagrams, and in the OS_c-n_c-diagrams. However, the Lake Shot sample exhibits a larger number of CHOS and CHOCl compounds than the Lake Dune sample. One possible explanation for the larger number of CHOS and CHOCl compounds at Lake Shot might be the higher contribution of daylight sampling, indicating the influence of photochemistry on the formation of CHOS and CHOCl.

A second sample collected at Lake Shot for a period of 82 hours in the mini OzCa chamber (Fig. 8c) exhibits a much larger number of individual compounds compared to the other samples (Fig. 8e). Particularly the highly oxidized CHO compounds with high O/C ratios increase. This also leads to the highest OS_c of CHO compounds (Fig. 8c, right), and higher n_c. Thus, with increasing sampling time the organic compounds reach higher oxidation levels, and oligomerization becomes important. In the van Krevelen diagram (Fig. 8c, left), the intensities of individual CHOS, CHON and CHOCl compounds are reduced, but the chemical diversity is increased, especially to higher O/C ratios. This implies further halogenation or sulfonation of highly oxidized CHO compounds.

In Fig. 8d, a sample collected in ambient air at Lake Bean is shown. The van Krevelen diagrams and the OS_c-n_c-diagrams of Lake Shot (Fig. 8b) and Lake Bean (Fig. 8d) show similar features, and a similar relative distribution of the compounds (Fig. 8e, right) implies that SOA formation in the mobile chamber is similar to SOA formation in ambient air. Despite a much longer sampling time at Lake Bean (73 hours) compared to Lake Shot (8.5 hours), the similar absolute number of individual compounds identified in the two samples (Fig. 8e, left) illustrates the concentration enrichment in the chamber.

Finally, a targeted FT-ICR/MS data analysis for organosulfates from monoterpenes (e.g. Surratt et al., 2008; Noziere et al., 2010) was performed. Organosulfates from α-pinene oxidation with a mass-to-charge ratio m/z = 265.075 ($C_{10}H_{17}O_6S$) were found in all four samples. Also, a potential organosulfate derived from 1,8-cineole ($C_{10}H_{17}O_9S$; m/z = 313.0593) was identified in the three-day sample collected at Lake Shot (mini OzCa; cf. Fig. 8c). In addition, two known atmospheric tracers for secondary organic aerosol from the oxidation of 1,8-cineole by OH, diaterebic acid acetate and diaterpenylic acid acetate (Iinuma et al., 2009), were identified in the samples. Thus, 1,8-cineole has been found in high concentrations in the gas phase, and oxidation products of 1,8-cineole were found in the aerosol phase, suggesting that 1,8-cineole was an important precursor for organic aerosol formation.

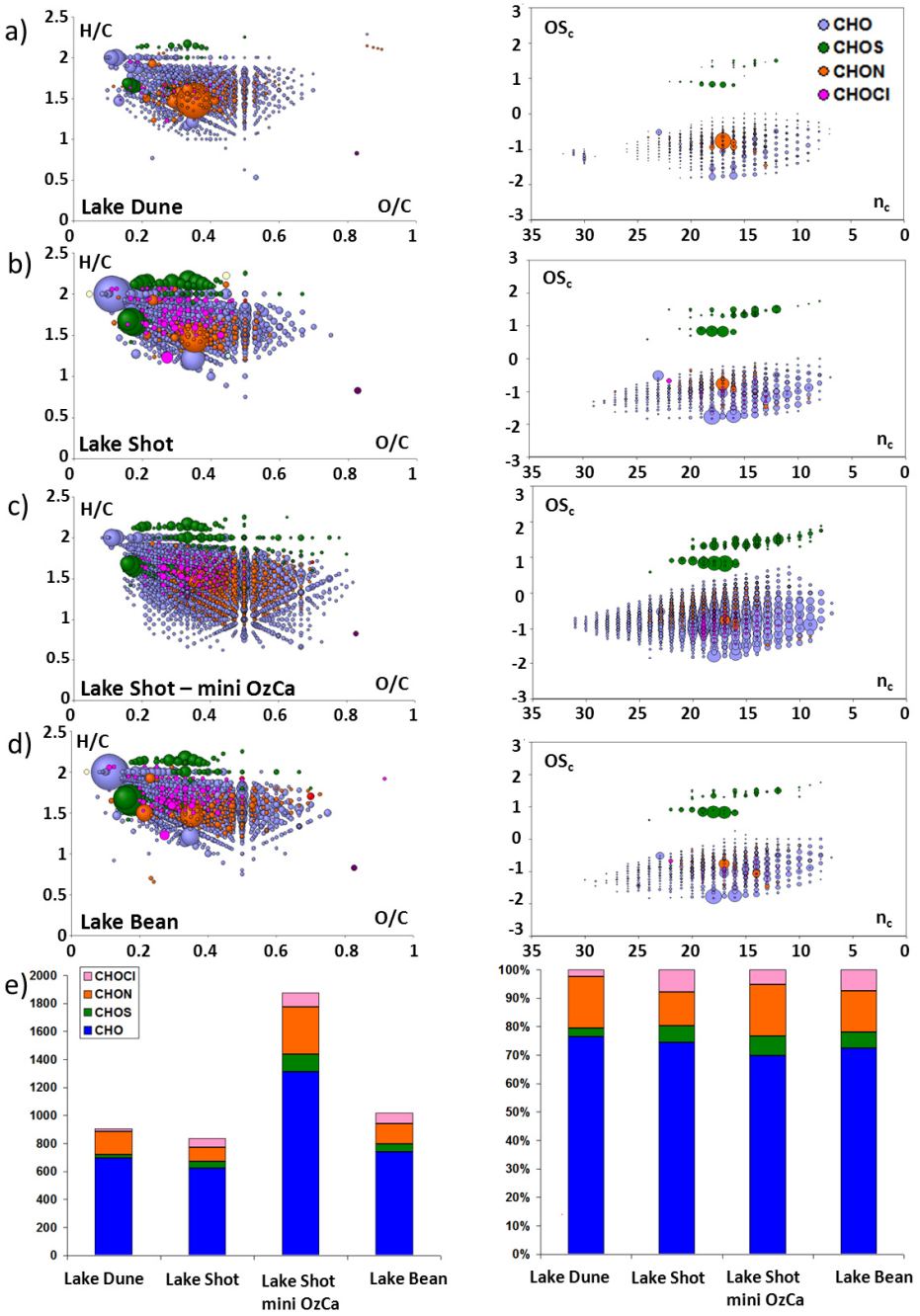

Figure 8. Van Krevelen diagrams (a-d, left) and the average carbon oxidation state (a-d, right) of the ultrahigh resolution mass spectra of filter samples taken during chamber experiments at a) Lake Dune starting in the afternoon to the next morning and b) Lake Shot from sunrise to the afternoon. With a small Teflon chamber (mini OzCa), samples were taken over a period of three days at c) Lake Shot, and ambient air samples were taken at d) Lake Bean for three complete days. The corresponding classification and relative distribution of individual compounds is depicted in e).

5 Conclusions

In situ measurements of new particle formation above salt lakes were carried out in Western Australia with a new approach using a mobile chamber. Aerosol formation was observed inside the chamber, and thus, directly linked to emissions from the salt lake. The soil layer located directly below the salt crust is enriched in organic compounds, which promotes the release of volatile organic compounds from the soil, and the accumulation of organic precursors in the chamber. This soil layer contains leaf litter primarily from decomposed leaves of the surrounding eucalyptus trees. Therefore, we expect soil emissions of volatile organic compounds characteristic of eucalyptus as well as reaction products of these compounds in the soil. In the chamber air, the emitted organic gases are oxidized, and oxidation products may contribute to new particle formation either by forming new particles, or by condensing on pre-existing particles and subsequent particle growth. NPF events have been observed above lakes with pH values ranging from 2.5 to 7.1.

The chemical processes inside of the mobile chamber OzCa are considered to be similar to atmospheric processes in ambient air. However, the total particle number concentration was typically enriched inside the chamber by a factor ranging from 2 to 16 after NPF. Also, trace gas concentrations were enriched inside the chamber. Consequently, particle growth by condensation is expected to proceed faster, and particle formation was observed earlier inside the chamber. Growth rates obtained in the chamber ranged from 2.9 to 25.4 nm h^{-1}. We attribute this finding to the enrichment of gases and particles inside the chamber.

The aerosol chemical composition above the salt lakes was investigated in detail by a combination of Raman spectroscopy, SEM-EDX, and ultrahigh resolution mass spectrometry. Due to field sampling limitations, chemical information about the freshly nucleated particles were not in the focus of this study. While halogenated organic compounds were found in the aerosol samples, a mixture of organic and sulfur-containing organic compounds (as identified with SEM-EDX, Raman spectroscopy, and ultrahigh resolution mass spectrometry) seems to control new particle formation in the study area. Also, the formation of organosulfates may indicate the potential influence of aqueous-phase chemistry, which has been further investigated in laboratory experiments (Kamilli et al., 2015).

In conclusion, this study directly linked new particle formation to salt lakes in Western Australia. To our knowledge, a comprehensive chemical characterization of the organic aerosol above Western Australian salt lakes combining Raman spectroscopy, SEM-EDX, and mass spectrometry has been given for the first time. Thus, these results contribute to a better understanding of new particle formation in salt lake environments, which may lead to enhanced numbers of cloud condensation nuclei, and potentially to a change in regional precipitation patterns.

Acknowledgements

The authors thank Franz X. Meixner (Max Planck Institute for Chemistry, Mainz) for providing the ozone monitor for this study. The research leading to these results has received funding from the German Research Foundation (DFG) grant HE 5214/5-1 and within the DFG research group HaloProc (FOR 763).

References

Addison, D.: Groundwater study of the Lake Grace townsite, Resource Management Technical Report 212, Agriculture Western Australia, Rural Towns Program, 2001.

Andreae, M. O., and Crutzen, P. J.: Atmospheric aerosols: Biogeochemical sources and role in atmospheric chemistry, Science, 276 (5315), 1052-1058, 1997.

Batonneau, Y., Sobanska, S., Laureyns, J., and Bremard, C.: Confocal Microprobe Raman Imaging of Urban Tropospheric Aerosol Particles, Environmental Science Technol., 40 (4), 1300–1306, 2006.

Boutegrabet, L., Kanawati, B., Gebefügi, I., Peyron, D., Cayot, P., Gougeon, R.D., Schmitt-Kopplin, P.: Chloride anion attachment to Sugars. Mechanistic investigation and discovery of a new dopant for efficient sugar ionization/detection in mass spectrometers, Chemistry, A European Journal, 18 (41), 13059-13067, 2012.

Buxmann, J., Balzer, N., Bleicher, S., Platt, U., and Zetzsch, C.: Observations of bromine explosions in smog chamber experiments above a model salt pan, Int. J. Chem. Kinet., 44, 312-326, 2012.

Cai, X., and Griffin, R. J.: Secondary aerosol formation from the oxidation of biogenic hydrocarbons by chlorine atoms, Journal of Geophysical Research: Atmospheres (1984–2012), 111, D14206, 2006.

Cai, X., Ziemba, L. D., and Griffin, R. J.: Secondary aerosol formation from the oxidation of toluene by chlorine atoms, Atmospheric Environment, 42 (32), 7348-7359, 2008.

Dal Maso, M., Kulmala, M., Riipinen, I., Wagner, R., Hussein, T., Aalto, P. P., and Lehtinen, K. E. J.: Formation and growth of fresh atmospheric aerosols: eight years of aerosol size distribution data from SMEAR II, Hyytiälä, Finland, Boreal Env. Res., 10, 323–336, 2005.

Dieing, T., Hollricher, O. and Toporski, J., Eds.: Confocal Raman Microscopy, Springer-Verlag, Berlin Heidelberg, 2011.

Esau, I. N., and Lyons, T. J.: Effect of sharp vegetation boundary on the convective atmospheric boundary layer, Agricultural and Forest Meteorology, 114, 3-13, 2002.

Ghauri, S.: Groundwater trends in the central agricultural region, Resource Management Technical Report 269, Department of Agriculture, 2004.

Gonser, S. G., and Held, A.: A chemical analyzer for charged ultrafine particles, Atmospheric Measurement Techniques, 6 (9), 2339-2348, 2013.

Held, A., Nowak, A., Birmili, W., Wiedensohler, A., Forkel, R., and Klemm, O.: Observations of particle formation and growth in a mountainous forest region in central Europe, Journal of Geophysical Research, 109, D23204, 2004.

Hope, P., Timbal, B., and Fawcett, R.: Associations between rainfall variability in the southwest and southeast of Australia and their evolution through time, Int. J. Climatol., 30, 1360–1371, 2010.

Hussein, T., Dal Maso, M., Petäjä, T., Koponen, I. K., Paatero, P., Aalto, P. P., Hämeri, K., and Kulmala, M.: Evaluation of an automatic algorithm for fitting the particle number size distributions, Boreal environment research, 10 (5), 2005.

Iinuma, Y., Böge, O., Keywood, M., Gnauk, T., and Herrmann, H.: Diaterebic Acid Acetate and Diaterpenylic Acid Acetate: Atmospheric Tracers for Secondary Organic Aerosol Formation from 1,8-Cineole Oxidation, Environmental Science & Technology, 43 (2), 280-285, 2009.

Junkermann, W., Hacker, J., Lyons, T., and Nair, U.: Land use change suppresses precipitation, Atmos. Chem. Phys., 9, 6531–6539, 2009.

Kamilli, K. A., Ofner, J., Lendl, B., Schmitt-Kopplin, P., Held, A.: New particle formation above a simulated salt lake in aerosol chamber experiments, Environmental Chemistry, 12, 489-503, 2015.

Kavouras, I. G., Mihalopoulos, N., and Stephanou, E. G: Formation of atmospheric particles from organic acids produced by forests, Nature, 395 (6703), 683-686, 1998.

Krause, T., Tubbesing, C., Benzing, K., and Schöler, H. F.: Model reactions and natural occurrence of furans from hypersaline environments, Biogeosciences, 11, 2871-2882, 2014.

Kulmala, M., Vehkamäki, H., Petäjä, T., Dal Maso, M., Lauri, A., Kerminen, V.-M., Birmili, W., and McMurry, P. H.: Formation and growth rates of ultrafine atmospheric particles: a review of observations, Journal of Aerosol Science, 35 (2), 143-176, 2004.

Lohninger, H., and Ofner, J.: Multisensor hyperspectral imaging as a versatile tool for image-based chemical structure determination, Spectroscopy Europe, 26 (5), 6-10, 2014.

Lyons, T. J.: Clouds prefer native vegetation, Meteorol. Atmos. Phys., 80, 131–140, 2002.

Nozière, B., Ekström, S., Alsberg, T., and Holmström, S.: Radical-initiated formation of organosulfates and surfactants in atmospheric aerosols, Geophys. Res. Lett., 37, L05806, 2010.

Nunes, T. V., and Pio, C. A.: Emission of volatile organic compounds from Portuguese eucalyptus forests, Chemosphere - Global Change Science, 3 (3), 239-248, 2001.

O'Dowd, C., Aalto, P., Hameri, K., Kulmala, M., and Hoffmann T.: Atmospheric particles from organic vapours, Nature, 416, 497–498, 2002.

Ofner, J., Balzer, N., Buxmann, J., Grothe, H., Schmitt-Kopplin, P., Platt, U. and Zetzsch, C.: Halogenation processes of secondary organic aerosol and implications on halogen release mechanisms, Atmos. Chem. Phys., 12(13), 5787–5806, doi:10.5194/acp-12-5787-2012, 2012.

Ofner, J., Kamilli, K.A., Held, A., Lendl, B., and Zetzsch, C.: Halogen-induced organic aerosol (XOA): A study on ultra-fine particle formation and time-resolved chemical characterization, Faraday Discussions, doi:10.1039/C3FD00093A, 2013.

Ofner, J., Kamilli, K.A., Eitenberger, E., Friedbacher, G., Lendl, B., Held, A. and Lohninger, H.: Chemometric analysis of multisensor hyperspectral images of precipitated atmospheric particulate matter, Analytical Chemistry, in press, DOI: 10.1021/acs.analchem.5b02272, 2015.

Pathak, R. K., Stanier, C. O., Donahue, N. M., and Pandis, S. N.: Ozonolysis of α-pinene at atmospherically relevant concentrations: Temperature dependence of aerosol mass fractions (yields), J. Geophy. Res., 112, D03201, doi:10.1029/2006JD007436, 2007.

Pesch, M., Grimm, H., Külz, T., Richter, M., and Albrecht, R.: Impact of size and concentration on the particle charging properties of an annular DBD, Res. Abstr. EAC, 2013.

Place Jr., P. F., Ziemba, L. D., and Griffin, R. J.: Observations of nucleation-mode particle events and size distributions at a rural New England site, Atmospheric Environment, 44 (1), 88-94, 2010.

Remucal, C. K., and Sedlak, D. L.: The Role of iron coordination in the production of reactive oxidants from ferrous iron oxidation by oxygen and hydrogen peroxide, Aquatic Redox Chemistry (ACS Symposium Series), 1071, 177–197, 2011.

Schmitt-Kopplin, P., Gelencser, A., Dabek-Zlotorzynska, E., Kiss, G., Hertkorn, N., Harir, M., Hong, Y., and Gebefugi, I.: Analysis of the Unresolved Organic Fraction in Atmospheric Aerosols with Ultrahigh-Resolution Mass Spectrometry and Nuclear Magnetic Resonance Spectroscopy: Organosulfates as Photochemical Smog Constituents, Anal. Chem., 82, 8017– 8026, 2010.

Schmitt-Kopplin, P., Liger-Belair, G., Koch, B. P., Flerus, R., Kattner, G., Harir, M., Kanawati, B., Lucio, M., Tziotis, D., Hertkorn, N., and Gebefügi, I.: Dissolved organic matter in sea spray: a transfer study from marine surface water to aerosols, Biogeosciences, 9 (4), 1571-1582, 2012.

Socrates, G.: Infrared and Raman Characteristic Group Frequencies – Tables and Charts, Third Edition, John Wiley & Sons Ltd., West Sussex, England, 2001.

Southworth, B. A., and Voelker, B. M.: Hydroxyl radical production via the photo-Fenton reaction in the presence of fulvic acid, Environ. Sci. Technol., 37, 1130‑1136, 2003.

Surratt, J. D., Gómez-González, Y., Chan, A. W. H., Vermeylen, R., Shahgholi M., Kleindienst, T. E., Edney, E. O., Offenberg, J. H., Lewandowski, M., Jaoui, M., Maenhaut, W., Claeys, M., Flagan, R. C., and Seinfeld, J. H.: Organosulfate Formation in Biogenic Secondary Organic Aerosol, The Journal of Physical Chemistry, A112 (36), 8345-8378, 2008.

Tang, Y., Thorn, R. P., Mauldin, R. L., Wine, P. H.: Kinetics and spectroscopy of the SO_4^- radical in aqueous-solution, J. Photochem. Photobiol. A., 44 (3), 243–258, 1988.

Wiedensohler, A.: Technical note: an approximation of the bipolar charge distribution for particles in the submicron size range, J. Aerosol Sci., 19, 387–389, 1988.

Zhang, S.-H., Akutsu, Y., Russell, L. M., Flagan, R. C., and Seinfeld, J. H.: Radial Differential Mobility Analyzer, Aerosol Science and Technology, 23 (3), 1995

Zhang, S.-H., Flagan, R. C.: Resolution of the radial differential mobility analyzer for ultrafine particles, J. Aerosol Sci., 27, 1179-1200, 1996.

Appendix III

New particle formation above a simulated salt lake in aerosol chamber experiments

K. A. Kamilli[A,E], J. Ofner[B], B. Lendl[B], P. Schmitt-Kopplin[C] and A. Held[A,D]

DOI: 10.1071/EN14225

[A]Atmospheric Chemistry, University of Bayreuth, Dr-Hans-Frisch-Straße 1-3, D-95448 Bayreuth, Germany.
[B]Institute of Chemical Technologies and Analytics, Vienna University of Technology, Getreidemarkt 9, AT-1060 Vienna, Austria.
[C]Research Unit Analytical BioGeoChemistry, Helmholtz Centre Munich, Ingolstädter Landstraße 1, D-85764 Neuherberg, Germany.
[D]Bayreuth Center of Ecology and Environmental Research BayCEER, Dr-Hans-Frisch-Straße 1-3, D-95448 Bayreuth, Germany.
[E]Corresponding author. Email: katharina.kamilli@uni-bayreuth.de

Environmental context. Deforestation in Western Australia beginning in the mid-19th century led to a considerable change of the land surface, and Western Australia is now suffering more often from droughts. Particle formation induced by Western Australian salt lakes has been identified as a potential control factor for changed precipitation patterns. This study aims to determine key factors involved in the particle formation process by simulating a simplified salt lake in an aerosol chamber in the laboratory.

Abstract

In recent field experiments, particle formation has been observed above salt lakes in Western Australia and related to changes in regional precipitation patterns. This work investigates the particle formation potential above a simulated salt lake in aerosol chamber experiments under various conditions. The salt lake mixture comprised fixed concentrations of NaBr, NaCl and Na_2SO_4, and varying concentrations of $FeSO_4$ and $FeCl_3$. Further, an organic mixture of 1,8-cineol and limonene was added under dark and light conditions. Both the presence of organic compounds and of light were found to be essential for new particle formation in our experiments. There were clear indications for conversion of Fe^{II} to Fe^{III}, which suggests a Fenton-like reaction mechanism in the system. Contrary to the idea that a Fenton-like reaction mechanism might intensify the oxidation of organic matter, thus facilitating secondary organic aerosol formation, the observed particle formation started later and with lower intensity under elevated Fe^{II} concentrations. The highest particle number concentrations were observed when excluding Fe^{II} from the experiments. Chemical analysis of the formed aerosol confirmed the important role of the Fenton-like reaction for particle formation in this study. Ultrahigh-resolution mass spectrometry and Raman spectroscopy provide analytical proof for the formation of organosulfates and halogenated organic compounds in the experiments presented. Even though

halogens and organic precursors are abundant in these experimental simulations, halogen-induced organic aerosol formation exists but seems to play a minor overall role in particle formation.

Introduction

Secondary aerosol formation from gaseous precursors is not completely understood because of the complex interplay of a vast number of chemical reactions, potential precursors and gas-particle-partitioning.[1, 2] Within the last years, a research focus has been placed on secondary organic aerosol (SOA) formation. In several field experiments, it has been shown that SOA contributes to a major fraction of the aerosol mass in the free troposphere. Contrary to global chemistry transport models predicting organic aerosol formation in the free troposphere[3], and forecasting an increasing fraction of SOA from oxidation of monoterpenes in the future[4], the experimentally measured SOA mass was typically one to two orders of magnitude larger than the modeled SOA mass.[5]

On a global scale, SOA released from anthropogenic sources plays a minor role.[6] Not considering methane, biogenic volatile organic compounds (VOC) emissions are estimated to range from 491 to 1150 Tg carbon per year, exceeding the emissions from anthropogenic sources by up to an order of magnitude.[7] The VOC emissions from trees alone exceed the level from man-made sources by a factor of 6.2[8], and are therefore a crucial source for organic aerosol precursors. Several studies have identified SOA coming from VOCs emitted by conifer forests.[9-13] Also, the emission from eucalyptus trees is the topic of some studies.[6, 14-16] To evoke new particle formation, the reactive VOCs are oxidised primarily by ozone, OH and NO_3 radicals.[14] Some studies have also investigated halogen-induced SOA formation.[17-19] Important sources for reactive halogen species (RHS) are halogen release from sea-salt aerosols (e.g. Finlayson-Pitts[20]), heterogeneous reactions on aerosol surfaces[21] and salt lakes.[22, 23] Saline soils and salt lakes will become even more important terrestrial sources for atmospheric chlorine and other halogens with the increase in human-caused salinisation.[24] Thus, in regions with high concentrations of RHS and VOC, the halogen-induced formation of SOA may contribute considerably to particle concentrations. However, the relative contribution of halogen-induced SOA formation has not been quantified in the natural environment. The aqueous phase has been established as an additional source for SOA over the past decade.[25-28] For example, the oxidation of organic compounds is catalysed by Fe^{II} as well as hydrogen peroxide (H_2O_2) in the so-called Fenton reaction, first described by Fenton[29] on the basis of the oxidation of tartaric acid in the presence of H_2O_2 and a low concentration of a ferrous salt. Enhanced solar radiation, which is important for a constant supply of H_2O_2 in surface waters and top soils[30], is typical for Western Australia. Indeed, both H_2O_2 as well as Fe^{II} were found in Australian salt-lake water samples.[31] The Fenton reaction can contribute to the production of OH radicals[32], even though the importance of OH production by this pathway is still controversial.[33] Aqueous-phase chemistry may also slow down or inhibit atmospheric SOA formation if oxidation in the aqueous phase leads to non-volatile products that cannot escape to the atmosphere. Here, simulation experiments of new particle formation above a salt lake model were conducted in a 700 L aerosol chamber in order to investigate aerosol formation processes in salt lake environments.

Measurement and methods

Aerosol chamber setup

The main experiments were conducted in a 700-L aerosol chamber. A detailed description of this chamber can be found in Ofner et al.[34] In this glass chamber, experiments can be performed under close-to-ambient light conditions using a solar simulator.[19] Contamination of the chamber is prevented by a constant flow of particle-free zero air during the experiments generating a slight excess pressure inside the chamber. Also, the chamber was flushed with zero air between the experiments.

The general chamber set-up consists of a cylindrical 700-L Duran glass body closed with Teflon film at the top and bottom, transparent to radiation coming from the solar simulator at the bottom.[34] This set-up was supplemented with a custom-made structure to position the simulated salt lake inside the chamber (Fig. 1).

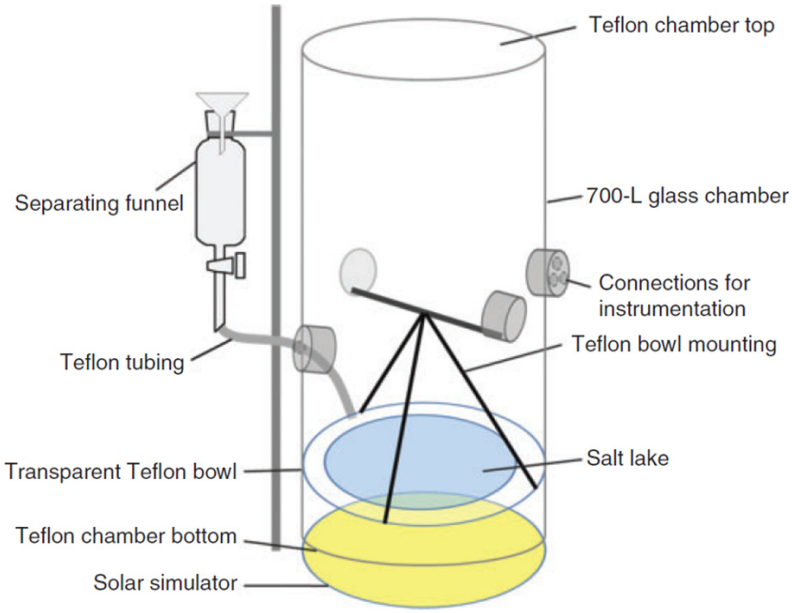

Fig. 1. Chamber set-up with additional structure to inject the salt lake mixture into the chamber.

A stainless-steel rod was fixed between two opposite glass ports to support the three-point mounting of a transparent Teflon bowl inside the chamber. This structure was built in order to avoid contamination of the chamber bottom made of Teflon film, and to increase the distance between the salt lake mixture and the solar simulator. Consequently, warming and potential vaporisation of the salt lake mixture due to the solar simulator is reduced. The salt lake mixture was injected into the Teflon bowl in the chamber through a separating funnel outside the chamber and Teflon tubing fed through a glass port of the chamber (Fig. 1). This allowed the introduction of the salt lake mixture and sampling from it without contaminating the chamber with ambient air. Placed on a transparent Teflon film, the simulated salt lake mixture was irradiated from below by the solar simulator, creating irradiation conditions comparable with those above Australian salt lakes after sunrise.

Instrumentation

The aerosol particle number size distribution inside the chamber was measured with a custom-built scanning mobility particle sizer (SMPS) (Tropos Leipzig, Germany) following the design recommended by Wiedensohler et al.[35] After achieving bipolar charge equilibrium, the aerosol population was size-segregated in a differential mobility analyser (DMA), and the particles were detected with a condensation particle counter (CPC Model 3772, TSI Inc., Shoreview, MN, USA). With a time resolution of 5 minutes, a full scan of the size distribution was measured in the mobility diameter range from particle diameter (*Dp*) = 10 to 772 nm in 71 bins or from *Dp* = 8 to 325 in 68 bins. In order to determine the onset of new particle formation with a better time resolution, and for comparison with the SMPS measurements, total particle number concentrations were measured with an additional condensation particle counter (CPC Model 5.400, GRIMM Aerosol Technik).

For subsequent chemical analysis, aerosol particles were collected on aluminium foils with a Sioutas impactor (SKC; Eighty Four, PA, USA) for 60 min at the end of the experiments. The flow rate was set to 9 L min^{-1} in order to sample on four separate stages in the aerodynamic diameter range from 250 nm to 10 µm. In addition, aerosol samples were collected on quartz-fiber filters (Whatman QMA, 25 mm, GE Healthcare, Little Chalfont, UK) with a stainless steel inline filter holder at a flow rate of 9 l min^{-1} for 80 min.

The impactor samples were analyzed by Raman microscopy and scanning electron microscopy with energy-dispersive x-ray spectroscopy (SEM-EDX). EDX of single aerosol particles was done using an Octane Pro Silicon Drift (SDD) EDX detector from AMETEK, coupled to the FEI Quanta 200 scanning electron microscope (FEI Europe, Eindhoven, Netherlands). Raman spectra of single aerosol particles were obtained using a Horiba LabRam 800 HR Raman microscope (Horiba, Bensheim, Germany) at an excitation wavelength of 532 nm with a 300-lines mm^{-1} grating at an initial laser power of 10 % (about 5 mW). By combining Raman spectroscopy and EDX, a detailed characterization of the collected aerosol particles with respect to elemental composition and vibrational behavior of the aerosol sample was obtained.[36] In addition, the quartz-fiber filters were analyzed by ultrahigh resolution mass spectrometry. The SolariX Fourier-transform ion cyclotron resonance mass spectrometer (FT-ICR/MS; Bruker; Bremen, Germany) was operated with a 12-T superconducting magnet and an Apollo II electrospray source in negative mode.[37] Because there were high salt concentrations in the sample, chlorine adducts[38] and organohalogens could not be clearly distinguished if the SOA sample was dissolved in methanol and directly injected into the ultrahigh-resolution mass spectrometer. Additionally, high salt-cluster concentrations would suppress some signals resulting from CHNOS compounds in the spectra. Therefore, the samples were desalted before analysis by extracting the filters with water and enriching the organic matter by solid phase extraction (SPE) using BAKERBOND spe Octadecyl (C18) Disposable Extraction Columns (Avantor, Center Valley, PA, USA).[39] A blank SPE extract of a non-loaded filter was also analyzed by FT-ICR/MS and did not show significant contamination from the filter material.

Ozone mixing ratios were measured during all chamber experiments using a photometric O_3 analyzer (Model 49i, Thermo Scientific, Franklin, MA, USA) with a lower detection limit of 1 ppb.

Simulated salt lake

A simplified salt lake mixture was prepared based on the chemical composition of various Australian salt lake samples determined in 2011 and 2012 by the Institute of Earth Science at the University of Heidelberg. With respect to inorganic salts, average concentrations of the main inorganic ions Na^+, Fe^{2+}, SO_4^{2-}, Cl^- and Br^- were calculated. Combining these ions in four inorganic salts, the standard salt lake mixture included NaBr (0.66 g L^{-1}), NaCl (307.71 g L^{-1}), Na_2SO_4 (32.11 g L^{-1}) and $Fe^{II}SO_4$ (0.52 g L^{-1}). In addition to the inorganic mixture, commercial eucalyptus oil (Primavera, Oy-Mittelberg, Germany) distilled from leaves and boughs of Portuguese *Eucalyptus globulus* trees was used as the organic model compound. The oil is a mixture of 85 % 1,8-cineol and 15 % limonene corresponding to the typical emission of *Eucalyptus globulus*. Owing to its moderate solubility, it was expected that the oil would be volatilised from the salt lake mixture in the course of the experiment, providing the gaseous organic precursor for SOA formation.

Experimental design

Three different series of chamber experiments were conducted studying the influence of light and the presence of an organic precursor (series A), the presence of Fe^{II} and Fe^{III} (series B), and the concentration of Fe^{II} (series C) in the simulated salt lake (cf. Table 1). Experimental conditions were varied by excluding the organic precursor, by using $FeCl_3$ instead of $FeSO_4$, by using a mixture of $FeSO_4$ and $FeCl_3$, or by changing the concentration of $FeSO_4$.

Table 1. Overview of experiments studying the effect of the organic precursor (A1-A2), Fe^{II} v. Fe^{III} (B1-B4), and varying Fe^{II} concentrations (C1-C3)

Volume of organic precursor added to the chamber; Fe^{II} and Fe^{III} concentration in salt lake mixture; observation of new particle formation (NPF); maximum particle number concentration (N_{max}); time when N_{max} occurred after turning on lights; maximum geometric mean diameter (GMD) within 60 min of turning on lights; maximum particle volume concentration (V_{max}) within 60 min after turning on lights; time when V_{max} occurred after turning on lights; particle growth rate GR

Experiment	Organic precursor (µL)	Fe^{II} (mg L^{-1})	Fe^{III} (mg L^{-1})	NPF (yes or no)	N_{max} (cm^{-3})	Time of N_{max} (min)	Max. GMD (nm)	V_{max} ($\mu m^3\ cm^{-3}$)	Time of V_{max} (min)	GR (nm h^{-1})
A1	0	520	0	No	–	–	–	–	–	–
A2	163	520	0	Yes	2.51×10^5	9	103	30.4	18	84
B1	163	520	0	Yes	1.1×10^5	7	71	6.0	29	70
B2	163	0	505	Yes	5.4×10^4	7	183	56.6	10	126
B3	163 + 80	260	253	No	3.3×10^3	–	–	–	–	–
B4	163	130	126	Yes	2.8×10^3	21	165	2.6	55	162
C1	163	520	0	Yes	8.3×10^4	10	95	6.8	44	95
C2	163	3640	0	Yes	2.2×10^4	15	148	13.0	24	170
C3	163	0	0	Yes	1.9×10^5	5	161	77.3	46	133

At first, the salt lake mixture was studied under dark and light conditions with and without the organic precursor to validate the role of light and the organic precursor in particle formation (Table 1, A1-2). The next set of experiments (Table 1, B1-4) was conducted using Fe^{III} instead of Fe^{II}, a mixture of Fe^{II} and Fe^{III}, and half of the concentration of Fe^{II} and Fe^{III} in the mixture. In this set of experiments, liquid samples were extracted with a syringe. The samples of the salt lake mixture were analyzed with test strips for H_2O_2 (Quantofix, Peroxyde 25, Machery-Nagel, Düren, Germany), for the total concentration of Fe^{III} (Quantofix, Fer total 100, Machery-Nagel), and for Fe^{II} (MQuant, Merck, Darmstadt, Germany). In a third set of experiments (Table 1, C1-3), the concentration of $Fe^{II}SO_4$ was varied between zero, 0.52 g L^{-1} and 3.64 g L^{-1}. The maximum concentration is based on the highest Fe^{II} concentration observed in Lake Boats in Western Australia. This concentration corresponds to the seven times the average Fe^{II} concentration observed in the field, represented by a concentration of 0.52 g L^{-1} $Fe^{II}SO_4$.

The pH of the salt lake mixture was typically adjusted to a value of 2.5 using HCl after analyzing the natural pH of several salt lakes in Western Australia (T.Krause, unpubl. data). In 11 samples of natural salt lakes taken in 2013, the pH varied from 2.5 to 7.1. Particle formation was strongest at lakes in the pH range 2-4, with a maximum particle number concentration of N_{max}= 2.50 x 10^5 cm^{-3} measured at Lake Dune with a daily average pH of 2.9. Four lakes were analyzed in detail, showing that the pH is not constant over the course of the day but fluctuates slightly. No clear trend can be observed in the field data, but the pH values seem to influence particle formation above the salt lakes. In most cases, new particle formation (NPF) started directly after a drop in the pH. For example, at Lake Boats, the pH was between 2.7 and 2.9, and NPF started on two occasions when the pH fell below 2.85. Therefore, a pH of 2.5 was chosen for the model lake in our simulation experiments in the laboratory in order to provide pH conditions favorable for NPF. However, when a mixture of $FeCl_3$ and $FeSO_4$ was used (Table 1, B3-4), the pH was set to 3.0 and 3.1.

Results and Discussion

Influence of experimental conditions on particle formation

As a first experiment, a pure salt mixture without the organic precursor was injected into the dark chamber (Table 1, A1). Under these conditions, particle formation, i.e. an increase of particle concentrations or particle growth, was not observed in the particle number size distributions. After 80 min, the solar simulator was switched on. Similarly, under daylight conditions, particle formation was not observed, and the particle concentration remained below 100 cm^{-3} (cf. Fig. 2a). This 'blank' experiment shows that the salt mixture of NaBr, NaCl, Na_2SO_4 and $Fe^{II}SO_4$ does not induce NPF in the aerosol chamber. Additionally, this experiment indicates that neither the aerosol chamber itself nor the chamber top or bottom made of Teflon film produce a significant number of particles under the influence of radiation.

In a second experiment (Table 1, A2), the organic precursor was added to the salt lake mixture. In order to evaluate the importance of light and photochemical reactions for particle formation in acidic, salty environments, the salt lake mixture remained in darkness for a time (<30 min). During this time no particle formation was observed, even though the salt lake mixture including 1,8-cineol and limonene was present in the chamber. This state is comparable with an Australian salt lake before sunrise, where NPF was not observed in the dark (K.A. Kamilli, unpubl. data). After switching on the solar simulator and initiating photochemistry in our experiments, particle formation started within 5 min, reaching a maximum particle

number concentration of 2.51 x 10^5 cm^{-3} (Fig. 2b). This confirms that both the organic precursor and light are essential for NPF in our experiments. No particles were formed in the illuminated chamber with only the salt mixture present (Fig. 2a), and no particles were formed under dark conditions.

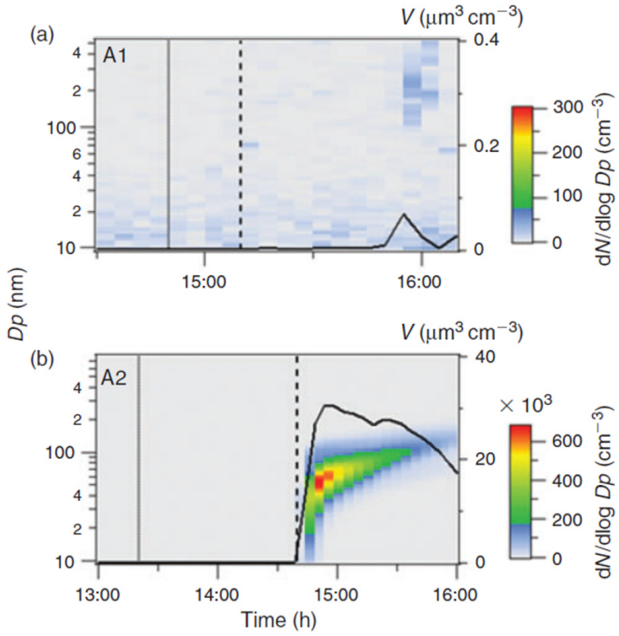

Fig. 2. (a) No particle formation was observed with a pure salt lake mixture under simulated sunlight without organic precursor. (b) The standard salt lake mixture with added organic precursor did not start particle formation until the solar simulator was switched on. The dotted lines refer to the salt lake injection, the dashed lines denote the moment of switching on the lights and the black solid lines show the course of the total particle volume.

During the experiments, the initial pH of 2.5 decreased continuously. On the one hand, this indicates that the pH of the simulated salt lakes changed owing to aqueous-phase chemistry. On the other hand, the pH values were not a key trigger of NPF in our simulation experiments, and NPF did not significantly change aqueous-phase chemistry. Also, contrary to the field measurements, H_2O_2 was not found in the samples of the simulated lake. In Western Australia, H_2O_2 was detected in the liquid layer of the salt lakes. However, in the field observations, it was striking that particle formation started at minimum H_2O_2 concentrations, which leads to the conclusion that H_2O_2 was typically consumed before particle formation.

Chamber experiments with mixtures of Fe^{II} and Fe^{III}

In a second series of experiments (Table 1, B1–B4), the experimental conditions concerning light, the concentration of the organic precursor and the concentrations of NaBr, NaCl and Na_2SO_4 were held constant. Only the concentration of iron-containing salts was varied to investigate the potential effect of iron in the aqueous phase on particle formation.

In order to investigate the effect of varying concentrations of Fe^{II} and Fe^{III} on particle formation, experiments B1–B4 were compared with respect to N_{max}, the time after switching on the solar simulator when N_{max} was reached, the maximum geometric mean diameter (GMD), the maximum particle volume concentration (V_{max}), the time after switching on the solar simulator when V_{max} was reached, and the particle

growth rate (GR) within 45 minutes after NPF started. For comparability, the maximum GMD was computed in the diameter range from 10 to 325 nm within 1 h after switching on the solar simulator for all experiments.

First, the standard salt lake mixture with a concentration of 520 mg L^{-1} of the Fe^{II} salt was used (Table 1, B1; Fig. 3a). After switching on the solar simulator, the maximum particle number concentration of 1.10 x 10^5 cm^{-3} was reached after 7 min. The GMD reached a value of 71 nm. In the second experiment, Fe^{III} was added to the salt lake mixture instead of Fe^{II} (Table 1, B2; Fig. 3b). Particle formation started directly after switching on the light, and the particle population grew to GMDs >100 nm within 10 min. The maximum particle number concentration was 5.4 x 10^4 cm^{-3}, and the maximum GMD was 183 nm. In a third experiment (Table 1, B3; Fig. 3c), a mixture of Fe^{II} and Fe^{III} salts showed no particle formation coming from the salt lake with the original mixture. After 20 min without any particle formation, an extra 80 µL of eucalyptol oil was added to the liquid layer. After 5 min, particle formation started, but the maximum particle number concentration of 3.3 x 10^3 cm^{-3} was quite low. Also, the particles grew to very large sizes outside the upper diameter limit of the measuring range. Reducing the concentrations of Fe^{II} as well as Fe^{III} to 50 % (Table 1, B4; Fig. 3d) led to NPF without further addition of dissolved organic compounds. However, the delay between switching on the lights and the start of NPF was longer than in experiments B1 and B2. The maximum particle number concentration was 2.8 x 10^3 cm^{-3}, and the maximum GMD was 165 nm.

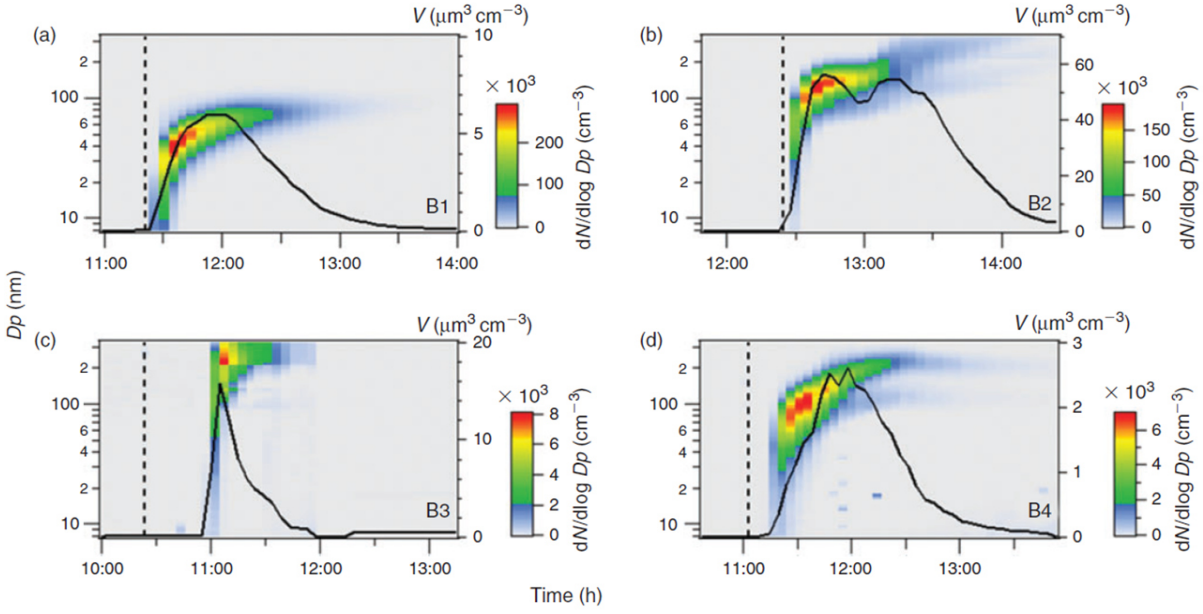

Figure 3 Contour plots of series B with varying concentration of Fe(II) and Fe(III). The dashed lines denote the moment of switching on the lights and the black solid lines show the course of the total particle volume. a) The standard salt lake mixture with a concentration of 520 mg l-1 of the Fe(II) salt; b) Fe(III) was added to the salt lake mixture instead of Fe(II); c) a mixture of Fe(II) and Fe(III) salts showed no particle formation until an extra 80 µl of eucalyptol were added to the liquid layer; d) reduced concentrations of Fe(II) as well as Fe(III) to 50 % led to NPF without further addition of dissolved organic.

Comparing the maximum particle number concentration and the maximum GMD of the four experiments B1 to B4, it is striking that in B1, the highest particle concentration was observed whereas the GMD was smallest. In experiment B2, the maximum particle number concentration was half of the value of experiment B1, but the GMD was the largest in this series. Even with the highest amount of organic precursor added to the experiment, the mixture of Fe^{II} and Fe^{III} in B3 led to a very low maximum particle number concentration of 3.3 x 10^3 cm^{-3}. Even though the subsequent addition of an extra amount of the organic precursor led to spontaneous NPF and a fast, obvious growth, experiment B3 was excluded from further consideration because of the different starting conditions. Using only half the concentrations of the iron salts in experiment B4 led to the lowest maximum particle number concentration in this series, whereas the GMD was large.

The maximum GMD reached within 60 min of turning on the solar simulator is related to the total aerosol mass or volume formed from the precursor gas and the particle growth rate. Assuming a fixed initial particle number size distribution, a more rapid increase in particle volume leads to a higher growth rate and a large maximum GMD. However, if the concentration of large particles is already high at the beginning of the experiment, even high particle formation intensities will yield low particle growth rates. Therefore, in addition to particle number concentrations and GMD, the maximum particle volume concentration and particle growth rates will be compared in the following text. Particle volume concentrations were estimated from the measured particle number size distributions assuming spherical particles and the GMD of each size bin as the typical diameter of all particles in this size bin.

Experiment B1 with the highest Fe^{II} concentration showed the lowest GR of 70 nm h^{-1}. The maximum particle volume concentration was reached 29 min after switching on the lights, with a value of 6 μm^3 cm^{-3}, which is quite low. Replacing Fe^{II} with Fe^{III} in the salt lake mixture resulted in clearly faster particle growth in experiment B2 and a high maximum particle volume concentration of 57 μm^3 cm^{-3}, which was already reached 10 minutes after starting the solar simulator. From this individual experiment, it remains unclear if excluding Fe^{II} from the mixture, the presence of Fe^{III}, or a combination of both have a promoting effect on particle formation and growth. Adding both Fe^{II} and Fe^{III} to the salt lake mixture in experiment B4 led to a high GR of 162 nm h^{-1}, and a low maximum particle volume concentration of 2.6 μm^3 cm^{-3} reached 55 min after switching on the solar simulator.
Apparently, even though the particle GR is quite high in experiment B4, the low maximum particle volume concentration reached late in the experiment indicates slow but constant particle formation over an extended time period when both Fe^{II} and Fe^{III} are present.
In experiments B1, B2 and B4, i.e. in experiments when NPF was observed, the color of the salt lake mixture changed from clear to orange-brownish more than 1 h after switching on the solar simulator. This color change is consistent with conversion of Fe^{II} to Fe^{III}. In addition, at the end of the experiments, recrystallisation of salt inside the salt lake mixture was observed. In order to quantify this process, batch experiments studying Fe^{II} and Fe^{III} concentrations during the evolution of the salt lake were performed. Over time, Fe^{II} concentrations clearly decreased in the solution. This suggests a Fenton-like reaction mechanism in the mixture of iron salts and organic compounds.

Effect of Fe^{II} concentration on new particle formation

In order to study the potential effect of a Fenton-like reaction on NPF, the effect of the Fe^{II} concentration in the simulated salt lake mixture on particle formation was studied in a third series of experiments (Table 1, C1–3). In a Fenton-like reaction, the oxidation of Fe^{II} by H_2O_2 yields Fe^{III}, a hydroxyl anion and a highly reactive OH radical (Reaction 1).[30, 40-42]

$$Fe^{2+} + H_2O_2 \rightarrow Fe^{3+} + HO^- + OH \qquad (R1)$$

Organic matter is acting as the electron donor for the Fenton reaction in iron-rich environments.[43, 44] Hydroxyl in the liquid phase may also be produced photochemically from hydrogen peroxide.[45] Herrmann et al.[46] have estimated that the main source for aqueous OH radicals is the Fenton reaction. Under the assumption that Reaction R1 actually takes place in the simulated salt lake mixture, more Fe^{II} would produce more OH radicals. Then, oxidation of the organic precursor and the formation of SOA would be facilitated. In the first experiment C1, the standard concentration of Fe^{II} was used as a reference experiment (Fig. 4a).

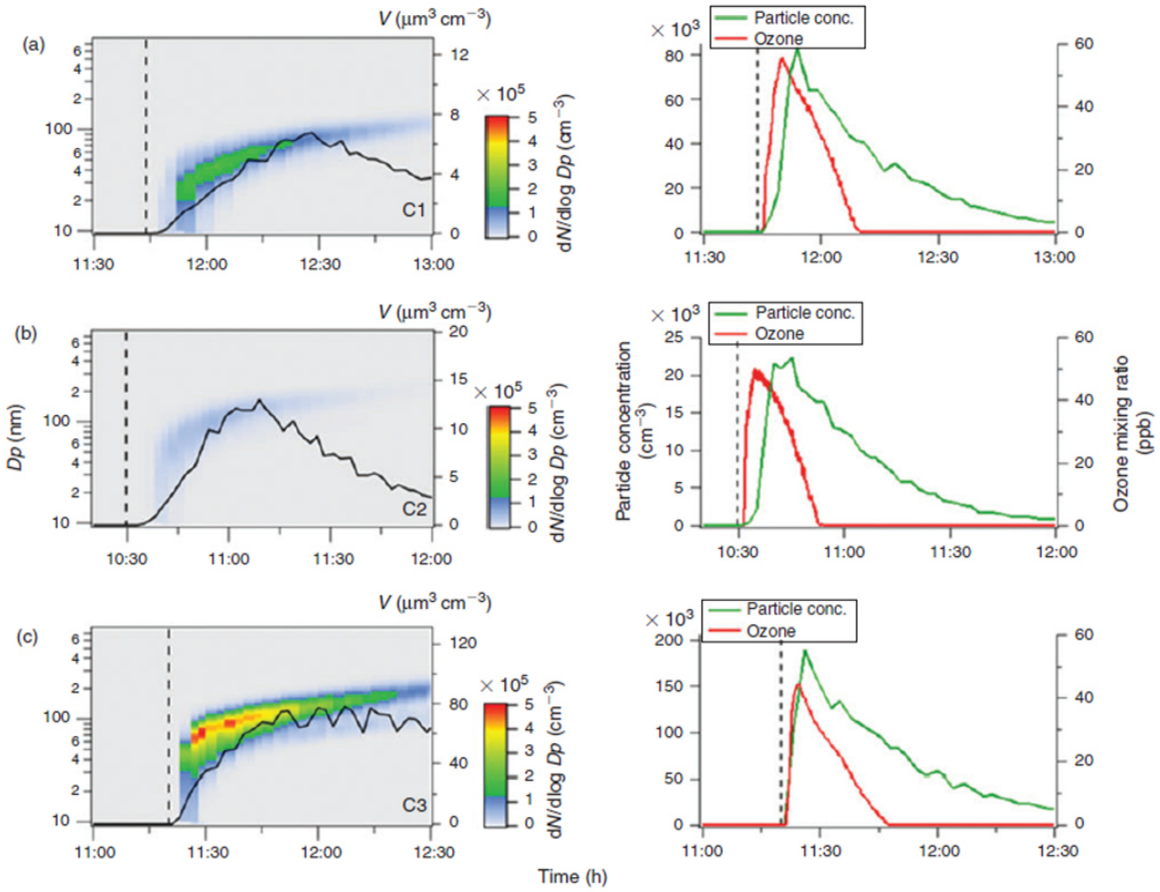

Fig. 4. During experiment series C, the concentration of Fe^{II} was varied: (a) standard concentration of Fe^{II}; (b) seven-fold higher concentration of Fe^{II}; and (c) no Fe^{II}. The dashed lines correspond to the moment when the solar simulator was switched on and the black solid lines show the course of the total particle volume. Corresponding particle number concentrations and ozone mixing ratios are shown on the right.

In experiment C2, the Fe^{II} concentration was increased by a factor of seven (Fig. 5b), representing the highest Fe^{II} concentration observed in natural salt lake samples of Western Australia in 2013. Owing to the fact that an increased concentration of Fe^{II} did not lead to more abundant particle formation, a third experiment C3 excluding Fe^{II} from the salt lake mixture was run for comparison (Fig. 4c).

Figure 4 shows that particle formation was observed quickly after switching on the solar simulator in all three experiments. Apparently, the time delay between illumination and the onset of particle formation increases when more Fe^{II} is added to the salt lake mixture. There is also a clear trend with respect to the maximum particle number concentration (cf. Table 1): With the standard Fe^{II} concentration in C1, the maximum particle number concentration was 8.3 x 10^4 cm^{-3}, whereas the maximum particle number concentration was much lower for increased Fe^{II} concentrations in C2 (2.2 x 10^4 cm^{-3}), and higher without Fe^{II} in C3 (1.9 x 10^5 cm^{-3}). This finding is consistent with recent work by Chu et al.[47], who observed reduced SOA formation in the aqueous phase with increased $FeSO_4$ concentrations. Ultrahigh-resolution mass spectrometry of aerosol samples also shows a loss of CHO oligomers (CH_2 homologous series) from iron-free experiment C3 to C1 and C2, and an increase of the chemical diversity in C1 and C2 with a maximum in experiment C1 (cf. *Aerosol chemical composition* section).

With respect to SOA formation, we have to consider oxidation of the organic precursor compounds 1,8-cineol and limonene both in the gas and in the aqueous phases. Owing to its moderate solubility in water, we assume that a certain fraction of the eucalyptus oil contained in the salt lake mixture will be released into the gas phase. In the gas phase, the OH radical is the main oxidant of 1,8-cineol [48], and diaterebic acid acetate and diaterpenylic acid acetate have been found to contribute to particle formation as OH oxidation products of 1,8-cineol.[49] Limonene is readily oxidised by ozone and OH radicals leading to a high aerosol yield.[50] The aqueous phase expands the possible reaction pathways for oxidation of organic compounds. For example, gas-phase ozonolysis of limonene yields water-soluble oligomers, which may be dissolved in the aqueous phase and undergo further oxidation.[51] Also, Fenton-like reactions (Reaction R1) are important aqueous-phase sources of OH radicals for further oxidation. Finally, oxidants other than ozone and OH may be produced in the aqueous phase. This includes the production of the sulfate radical (e.g. Herrmann [52]):

$$OH + HSO_4^- \rightarrow SO_4^- + H_2O \qquad \text{(R2)}$$

leading to the potential production of organosulfates.[37, 53] Aqueous-phase ozone may also react with dissolved chloride to form reactive chlorine species like HOCl:

$$O_3 + Cl^- \rightarrow ClO^- + O_2 \qquad \text{(R3a)}$$
$$ClO^- + H^+ \rightarrow HOCl \qquad \text{(R3b)}$$

HOCl may further react with dissolved chloride to produce molecular chlorine, which is quickly released to the gas phase and, in the presence of light, photolysed yielding Cl radicals. Previous studies by Lim et al.[54] and Wittmer et al.[55] suggest that Fe^{III} in NaCl solution promotes the release of chlorine from the aqueous phase. In our experiments, the presence of Fe^{II} and organic compounds may lead to the production of OH and Fe^{III} by the Fenton-like Reaction R1, subsequently facilitating the release of chlorine. HOCl also reacts with the organic precursor in the aqueous phase to form chlorinated organic matter (cf. *Aerosol chemical composition* section). Volatile organohalogens (VOX) may be released into the gas phase. By photolytic

cleavage of the C–Cl bond, a free halogen radical and a free organic radical are formed. VOX production in the aqueous phase and release into the gas phase are therefore a source for atmospheric reactive halogen species, which could oxidise SOA precursors in the gas phase.[19] It should be noted that the potential oxidation of 1,8-cineol by chlorine radicals is not well quantified yet.

In our experiments C1–C3, when the solar simulator was switched on, illumination initiated the oxidation of VOC and the simultaneous production of photochemical oxidants and ozone.[14] Ozone production was similar in all three experiments C1 to C3. Maximum ozone mixing ratios were reached ~5 min after illumination, ranging from 45 to 55 ppb (cf. Fig. 4). The lowest ozone production was observed in experiment C3 without any Fe^{II} in the simulated salt lake. In comparison with α-pinene and limonene, 1,8-cineol tends to produce higher ozone mixing ratios, as found in previous experiments comparing 1,8-cineol, α-pinene and limonene. The ozone mixing ratios observed in experiments with monoterpenes not carrying an oxygen atom were typically only 10 % of the ozone mixing ratios observed in experiments with 1,8-cineol. Ozone can either act as the primary oxidant of limonene, which is the minor constituent of the eucalyptus oil used in this study, or alternatively, under light conditions, ozone may produce OH radicals, which react with both limonene and 1,8-cineol.

In experiment C1 with the standard Fe^{II} concentration, particle formation is observed (Fig. 4a). Increasing the Fe^{II} concentration in the salt lake mixture is expected to enhance the production of OH radicals from H_2O_2 in the aqueous phase. Higher OH concentrations would suggest faster oxidation of the organic precursor compounds, and thus, an increased number and faster formation of particles compared with standard Fe^{II} conditions. However, with elevated Fe^{II} concentrations in experiment C2 (Fig. 4b), the observed particle formation starts later and with lower intensity. One possible reason is the complexing of organic compounds by irradiated iron oxide.[41] Joshi et al.[56] found a moderate to good chelating activity of Fe^{II} and mainly 1,8-cineol-containing oils. This suggests that more organic matter is potentially bound by additional Fe^{II} in the aqueous phase than without Fe^{II}, and less organic compounds may be released into the gas phase for subsequent participation in particle formation. Without the addition of Fe^{II} to the salt lake mixture in experiment C3, strong particle formation and CH_2 homologous series of oligomers are observed. In this case, it is expected that the organic precursors are mainly oxidised in the gas phase by OH and ozone, and competitive reactions in the aqueous phase are negligible.

Aerosol chemical composition

Analyzing the chemical composition of aerosol particles formed in experiments C1 to C3 by EDX, Raman spectroscopy and ultrahigh-resolution mass spectrometry may help to evaluate the relative importance of some of the potential particle formation pathways discussed above.

Electron-dispersive X-ray spectroscopy (Fig. 5) reveals $CaSO_4$ and $CaCO_3$ as the main inorganic species in the aerosol phase. These inorganic species are confirmed by Raman spectroscopy (Fig. 6), also indicating the presence of $CaSO_4$ and $CaCO_3$. The Ca^{2+} ions appear to originate from impurities in the salt mixture, and further display a phase separation of the involved Ca and Na ions. In addition, in case of the Fe^{II} experiments C2, small contributions of haematite (Fe_2O_3) were identified (Fig. 6).

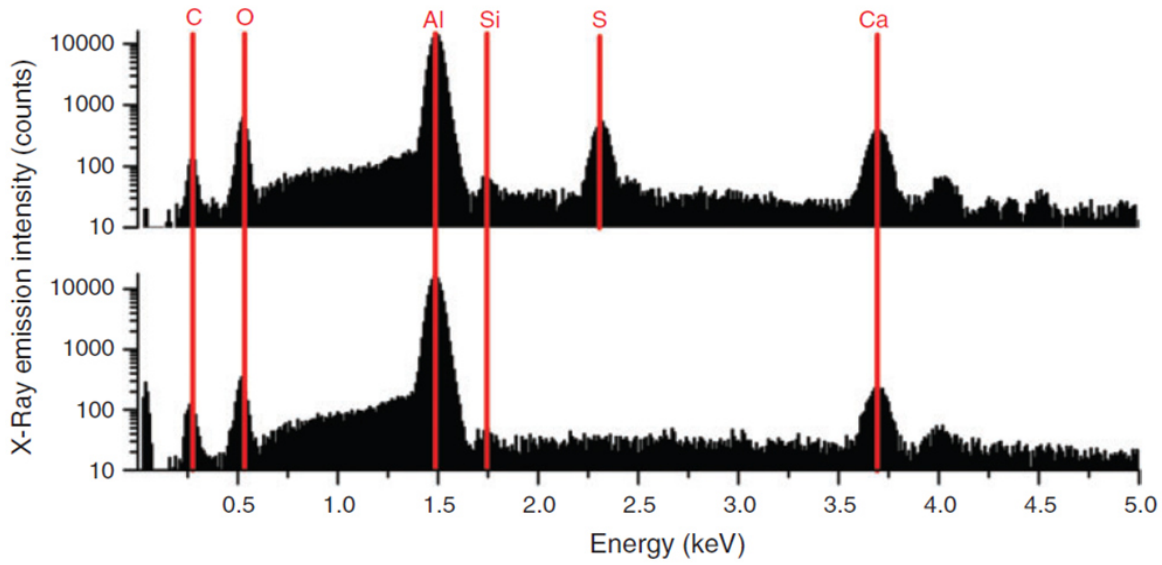

Fig. 5. Scanning electron microscopy with energy-dispersive X-ray spectroscopy (SEM-EDX) spectra of inorganic components of aerosol particles, indicating $CaSO_4$ and $CaCO_3$ as the major species.

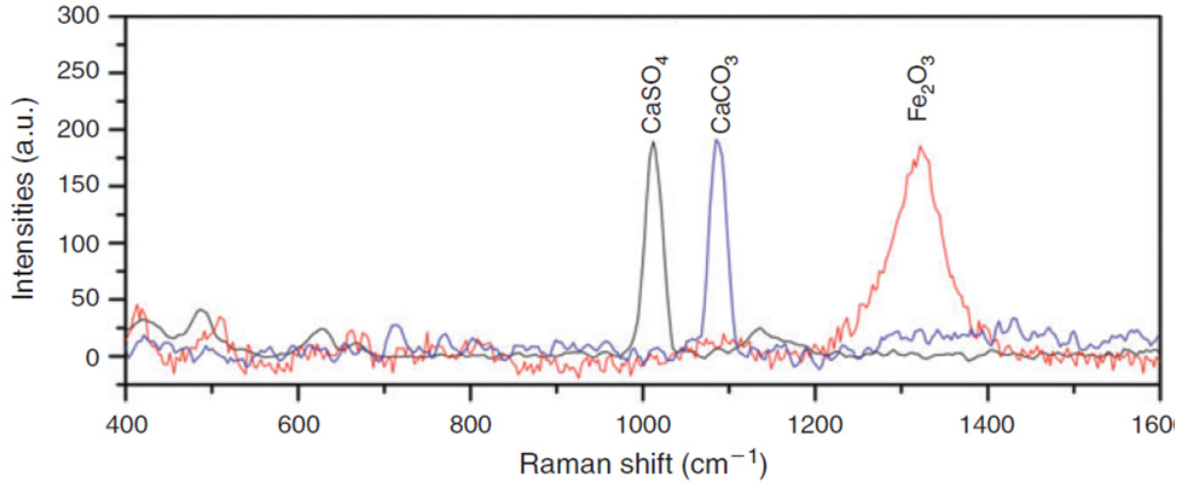

Fig. 6. Raman spectra of inorganic components of aerosol particles, indicating $CaSO_4$, $CaCO_3$ and haematite (Fe_2O_3) as the major species.

However, a large fraction of the collected aerosol particles exhibits secondary organic features, indicating particle formation based on eucalyptol. All inorganic Raman spectra were referenced to the RRUFF database.[57] To characterize significant changes of the precursor oil (derived from *Eucalyptus globulus*) related to the chemical process during aerosol formation, reference spectra of the eucalyptus oil and its individual components were recorded (Fig. 7). The main component of the eucalyptus oil used is 1,8-cineol. Further, small contributions of limonene were identified. Beside the dominance of the different deformation and stretching vibrations related to C–H species, the ether group of 1,8-cineol is very predominant at 740 cm^{-1}.

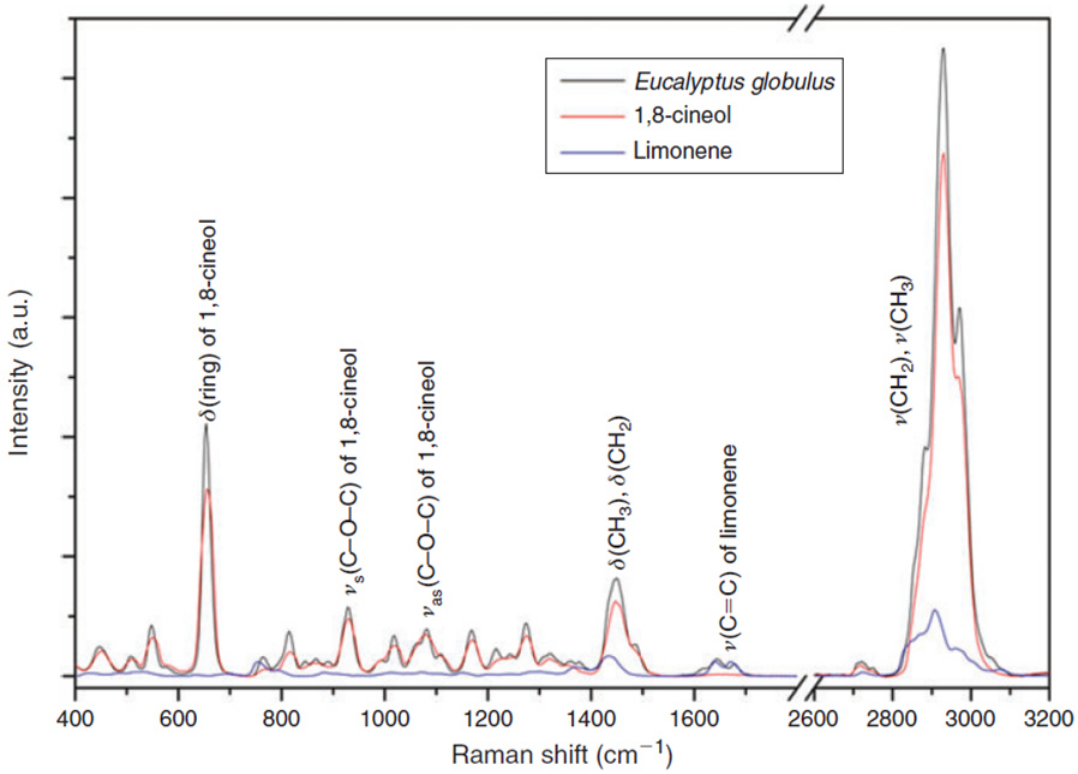

Fig.7. Raman spectra of the organic precursor oil derived from *Eucalyptus globulus* (black), and reference spectra of 1,8-cineol (red) and limonene (blue).

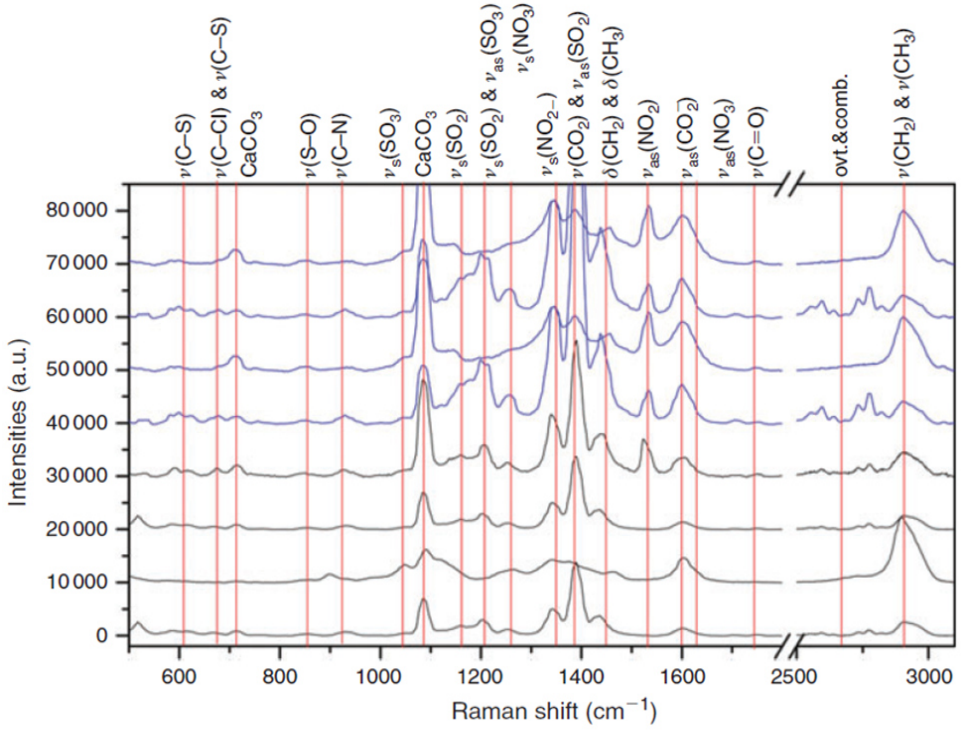

Fig. 8. Raman spectra of aerosol particles collected in experiment C2 with increased Fe^{II} concentrations (blue spectra), and collected in experiment C3 without Fe^{II} (black spectra). (ovt., overtone bands; comb., combination bands.)

Raman spectra were obtained of aerosol particles collected in the C2 experiments (increased Fe^{II} concentrations; Fig. 8, blue) and C3 (without Fe^{II}; Fig. 8, black). The following interpretation of the Raman spectra is based on Socrates.[58] Many particles exhibit Raman excitations related to $CaCO_3$ at 1085 and 710 cm^{-1}. Owing to the position of the Raman shifts of $CaCO_3$, the interpretation of the Raman spectra is hampered in these spectral regions. All spectra examined in the present work can be related to organic species, indicated by a predominant C–H stretch vibration. The predominance of the CH_3 group in the reference spectra (Fig. 7) is also present in the Raman spectra of the aerosol particles (Fig. 8), indicating organic precursors as the main origin of the secondary particles collected. This is also confirmed by the highest number of CHO formula with mainly CH_2-homologous series as observed in the mass spectra of experiment C3 (Fig. 9a).

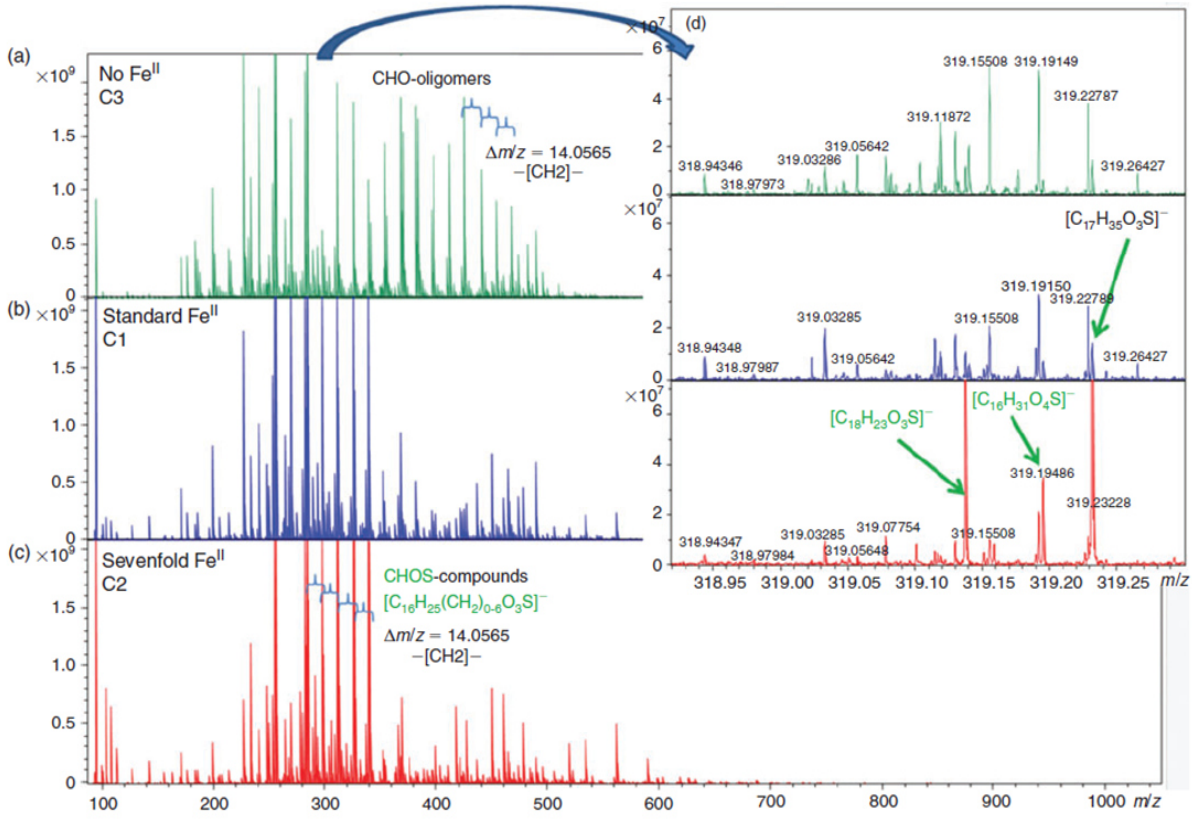

Fig. 9. Ultrahigh-resolution mass spectra of aerosol samples collected in experiment series C. Increasing the concentration of Fe^{II} from (a) to (c) directly affects the CHO oligomers, with increasing production of CHOS compounds visible in the total spectra (c) and in the single nominal mass signatures (inset d).

Further, the related deformation vibrations at 1430-1450 cm^{-1} are present. The predominant δ(ring) of the ether group (Fig. 7) of 1,8-cineol was not found in the aerosol phase. Thus, ring-opening at the position of the ether group appears to be a major step in the oxidation mechanism of 1,8-cineol. Predominant species, especially in case of the Raman spectra of the aerosol samples collected in the Fe^{II}-rich experiment C2, are $\nu_s(CO_2^-)$ at 1400 cm^{-1} and $\nu_{as}(CO_2^-)$ at 1600 cm^{-1}. The $\nu_s(CO_2^-)$ consist of several strong bands, covering other spectral features in this region. These vibrations belong to carboxylic acid salts and can explain the formation of $CaCO_3$ by further decarboxylation. Hence, the simultaneous occurrence of carboxylic acid salts

and $CaCO_3$ can be explained. Further, weak ν(C=O) vibrations at ~1730 cm^{-1} suggest the presence of oxygen-containing species. Indications of various nitrogen- and sulfur-containing species and organosulfates can be found in the Raman spectra of the aerosol particles, and appear to be enhanced in the Fe^{II}-rich experiment C2 compared with the Fe^{II}-free experiment C3. Bands at 1360 cm^{-1} ($\nu_s(NO_2)$) and 1530 cm^{-1} ($\nu_{as}(NO_2)$) indicate the presence of R–NO_2 species. Organic nitrates are represented by the $\nu_{as}(NO_3)$ band at 1630 cm^{-1} and the $\nu_s(NO_3)$ band at 1250 cm^{-1}. The related basic ν(C–N) can be found at ~920 cm^{-1}. Further, the presence of organic sulfate species is demonstrated by the Raman spectra. Organic sulphonates are indicated by $\nu_s(SO_2)$ at 1210 cm^{-1} and $\nu_{as}(SO_2)$ at 1400 cm^{-1}, which is masked by the strong $\nu_s(CO_2^-)$. The related ν(C–S) can be found at ~620 cm^{-1}. Higher oxidised sulfur species, especially sulphonic acid salts, can be found at 1050 ($\nu_s(SO_3)$, covered by $CaCO_3$, and 1200 ($\nu_{as}(SO_3)$) cm^{-1}. The corresponding ν(S–O) is located at ~850 cm^{-1}. Bands between 680 and 720 cm^{-1} suggest the presence of C–Cl or further C–S species. However, this spectral region is difficult to evaluate owing to the presence of $CaCO_3$.

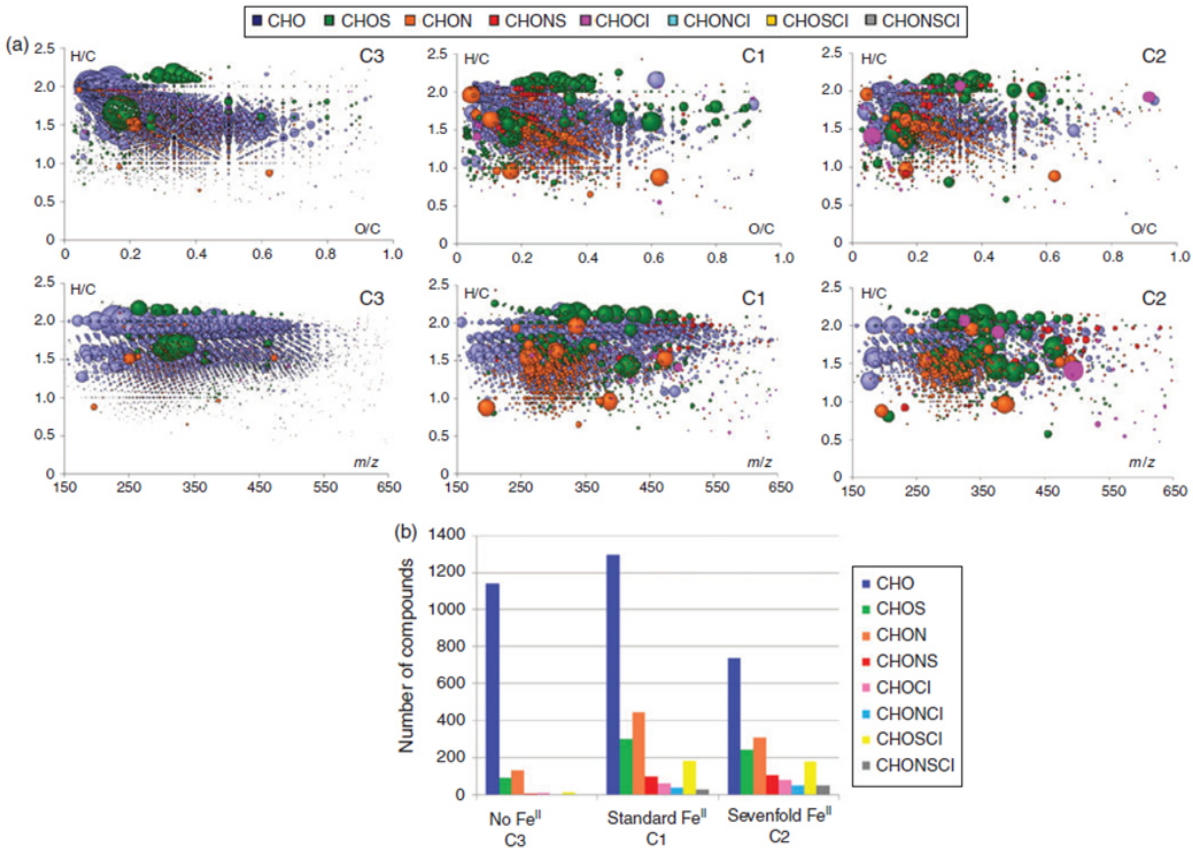

Fig. 10. Van Krevelen diagrams of the ultrahigh-resolution mass spectra in (a) show the increasing chemical diversity of compounds contained in the aerosol particles with increasing Fe^{II} concentration, which is summarised in (b). The bubble size is proportional to the signal intensity in the mass spectra and the colour code indicates the type of compositions. The relative contribution of CHO compounds decreases with increasing Fe^{II} concentration, whereas the contribution of organosulfates and halogenated organic compounds increases with increasing Fe^{II} concentration.

Ultrahigh-resolution mass spectra clearly show CH_2 homologous series of CHO compounds in the SOA fraction (Fig. 9), resulting in very regular CHO profiles in the van Krevelen Diagrams and continuity in the entire mass range (Fig. 10a). The addition of iron directly affects these CHO oligomers, with increasing production of CHOS compounds with iron addition as observed in the total spectra (Fig. 9c) and in the single nominal-mass signatures (Fig. 9d). Converting all exact masses into thousands of elementary compositions enabled the description of the iron addition in terms of chemical diversity of the compositional space. This is illustrated in Fig. 10b by number of formulas of specific atomic compositions including CHO, CHOS, CHOCl and others. In a first step, the addition of iron enhances the formation of CHO and generates a series of CHOS and halogenated organic compounds. Further increase in iron (C1 to C2) decreases on average the number of formulas but increases the relative abundance of CHOS and halogenated organic compounds. This is further confirmed when determining the formulas that increase or decrease with addition of iron in the series C3 → C1 → C2 (Fig. 11a, b). It is interesting to note that particularly the number of less oxidised CHO compounds with low O/C ratios decreases when Fe^{II} is increased, whereas CHOS and halogenated organic compounds appear or increase in intensity.

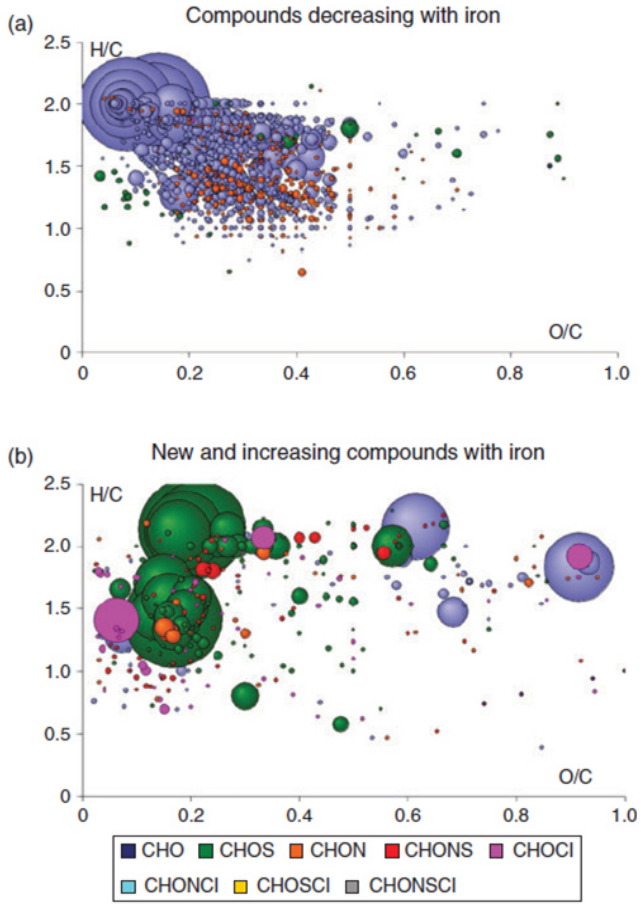

Fig. 11. (a) O/C and H/C ratios of individual compounds decreasing in intensity with increasing Fe^{II} concentrations. (b) O/C and H/C ratios of individual compounds appearing or increasing in intensity with increasing Fe^{II} concentrations. Colours indicate classification of organic compounds as CHO, CHOS, CHOCl and others.

In general, a larger contribution of oxidised species such as carboxylic acid salts and sulfates is visible in the Raman spectra of the Fe^{II}-enhanced experiment C2 (Fig. 8, blue spectra) compared with the Fe^{II}-free experiment C3 (Fig. 8, black spectra). This larger contribution of CHOS compounds was confirmed by ultrahigh-resolution mass spectrometry (Fig. 9, 10), and is consistent with an important contribution of the Fenton-like Reaction R1, which causes oxidation of the initial organic precursor in the aqueous phase, and formation of organosulfates potentially by the sulfate radical formed in the aqueous-phase Reaction R2.

With respect to the role of reactive halogen species potentially leading to halogen-induced organic aerosol formation or halogenation reactions of pre-existing organic aerosol[19], the analysis by Raman spectroscopy remains inconclusive. There are no clear indications for a strong contribution of halogen-induced reactions to NPF in the experiments presented, even though organic compounds and halogen species were simultaneously present. However, halogenated organic compounds were detected by ultrahigh-resolution mass spectrometry (Fig. 10).

Finally, diaterebic acid acetate and diaterpenylic acid acetate, tracers of OH oxidation of 1,8-cineol[49], were confirmed in all aerosol samples collected during the chamber experiments series C with ultrahigh-resolution mass spectrometry (Fig. 12). The fraction of these tracer compounds decreases with the presence of iron showing their further implication in the formation of sulfur-containing and halogenated species. This indicates that the gas-phase oxidation of the organic precursor compounds always contributed to the particle formation process in our simulation experiments.

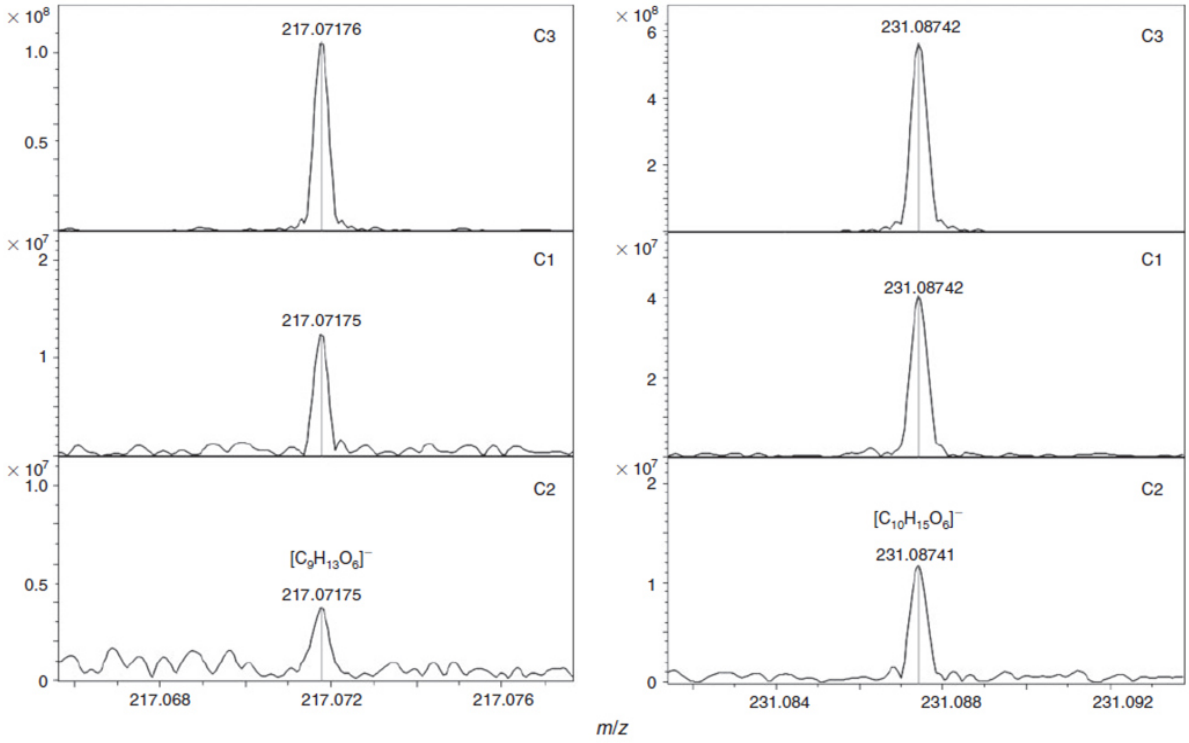

Fig. 12. Two tracers of OH oxidation of 1,8-cineol, diaterebic acid acetate (left) and diaterpenylic acid acetate (right), were confirmed in all aerosol samples collected during the chamber experiments series C with ultrahigh-resolution mass spectrometry. The fraction of these tracer compounds decreases in intensity with increasing Fe^{II} concentrations (C3 → C1 → C2).

Conclusions

In the present study, particle formation was observed in an aerosol chamber above a simulated salt lake mixture containing 1,8-cineol and limonene as organic precursor compounds for SOA formation. By evaluating maximum particle number and volume concentrations, the maximum geometric mean diameter and particle growth rates in various chamber experiments (cf. Table 1), the concentration of Fe^{II} in the salt lake mixture was identified to be a key control factor in the intensity of particle formation. In salt lake environments with low pH values and high solar irradiation, Fe^{II} is converted to Fe^{III} in the presence of organic matter in a Fenton-like reaction, which is the main source of highly reactive OH radicals in the aqueous phase.[46] The fact that the variation of Fe^{II} concentrations in the salt lake mixtures affects the intensity of particle formation in our experiments suggests a coupling of aqueous-phase chemistry and particle formation.

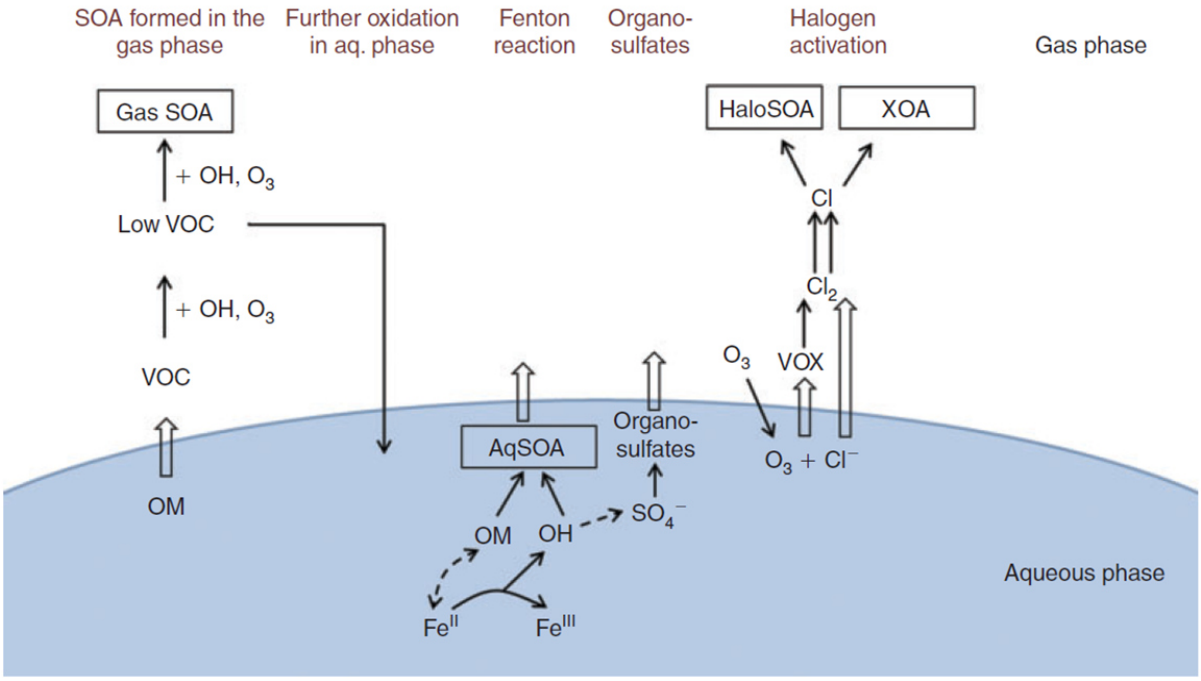

Fig. 13. Interaction between aqueous- and gas-phase chemistry in a system containing salts and organic matter (OM) under light conditions leading to secondary organic aerosol (SOA) formation. (HaloSOA, halogenated SOA or halogenations of pre-existing secondary organic aerosol; XOA, halogen-induced organic aerosol; VOX, volatile organohalogens; low VOC, low volatile organic compounds; AqSOA, SOA formed in the aqueous phase; Gas SOA, SOA formed in the gas phase.)

Release of 1,8-cineol and limonene from the aqueous phase into the gas phase and subsequent oxidation of 1,8-cineol by OH radicals[48], and of limonene by ozone and OH radicals[50], contribute to secondary aerosol formation in the gas phase (Fig. 13). Water-soluble products formed in the gas phase, e.g. water-soluble oligomers formed during limonene ozonolysis, may be dissolved in the liquid phase and undergo further aqueous phase oxidation.[51] The detection of diaterebic acid acetate and diaterpenylic acid acetate in aerosols collected in experiments C1-3 confirms particle formation from the oxidation of 1,8-cineol by OH radicals.[49] Fenton-like reactions suggest additional production of OH radicals in the aqueous phase, and

consequently, an increased potential for oxidation of the organic precursor compounds in the aqueous phase leading to less-volatile organic compounds (cf. Fig. 13). If these low-volatility compounds are released from the aqueous phase, they may contribute to SOA formation. However, the experiments C1 to C3 show that increased Fe^{II} concentrations reduce the intensity of particle formation observed in the gas phase. The highest particle concentrations were observed when Fe^{II} was excluded from the salt lake mixture (experiment C3). This is consistent with recent work by Chu et al.[47], who observed reduced SOA formation in the presence of $FeSO_4$ in their experiments under wet conditions (50 % relative humidity) in α-pinene-NOx and α-pinene-HONO photooxidation systems. They propose oxidation processes on the wet surface of the SOA layer by OH radicals breaking down the organic oxidation products into smaller molecules, which may be released into the gas phase, thereby reducing the aerosol mass concentration. We suggest that the complexing of organic compounds by irradiated iron oxide[44], as well as the chelating effect of Fe^{II} on 1,8-cineol as observed by Joshi et al.[49], may also reduce the availability of 1,8-cineol, limonene and their first-generation oxidation products for reactions leading to SOA. The competition of Fe^{II}-controlled aqueous-phase chemistry with secondary aerosol formation in the gas phase led to reduced particle formation in our experiments.

Besides this competitive effect, however, aqueous-phase chemistry expands the potential oxidation pathways of 1,8-cineol and limonene. The presence of Fe^{II} clearly increases the chemical diversity of the organic aerosol (cf. Figs. 10, 11). For example, formation of sulfate radicals provides an additional oxidant and the potential for organosulfate formation in the aqueous phase.[53] Contributions of organosulfates to particle formation have been found in the mass spectra and Raman spectra of aerosol collected in experiments C2 and C3. Also, ozone in the aqueous phase may react with dissolved chloride to form reactive chlorine species like HOCl. HOCl may either react with dissolved chloride to produce molecular chlorine, which can produce Cl radicals under irradiation once released into the gas phase, or HOCl may react with organic compounds in the aqueous phase to form chlorinated organic matter as observed, e.g., in the formation of chlorinated by-products in drinking-water production.[59] Volatile organohalogens (VOX) may be released into the gas phase. Both pathways are possible sources for atmospheric reactive halogen species, which may oxidise SOA precursors in the gas phase.[19] Halogenated organic compounds were detected unequivocally by ultrahigh-resolution mass spectrometry (Fig. 10). However, even though dissolved chloride as well as 1,8-cineol and limonene were abundant in our experiments, the formation of halogen-induced organic aerosol (XOA) or halogenation of pre-existing SOA (HaloSOA) as described in Ofner et al.[19] seems to play a minor overall role in NPF in our experiments.

The obvious influence of Fenton-like reactions in the present study emphasises the relevance of the interaction of gas-phase and aqueous-phase chemistry in particle formation. For a better understanding of the relative contributions of these different pathways to particle formation under various atmospherically relevant conditions, more studies have to be carried out analyzing systematically the interplay of gas-phase and aqueous-phase chemistry. With respect to Fe^{II}, a more detailed and quantitative analysis of the control of Fe^{II} over competitive aqueous-phase oxidation pathways of organic compounds is a prerequisite to quantitatively assess its influence on atmospheric particle formation.

Acknowledgements

We are indebted to the HaloProc partners, especially the Western Australia field teams in 2012 and 2013, for field data, ideas and discussions leading to this study. Further, we thank Gernot Friedbacher and Elisabeth Eitenberger (Vienna University of Technology, Institute of Chemical Technologies and Analysis) for obtaining the SEM-EDX data. Funding by the German Research Foundation (DFG) grant HE 5214/5-1 and within the DFG research group HaloProc (FOR 763) is gratefully acknowledged.

References

[1] A. G. Carlton, C. Wiedinmyer, J. H. Kroll, A review of secondary organic aerosol (SOA) formation from isoprene. *Atmos. Chem. Phys.* **2009**, *9*, 4987. doi:10.5194/ACP-9-4987-2009

[2] M. Kulmala, V.-M. Kerminen, T. Anttila, A. Laaksonen, C. D. O'Dowd, Organic aerosol formation via sulphate cluster activation. *J. Geophys. Res.* **2004**, *109*, D04205. doi:10.1029/2003JD003961

[3] K. Tsigaridis, J. Lathière, M. Kanakidou, D. A. Hauglustaine, Naturally driven variability in the global secondary organic aerosol over a decade. *Atmos. Chem. Phys.* **2005**, *5*, 1891. doi:10.5194/ACP-5-1891-2005

[4] K. Tsigaridis, M. Kanakidou, Secondary organic aerosol importance in the future atmosphere. *Atmos. Environ.* **2007**, *41*, 4682. doi:10.1016/J.ATMOSENV.2007.03.045

[5] C. L. Heald, D. J. Jacob, R. J. Park, L. M. Russell, B. J. Huebert, J. H. Seinfeld, H. Liao, R. J. Weber, A large organic aerosol source in the free troposphere missing from current models. *Geophys. Res. Lett.* **2005**, *32*, L18809. doi:10.1029/2005GL023831

[6] C. He, F. Murray, T. Lyons, Monoterpene and isoprene emissions from 15 *Eucalyptus* species in Australia. *Atmos. Environ.* **2000**, *34*, 645. doi:10.1016/S1352-2310(99)00219-8

[7] A. Guenther, C. N. Hewitt, D. Erickson, R. Fall, C. Geron, T. Graedel, P. Harley, L. Klinger, M. Lerdau, W. A. Mckay, T. Pierce, B. Scholes, R. Steinbrecher, R. Tallamraju, J. Taylor, P. Zimmerman, A global- model of natural volatile organic compound emissions. *J. Geophys. Res.–Atmos.* **1995**, *100*, 8873. doi:10.1029/94JD02950

[8] R. A. Rasmussen, What do the hydrocarbons from trees contribute to air pollution?. *J. Air Pollut. Contr. Assoc.* **1972**, *22*, 537. doi:10.1080/ 00022470.1972.10469676

[9] A. Held, A. Nowak, W. Birmili, A. Wiedensohler, R. Forkel, O. Klemm, Observations of particle formation and growth in a mountainous forest region in central Europe. *J. Geophys. Res.* **2004**, *109*, D23204. doi:10.1029/2004JD005346

[10] J. G. Isebrands, A. B. Guenther, P. Harley, D. Helmig, L. Klinger, L. Vierling, P. Zimmerman, C. Geron, Volatile organic compound emission rates from mixed deciduous and coniferous forests in Northern Wisconsin, USA. *Atmos. Environ.* **1999**, *33*, 2527. doi:10.1016/S1352-2310(98)00250-7

[11] H. Hakola, V. Tarvainen, T. Laurila, V. Hiltunen, H. Hellén, P. Keronen, Seasonal variation of VOC concentrations above a boreal coniferous forest. *Atmos. Environ.* **2003**, *37*, 1623. doi:10.1016/ S1352-2310(03)00014-1

[12] A. Plewka, T. Gnauk, E. Brüggemann, H. Herrmann, Biogenic contributions to the chemical composition of airborne particles in a coniferous forest in Germany, Atmospheric Environment **2006**, *40*, 103-115. doi:10.1016/J.ATMOSENV.2005.09.090

[13] I. Kourtchev, T. Ruuskanen, W. Maenhaut, M. Kulmala, M. Claeys, Observation of 2-methyltetrols and related photooxidation products of isoprene in boreal forest aerosols from Hyytiälä, Finland. *Atmos. Chem. Phys.* **2005**, *5*, 2761. doi:10.5194/ACP-5-2761-2005

[14] T. V. Nunes, C. A. Pio, Emission of volatile organic compounds from Portuguese eucalyptus forests. *Chemosphere, Glob. Chang. Sci.* **2001**, *3*, 239. doi:10.1016/S1465-9972(01)00007-1

[15] A. J. Winters, M. A. Adams, T. M. Bleby, H. Rennenberg, D. Steigner, R. Steinbrecher, J. Kreuzwieser, Emissions of isoprene, monoterpene and short-chained carbonyl compounds from *Eucalyptus* spp. in southern Australia. *Atmos. Environ.* **2009**, *43*, 3035. doi:10.1016/ J.ATMOSENV.2009.03.026

[16] F. Loreto, S. Delfine, Emission of isoprene from salt-stressed *Euca- lyptus globulus* leaves. *Plant Physiol.* **2000**, *123*, 1605. doi:10.1104/ PP.123.4.1605

[17] Q. K. Timerghazin, P. A. Ariya, Kinetics of the gas-phase reaction of atomic chlorine with selected monoterpenes. *PCCP Phys. Chem. Ch. Ph.* **2001**, *3*, 3981. doi:10.1039/B101380G

[18] X. Cai, R. J. Griffin, Secondary aerosol formation from the oxidation of biogenic hydrocarbons by chlorine atoms. *J. Geophys. Res.* **2006**, *111*, D14206. doi:10.1029/2005JD006857

[19] J. Ofner, K. A. Kamilli, A. Held, B. Lendl, C. Zetzsch, Halogen- induced organic aerosol (XOA): a study on ultrafine particle formation and time-resolved chemical characterization. *Faraday Discuss.* **2013**, *165*, 135. doi:10.1039/C3FD00093A

[20] B. J. Finlayson-Pitts, The tropospheric chemistry of sea salt: A molecular-level view of the chemistry of NaCl and NaBr. *Chem. Rev.* **2003**, *103*, 4801–4822. doi:10.1021/cr020653t

[21] M. J. Rossi, Heterogeneous reactions on salts. *Chem. Rev.* **2003**, *103*, 4823. doi:10.1021/CR020507N

[22] W. Junkermann, J. Hacker, T. Lyons, U. Nair, Land-use change suppresses precipitation. *Atmos. Chem. Phys.* **2009**, *9*, 6531. doi:10.5194/ACP-9-6531-2009

[23] J. Stutz, R. Ackermann, J. D. Fast, L. Barrie, Atmospheric reactive chlorine and bromine at the Great Salt Lake, Utah. *Geophys. Res. Lett.* **2002**, *29*, 18-1. doi:10.1029/2002GL014812

[24] W. D. Williams, Salinisation: a major threat to water resources in the arid and semi-arid regions of the world. *Lakes Reservoirs: Res. Manage.* **1999**, *4*, 85. doi:10.1046/J.1440-1770.1999.00089.X

[25] M. Hallquist, J. C. Wenger, U. Baltensperger, Y. Rudich, D. Simpson, M. Claeys, J. Dommen, N. M. Donahue, C. George, A. H. Goldstein, J. F. Hamilton, H. Herrmann, T. Hoffmann, Y. Iinuma, M., Jang, M. E. Jenkin, J. L. Jimenez, A. Kiendler-Scharr, W. Maenhaut, G. McFiggans, Th. F. Mentel, A. Monod, A. S. H. Prévôt, J. H. Seinfeld, J. D. Surratt, R. Szmigielski, J. Wildt, The formation, properties and impact of secondary organic aerosol: current and emerging issues. *Atmos. Chem. Phys.* **2009**, *9*, 5155–5236. doi:10.5194/ ACP-9-5155-2009

[26] Y. B. Lim, Y. Tan, M. J. Perri, S. P. Seitzinger, B. J. Turpin, Aqueous chemistry and its role in secondary organic aerosol (SOA) formation. *Atmos. Chem. Phys.* **2010**, *10*, 10521. doi:10.5194/ACP-10-10521-2010

[27] M. Claeys, W. Wang, A. C. Ion, I. Kourtchev, A. Gelencsér, W. Maenhaut, Formation of secondary organic aerosols from isoprene and its gas-phase oxidation products through reaction with hydrogen peroxide. *Atmos. Environ.* **2004**, *38*, 4093. doi:10.1016/J.ATMO SENV.2004.06.001

[28] A. G. Carlton, B. J. Turpin, H.-J. Lim, K. E. Altieri, S. Seitzinger, Link between isoprene and secondary organic aerosol (SOA): pyruvic acid oxidation yields low-volatility organic acids in clouds. *Geophys. Res. Lett.* **2006**, *33*, L06822. doi:10.1029/2005GL025374

[29] H. J. H. Fenton, Oxidation of tartaric acid in presence of iron. *J. Chem. Soc.* **1894**, *65*, 899. doi:10.1039/CT8946500899

[30] W. J. Cooper, R. G. Zika, R. G. Petasne, J. M. C. Plane, Photochemical formation of H_2O_2 in natural waters exposed to sunlight. *Environ. Sci. Technol.* **1988**, *22*, 1156. doi:10.1021/ES00175A004

[31] T. Krause, C. Tubbesing, K. Benzing, H. F. Schöler, Model reactions and natural occurrence of furans from hypersaline environments. *Biogeosciences* **2014**, *11*, 2871-2882. doi:10.5194/BG-11-2871-2014

[32] H. B. Dunford: Oxidation of iron(II)/(III) by hydrogen peroxide: from aquo to enzyme. *Coord. Chem. Rev.* **2002**, *233– 234*, 311–318. doi:10.1016/ S0010-8545(02)00024-3

[33] L. Deguillaume, M. Leriche, N. Chaumerliac, Impact of radical versus non-radical pathway in the Fenton chemistry on the iron redox cycle in clouds. *Chemosphere* **2005**, *60*, 718. doi:10.1016/J.CHEMO SPHERE.2005.03.052

[34] J. Ofner, H.-U. Krüger, H. Grothe, P. Schmitt-Kopplin, K. Whitmore, C. Zetzsch, Physico-chemical characterization of SOA derived from catechol and guaiacol – a model substance for the aromatic fraction of atmospheric HULIS. *Atmos. Chem. Phys.* **2011**, *11*, 1. doi:10.5194/ ACP-11-1-2011

[35] A. Wiedensohler, W. Birmili, A. Nowak, A. Sonntag, K. Weinhold, M. Merkel, B. Wehner, T. Tuch, S. Pfeifer, M. Fiebig, A. M. Fjäraa, E. Asmi, K. Sellegri, R. Depuy, H. Venzac, P. Villani, P. Laj, P. Aalto, J. A. Ogren, E. Swietlicki, P. Williams, P. Roldin, P. Quincey, C. Hüglin, R. Fierz-Schmidhauser, M. Gysel, E. Weingartner, F. Riccobono, S. Santos, C. Grüning, K. Faloon, D. Beddows, R. Harrison, C. Monahan, S. G. Jennings, C. D. O'Dowd, A. Marinoni, H.-G. Horn, L. Keck, J. Jiang, J. Scheckman, P. H. McMurry, Z. Deng, C. S. Zhao, M. Moerman, B. Henzing, G. de Leeuw, G. Löschau, S. Bastian, Mobility particle size spectrometers: harmonization of technical standards and data structure to facilitate high-quality long- term observations of atmospheric particle number size distributions. *Atmos. Meas. Tech.* **2012**, *5*, 657. doi:10.5194/AMT-5-657-2012

[36] Y. Batonneau, S. Sobanska, J. Laureyns, C. Bremard, Confocal microprobe Raman imaging of urban tropospheric aerosol particles. *Environ. Sci. Technol.* **2006**, *40*, 1300. doi:10.1021/ES051294X

[37] P. Schmitt-Kopplin, A. Gelencser, E. Dabek-Zlotorzynska, G. Kiss, N. Hertkorn, M. Harir, Y. Hong, I. Gebefugi, Analysis of the unresolved organic fraction in atmospheric aerosols with ultrahigh-resolution mass spectrometry and nuclear magnetic resonance spectroscopy: organosulfates as photochemical smog constituents. *Anal. Chem.* **2010**, *82*, 8017. doi:10.1021/AC101444R

[38] L. Boutegrabet, B. Kanawati, I. Gebefügi, D. Peyron, Ph. Cayot, R. D. Gougeon, Ph. Schmitt-Kopplin, Chloride anion attachment to sugars. Mechanistic investigation and discovery of a new dopant for efficient sugar ionization/detection in mass spectrometers. *Chemistry* **2012**, *18*, 13059. doi:10.1002/CHEM.201103788

[39] Ph. Schmitt-Kopplin, G. Liger-Belair, B. P. Koch, R. Flerus, G. Kattner, M. Harir, B. Kanawati, M. Lucio, D. Tziotis, N. Hertkorn, Gebefügi, Dissolved organic matter in sea spray: a transfer study from marine surface water to aerosols. *Biogeosciences* **2012**, *9*, 1571. doi:10.5194/BG-9-1571-2012

[40] F. Haber, J. Weiss, Über die Katalyse des Hydroperoxydes. *Naturwissenschaften* **1932**, *20*, 948. doi:10.1007/BF01504715

[41] P. Mazellier, B. Sulzberger, Diuron degradation in irradiated, hetero- geneous iron/oxalate systems: the rate-determining step. *Environ. Sci. Technol.* **2001**, *35*, 3314. doi:10.1021/ES001324Q

[42] C. K. Remucal, D. L. Sedlak, The role of iron coordination in the production of reactive oxidants from ferrous iron oxidation by oxygen and hydrogen peroxide. *ACS Symposium Series* **2011**, *1071*, 177. doi:10.1021/BK-2011-1071.CH009

[43] B. M. Voelker, B. Sulzberger, Effects of fulvic acid on Fe (II) oxidation by hydrogen peroxide. *Environ. Sci. Technol.* **1996**, *30*, 1106-1114. doi:10.1021/ES9502132

[44] B. M. Voelker, F. M. M. Morel, B. Sulzberger, Iron Redox Cycling in Surface Waters: Effects of Humic Substances and Light. *Environ. Sci.Technol.* **1997**, *31*, 1004-1011. doi:10.1021/ES9604018

[45] P. Warneck, The relative importance of various pathways for the oxidation of sulfur dioxide and nitrogen dioxide in sunlit continental fair weather clouds. *Phys. Chem. Chem. Phys.* **1999**, *1*, 5471. doi:10.1039/A906558J

[46] H. Herrmann, A. Tilgner, P. Barzaghi, Z. Majdik, S. Gligorovski, L. Poulain, A. Monod, Towards a more detailed description of tropospheric aqueous phase organic chemistry: CAPRAM 3.0. *Atmos. Environ.* **2005**, *39*, 4351. doi:10.1016/J.ATMOSENV.2005. 02.016

[47] B. Chu, Y. Liu, J. Li, H. Takekawa, J. Liggio, S.-M. Li, J. Jiang, J. Hao, H. He, Decreasing effect and mechanism of $FeSO_4$ seed particles on secondary organic aerosol in a-pinene photooxidation. *Environ. Pollut.* **2014**, *193*, 88. doi:10.1016/J.ENVPOL.2014.06.018

[48] S. B. Corchnoy, R. Atkinson, Kinetics of the gas-phase reactions of hydroxyl and nitrogen oxide (NO_3) radicals with 2-carene, 1,8- cineole, *p*-cymene, and terpinolene. *Environ. Sci. Technol.* **1990**, *24*, 1497. doi:10.1021/ES00080A007

[49] Y. Iinuma, O. Böge, M. Keywood, T. Gnauk, H. Herrmann, Diaterebic acid acetate and diaterpenylic acid acetate: atmospheric tracers for secondary organic aerosol formation from 1,8-cineole oxidation. *Environ. Sci. Technol.* **2009**, *43*, 280. doi:10.1021/ES802141V

[50] A. Calogirou, B. R. Larsen, D. Kotzias, Gas-phase terpene oxidation products: a review. *Atmos. Environ.* **1999**, *33*, 1423. doi:10.1016/ S1352-2310(98)00277-5

[51] A. P. Bateman, S. A. Nizkorodov, J. Laskin, A. Laskin, Photolytic processing of secondary organic aerosols dissolved in cloud droplets. *PCCP Phys. Chem. Ch. Ph.* **2011**, *13*, 12199. doi:10.1039/ C1CP20526A

[52] H. Herrmann, Kinetics of aqueous-phase reactions relevant for atmospheric chemistry. *Chem. Rev.* **2003**, *103*, 4691. doi:10.1021/ CR020658Q

[53] B. Nozière, S. Ekström, T. Alsberg, S. Holmström, Radical-initiated formation of organosulfates and surfactants in atmospheric aerosols. *Geophys. Res. Lett.* **2010**, *37*, L05806. doi:10.1029/2009GL041683

[54] M. Lim, K. Chiang, R. Amal, Photochemical synthesis of chlorine gas from iron(III) and chloride solution. *J. Photochem. Photobiol. Chem.* **2006**, *183*, 126. doi:10.1016/J.JPHOTOCHEM.2006. 03.005

[55] J. Wittmer, S. Bleicher, C. Zetzsch, Iron(III)-induced activation of chloride and bromide from modeled saltpans. *J. Phys. Chem. A* **2015**, *119*, 4373. doi:10.1021/JP508006S

[56] S. Joshi, C. S. Chanotiya, G. Agarwal, O. Prakash, A. K. Pant, C. S. Mathela, Terpenoid compositions, and antioxidant and anti- microbial properties of the rhizome essential oils of different *Hedychium* species. *Chem. Biodivers.* **2008**, *5*, 299. doi:10.1002/ CBDV.200890027

[57] R. T. Downs, The RRUFF Project: an integrated study of the chemistry, crystallography, Raman and infrared spectroscopy of minerals, in *Program and Abstracts of the 19th General Meeting of the International Mineralogical Association in Kobe, Japan* **2006**, O03–13. Available at http://www.geo.arizona.edu/xtal/group/pdf/ IMA19_O03-13.pdf [Verified 23 May 2015].

[58] G. Socrates, *Infrared and Raman Characteristic Group Frequencies*, 3rd edn **2011** (Wiley: Chichester, UK).

[59] E. E. Lavonen, M. Gonsior, L. J. Tranvik, Ph. Schmitt-Kopplin, S. J. Köhler, Preferential chlorination of oxidized natural organic matter – identification of new disinfection by-products. *Environ. Sci. Technol.* **2013**, *47*, 2264. doi:10.1021/ES304669P

Acknowledgements

First of all I like to thank my supervisor Prof. Dr. Andreas Held, who gave me the opportunity to work on the exciting and exceptional topic of SOA formation. The time at the Professorship in Atmospheric Chemistry was the perfect mixture between practical work in the field or lab and theoretical office work. Thanks to Prof. Dr. Andreas Held encouragement I participated in international conferences, which topped my experiences off. He always came with good ideas and helped with motivation. I am deeply grateful for the last 4 years.

My colleagues, who shared the time in Australia, Prof. Dr. Andreas Held, Prof. Dr. Andreas Kappler, Prof. Dr. Heinfried Schöler, Prof. Dr. Cornelius Zetzsch, Alexander Rücker, Pascal Weigold, and especially Dr. Thorsten Krause and Dr. Johannes Ofner I wanna say thanks for the memorable and magnificent time in 2012 and 2013. The colleagues of the Dead Sea campaign Prof. Dr. Frank Keppler, Christoph Tubbesing, Dr. Karsten Kotte, Dr. Robert Holla, Stefan Schmitt and Dr. Jutta Zingler for the support and the good time in 2012. Even if the results did not have an influence on the presented thesis, I learned a lot.

My students Anna-Rabea Schmidt, Lisa Güntner and Florian Lang I gratefully thank for the good cooperation in the lab, the help in optimizing the chamber setup and the experimental procedures and also the resulting friendships.

With Dr. Johannes Ofner, Dr. Torsten Krause and Tobias Sattler I could spend a splendid cooperation during lab experiments with constructive scientific discussions and support during and after the experimental phase. Additionally they provided the opportunity to work really experimentally in the lab. The burning shoes and the bubbling lake in the chamber will remain unforgotten. Thanks for the great time with you.

For scientific discussions, technical- and scientific support I also like to thank Paulo Alarcón, Dr. Stefan G. Gonser, Julian Wittmer, Dr. Malte Julian Deventer, Dr. Robert Holla, Stefan Schmitt, Prof. Dr. Philippe Schmitt-Kopplin, Agnes Bednorz, Dr. Sergej Bleicher, Andrej Einhorn, Heinz-Ullrich Krüger†, Gerhard Küfner, Dr. Matthias Sörgel, and Prof. Dr. Cornelius Zetzsch. Also all my Haloproc-colleagues not mentioned by name I like to thank for the scientific support with an active give-and-take. The Haloproc meetings were always interesting, educational and also fun.

This work was funded from the German Research Foundation (DFG) grant HE 5214/5-1 and within the DFG research group HaloProc (FOR 763).

My especially warm thanks are due to my family and friends for their continuous support, the understanding during timing constraints, the given hold and for always believing in me.

Affidavit

(Eidesstattliche) Versicherungen und Erklärungen

(§ 5 Nr. 4 PromO)

Hiermit erkläre ich, dass keine Tatsachen vorliegen, die mich nach den gesetzlichen Bestimmungen über die Führung akademischer Grade zur Führung eines Doktorgrades unwürdig erscheinen lassen.

(§ 8 S. 2 Nr. 5 PromO)

Hiermit erkläre ich mich damit einverstanden, dass die elektronische Fassung meiner Dissertation unter Wahrung meiner Urheberrechte und des Datenschutzes einer gesonderten Überprüfung hinsichtlich der eigenständigen Anfertigung der Dissertation unterzogen werden kann.

(§ 8 S. 2 Nr. 7 PromO)

Hiermit erkläre ich eidesstattlich, dass ich die Dissertation selbständig verfasst und keine anderen als die von mir angegebenen Quellen und Hilfsmittel benutzt habe.

(§ 8 S. 2 Nr. 8 PromO)

Ich habe die Dissertation nicht bereits zur Erlangung eines akademischen Grades anderweitig eingereicht und habe auch nicht bereits diese oder eine gleichartige Doktorprüfung endgültig nicht bestanden.

(§ 8 S. 2 Nr. 9 PromO)

Hiermit erkläre ich, dass ich keine Hilfe von gewerbliche Promotionsberatern bzw. -vermittlern in Anspruch genommen habe und auch künftig nicht nehmen werde.

…….

Ort, Datum, Unterschrift